

**DEVELOPMENT OF A  
THERMOELECTRIC GENERATOR SYSTEM  
FOR IOT APPLICATIONS**

**WONG WEN KANG**

**UNIVERSITI TUNKU ABDUL RAHMAN**

**DEVELOPMENT OF A  
THERMOELECTRIC GENERATOR SYSTEM  
FOR IOT APPLICATIONS**

**WONG WEN KANG**


**A project report submitted in partial fulfilment of the  
requirements for the award of Bachelor of Mechanical Engineering  
with Honours**

**Lee Kong Chian Faculty of Engineering and Science  
Universiti Tunku Abdul Rahman**

**May 2023**

## DECLARATION

I hereby declare that this project report is based on my original work except for citations and quotations which have been duly acknowledged. I also declare that it has not been previously and concurrently submitted for any other degree or award at UTAR or other institutions.

Signature :  \_\_\_\_\_

Name : Wong Wen Kang \_\_\_\_\_

ID No. : 000408-14-1465 \_\_\_\_\_

Date : 22<sup>nd</sup> May 2023 \_\_\_\_\_

**APPROVAL FOR SUBMISSION**

I certify that this project report entitled “**DEVELOPMENT OF A THERMOELECTRIC GENERATOR SYSTEM FOR IOT APPLICATIONS**” was prepared by **WONG WEN KANG** has met the required standard for submission in partial fulfilment of the requirements for the award of Bachelor of Mechanical Engineering with Honours at Universiti Tunku Abdul Rahman.

Approved by,

Signature : *yeongjin*

Supervisor : Ts Dr King Yeong Jin

Date : 22<sup>nd</sup> May 2023



The copyright of this report belongs to the author under the terms of the copyright Act 1987 as qualified by Intellectual Property Policy of Universiti Tunku Abdul Rahman. Due acknowledgement shall always be made of the use of any material contained in, or derived from, this report.

© 2023, Wong Wen Kang. All right reserved.

## ACKNOWLEDGEMENTS

I would like to thank everyone who had contributed to the successful completion of this project. I would like to express my gratitude to my research supervisor, Ts Dr. King Yeong Jin for his invaluable advice, guidance, and his enormous patience throughout the development of the research.

In addition, I would also like to express my gratitude to my loving parents and friends who had helped and given me encouragement to work on this project.

## ABSTRACT

Waste heat is produced as a by-product from various manufacturing process. In most of the industry, low-temperature waste heat is released into the atmosphere instead of recovering it due to low-grade heat energy that is unable to provide any useful work. Thermoelectric generator (TEG) is one of the waste heat recovery devices to generate electricity from the heat source. Along with the evolution of Industry 4.0, thermoelectric generator (TEG) encourages the acceptance of the recent technologies such as Internet of Things (IoT) devices into the manufacturing industry. IoT devices are the key components to build a powerful industrial system to boost the production rate. This is done by using real-time data to optimise the manufacturing process. However, installation of IoT system is costly as they require power source and the production plant must be shut down for installation purpose. For this reason, TEG system provides a solution by eliminating power cable to power up the additional devices. A plug and play IoT device that is completely wireless can be fabricated where system is maintenance-free as it does not have any moving part. To achieve that, this study aims to recover low-temperature waste heat using TEG module and convert them into electricity to power up small IoT device. In this study, the power generated by different type of heat sink, thermal conductive paste and TEG module were compared. Then, the configurations of the TEG to generate sufficient electricity to power up small IoT device were compared. Lastly, a wireless sensor device powered up by TEG was developed. The power output of the TEG system for each design was measured to analyse the performance of each design. From the experiment, it was found that the height of the fins for the heat sink is critical where heat sink with higher fins height can dissipate heat at a faster rate. As a result, higher temperature gradient is achieved and power output by the TEG is higher. In addition, air flow of the system is having significant impact on the overall performance of the system. At the end of this study, a feasible prototype of TEG system was built successfully. It managed to operate at surface temperature of 115 °C and above and atmospheric temperature of 30 °C.

## TABLE OF CONTENTS

<b>DECLARATION</b>		<b>i</b>
<b>APPROVAL FOR SUBMISSION</b>		<b>ii</b>
<b>ACKNOWLEDGEMENTS</b>		<b>iv</b>
<b>ABSTRACT</b>		<b>v</b>
<b>TABLE OF CONTENTS</b>		<b>vi</b>
<b>LIST OF TABLES</b>		<b>x</b>
<b>LIST OF FIGURES</b>		<b>xii</b>
<b>LIST OF SYMBOLS / ABBREVIATIONS</b>		<b>xvii</b>
<b>LIST OF APPENDICES</b>		<b>xviii</b>
<b>CHAPTER</b>		
<b>1</b>	<b>INTRODUCTION</b>	<b>1</b>
1.1	General Introduction	1
1.2	Importance of the Study	2
1.3	Problem Statement	3
1.4	Aim and Objectives	3
1.5	Scope and Limitation of the Study	4
1.6	Contribution of the Study	5
1.7	Outline of the Report	5
<b>2</b>	<b>LITERATURE REVIEW</b>	<b>6</b>
2.1	Introduction	6
2.2	Current Research Development on TEG	6
2.3	Working Principle of TEG	7
2.3.1	Seebeck Effect	7
2.3.2	Peltier Effect	8
2.4	Configuration of TEG	8
2.4.1	Material of TEG	9
2.4.2	Materials Arrangements of TEG	10
2.5	Waste Heat Recovery	12

	2.5.1 Low Temperature Waste Heat	15
	2.5.2 High Temperature Waste Heat	17
2.6	Application	17
	2.6.1 Industry 4.0 and Internet of Things (IoT)	17
	2.6.2 Medical Devices	18
	2.6.3 Wearable Devices	19
	2.6.4 Automotive	20
	2.6.5 Aerospace	21
2.7	Heat Sink	22
2.8	Efficiency of TEG	22
2.9	Air Flow of Fan	23
2.10	Summary	23
<b>3</b>	<b>METHODOLOGY AND WORK PLAN</b>	<b>24</b>
3.1	Introduction	24
3.2	Equipment and Material	26
	3.2.1 Thermoelectric Generator (TEG) Module	26
	3.2.2 Heat Sink	28
	3.2.3 Electric Fan	30
	3.2.4 Aluminium Plate	31
	3.2.5 Thermal Conductive Paste	31
	3.2.6 Insulation	33
	3.2.7 Step-Down Power Module	35
	3.2.8 ESP32 Arduino Module	36
	3.2.9 DHT11 Humidity and Temperature Sensor Module	36
3.3	Theoretical Analysis of TEG Module and Load	37
	3.3.1 Theoretical Output of SP1848-27145 TEG Module	37
	3.3.2 Theoretical Output of TEC1-12730 TEC Module	38
	3.3.3 Theoretical Output of TEG-127-3.5- 2.8T250D TEG Module	39
	3.3.4 Theoretical Loads	40
3.4	Methodology	40

	3.4.1	Methods of Data Collection	41
	3.4.2	Air Flow	42
	3.4.3	Experimental Procedure	44
3.5		Experiment 1 – Compare Different Type of Heat Sink, Thermal Conductive Paste and TEG Module	52
3.6		Experiment 2 – Compare the Configuration of TEG Module	54
	3.6.1	Design 1	55
	3.6.2	Design 2	56
	3.6.3	Design 3	58
	3.6.4	Design 4	60
	3.6.5	Design 5	62
	3.6.6	Design 6	63
	3.6.7	Design 7	65
	3.6.8	Design 8	67
3.7		Develop Arduino Module – Wireless Device	69
3.8		Summary	70
<b>4</b>		<b>RESULTS AND DISCUSSION</b>	<b>71</b>
	4.1	Introduction	71
	4.2	Experiment 1 - Compare Different Type of Heat Sink, Thermal Conductive Paste and TEG Module	71
	4.2.1	Comparison of Heat Sink	71
	4.2.2	Comparison of Thermal Conductive Paste	74
	4.2.3	Comparison of Thermoelectric Generator (TEG) Module	75
	4.3	Experiment 2 - Compare the Configuration of TEG	76
	4.3.1	Design 1	76
	4.3.2	Design 2	77
	4.3.3	Design 3	78
	4.3.4	Design 4	78
	4.3.5	Design 5	79

4.3.6	Design 6	82
4.3.7	Design 7	84
4.3.8	Design 8	86
4.3.9	Design 8 Under Load	87
4.3.10	Summary of the Comparison on the Designs	92
4.4	Efficiency of the Prototype	94
4.5	Develop Arduino Module – Wireless Device	94
4.6	Summary	96
<b>5</b>	<b>CONCLUSIONS AND RECOMMENDATIONS</b>	<b>97</b>
5.1	Conclusions	97
5.2	Limitations	97
5.3	Recommendations for Future Work	98
	<b>REFERENCES</b>	<b>99</b>
	<b>APPENDICES</b>	<b>105</b>

## LIST OF TABLES

Table 1.1:	Details of Scopes of the Study.	4
Table 2.1:	Categories of Thermoelectric Materials (Li et al., 2011; LaGrandeur et al., 2006; Espinosa et al., 2010).	10
Table 2.2:	Statistics of Waste Heat in US, China and EU (Xu, Wang and Yang, 2019).	13
Table 2.3:	Summary Table of Current Waste Heat Recovery Technologies (Jouhara et al., 2018).	13
Table 2.4:	Typical Processes and Temperature Ranges in Food and Beverage Industry (Fluch, Brunner and Grubbauer, 2017).	16
Table 2.5:	Efficiency of Waste Heat Recovery System in Automobiles using TEG.	22
Table 3.1:	Equipment Required for the Experiment.	26
Table 3.2:	Materials Required for the Experiment.	26
Table 3.3:	Insulation Material With Respective Thermal Conductivity.	33
Table 3.4:	Thermoelectric Parameter for a Single SP1848-27145TEG Module.	38
Table 3.5:	Thermoelectric Parameter for a Single TEG-127-3.5-2.8T250D TEG Module.	39
Table 3.6:	Calculation of Loads.	40
Table 3.7:	Theoretical Output for Design 1.	56
Table 3.8:	Theoretical Output for Design 2.	57
Table 3.9:	Theoretical Output for Design 3.	59
Table 3.10:	Theoretical Output for Design 4.	61
Table 3.11:	Theoretical Output for Design 5.	63
Table 3.12:	Theoretical Output for Design 6.	65
Table 3.13:	Theoretical Output for Design 7.	67



Table 3.14:	Theoretical Output for Design 8.	69
Table 4.1:	Data Obtained from Experiment 1.	72
Table 4.2:	Comparison of Heat Sink.	73
Table 4.3:	Comparison of Thermal Conductive Paste.	74
Table 4.4:	Comparison of TEG Modules.	75
Table 4.5:	Experimental Data for Design 1.	77
Table 4.6:	Experimental Data for Design 2.	77
Table 4.7:	Experimental Data for Design 3.	78
Table 4.8:	Experimental Data for Design 4.	79
Table 4.9:	Experimental Data for Design 5.	81
Table 4.10:	Experimental Data for Design 6.	82
Table 4.11:	Experimental Data for Design 7.	85
Table 4.12:	Experimental Data for Design 8.	87
Table 4.13:	Standard Deviation for All Trials of Design 8.	92
Table 4.14:	Comparison of the Designs.	93
Table 4.15:	Measured Power of the Energy Input and Output.	94
Table B-1:	Experimental Data for Design 8 for First Trial.	106
Table B-2:	Experimental Data for Design 8 for Second Trial.	106
Table B-3:	Experimental Data for Design 8 for Third Trial.	107
Table B-4:	Mean Data for Design 8 From All Trials.	107

## LIST OF FIGURES

Figure 1.1:	Distribution and Reuse of Waste Heat Resources (Xiao et al., 2022).	2
Figure 2.1:	Graphical View of Seebeck Effect and Peltier Effect (Reardon Hazel, 2022).	8
Figure 2.2:	Arrangements of Peltier Module for (a) Standard Thermocouple, (b) Segmented Thermocouple.	11
Figure 2.3:	Schematic Diagram of Cascaded Three Stages TEG Modules (Zhang et al., 2008).	12
Figure 2.4:	Cooker of Rice	16
Figure 2.5:	Cooker of Instant Noodle.	16
Figure 2.6:	Electroencephalography (EEG) Headband (CMP (Firm), Institute of Electrical and Electronics Engineers. and Components, 2009).	19
Figure 2.7:	Electrocardiography (ECG) Shirt (Leonov, 2013).	19
Figure 2.8:	Matrix PowerWatch Powered by TEG and Body Heat (Tech4All, n.d.).	20
Figure 2.9:	Heat Exchanger Subassemblies of Automobile Exhaust (Meisner, 2010).	21
Figure 2.10:	Locations of TEG Used on an Aircraft (Pearson et al., 2012).	21
Figure 3.1:	Flowchart of the Building of Prototype.	25
Figure 3.2:	SP1848-27145 TEG Module.	27
Figure 3.3:	TEC1-12730 TEC Module.	28
Figure 3.4:	TEG-127-3.5-2.8T250D TEG Module.	28
Figure 3.5:	Aluminium Heat Sink With 11 mm Fins.	29
Figure 3.6:	Copper Heat Sink With 2 mm Fins.	29
Figure 3.7:	Aluminium Heat Sink With 36 mm Fins.	29
Figure 3.8:	Aluminium Heat Sink With 20 mm Fins.	30

Figure 3.9:	Electric Fan 5 V 0.15 A.	30
Figure 3.10:	Aluminium Plate.	31
Figure 3.11:	Ice Fusion V2 Thermal Paste With 5 W/m-K Thermal Conductivity.	32
Figure 3.12:	HY510 Thermal Paste With 1.93 W/m-K Thermal Conductivity.	32
Figure 3.13:	HTK-002 Thermal Paste With 0.8 W/m-K Thermal Conductivity.	33
Figure 3.14:	Frost X25 Thermal Paste With 10.5 W/m-K Thermal Conductivity.	33
Figure 3.15:	PVC Board.	34
Figure 3.16:	Cork Sheet.	34
Figure 3.17:	Ethylene Vinyl Acetate (EVA) Foam.	35
Figure 3.18:	DC-DC Step-Down Power Module.	35
Figure 3.19:	ESP32 Arduino Module With Wi-Fi and Bluetooth.	36
Figure 3.20:	DHT11 Temperature and Humidity Sensor Module.	37
Figure 3.21:	Graph of Voltage and Current Produced from Temperature Difference of a Single SP1848-27145 TEG Module.	38
Figure 3.22:	Graph of Voltage and Current Produced from Temperature Difference of a Single TEG-127-3.5-2.8T250D TEG Module.	40
Figure 3.23:	Set-up of Single TEG Module.	41
Figure 3.24:	Set-up of Multiple TEG Module.	42
Figure 3.25:	Air Flow Simulation of Fan Without Fins.	43
Figure 3.26:	Fins for Fan.	43
Figure 3.27:	Air Flow Simulation of Fan with Fins.	44
Figure 3.28:	Prototype Design in SolidWorks.	45
Figure 3.29:	Fabrication of Metal Plate.	45
Figure 3.30:	3D Printing of Case.	46

Figure 3.31: Prepared Surface of Aluminium Plate.	46
Figure 3.32: Aluminium Plate with Thermal Conductive Paste.	47
Figure 3.33: TEG Modules on Aluminium Plate.	47
Figure 3.34: TEG Modules with Thermal Conductive Paste on the Cold Side.	48
Figure 3.35: Heat Sink Placed on TEG Modules.	48
Figure 3.36: Case Assembled with Fan.	49
Figure 3.37: Placing of Thermocouples on the Heat Sink.	49
Figure 3.38: Insulation Board.	50
Figure 3.39: Fully Assembled Prototype.	50
Figure 3.40: Soldering of the Connection of TEG Modules.	50
Figure 3.41: Soldering of the Connection of Step-Down Power Module.	51
Figure 3.42: Connection of Voltmeter and Ammeter.	51
Figure 3.43: Temperature Setting of Heater.	52
Figure 3.44: Prototype Testing in Experiment 2.	52
Figure 3.45: Set-up of Single TEG Module.	53
Figure 3.46: Connection of Voltmeter and Ammeter.	54
Figure 3.47: Set-up of Four TEG Modules Connecting in Series with Fan.	55
Figure 3.48: Circuit Diagram of Four TEG Modules.	56
Figure 3.49: Set-up of Six TEG Modules Connecting in Series and Parallel with Fan.	57
Figure 3.50: Circuit Diagram of Six TEG Modules.	58
Figure 3.51: Set-up of Nine TEG Modules Connecting in Series with Fan.	59
Figure 3.52: Circuit Diagram of Nine TEG Modules.	60

Figure 3.53: Set-up of Eight TEG Modules Connecting in Series with Fan.	61
Figure 3.54: Circuit Diagram of Eight TEG Modules.	61
Figure 3.55: Set-up of 15 TEG Modules Connecting in Series with Fan.	62
Figure 3.56: Circuit Diagram of 15 TEG Modules.	63
Figure 3.57: Set-up of 16 TEG Modules Connecting in Series and Parallel.	64
Figure 3.58: Set-up of 16 TEG Modules Connecting in Series and Parallel with Case and Fan.	64
Figure 3.59: Circuit Diagram of 16 TEG Modules.	65
Figure 3.60: Set-up of Nine TEG Modules Connecting in Series.	66
Figure 3.61: Set-up of Nine TEG Modules Connecting in Series with Case and Fan.	66
Figure 3.62: Circuit Diagram of Nine TEG Modules.	67
Figure 3.63: Set-up of 12 TEG Modules Connecting in Series and Parallel.	68
Figure 3.64: Set-up of 12 TEG Modules Connecting in Series and Parallel with Case and Fan.	68
Figure 3.65: Circuit Diagram of 12 TEG Modules.	69
Figure 3.66: Schematic Diagram of Prototype.	70
Figure 4.1: Prototype of Design 1.	76
Figure 4.2: Prototype of Design 2.	77
Figure 4.3: Prototype of Design 3.	78
Figure 4.4: Prototype of Design 4.	79
Figure 4.5: Prototype of Design 5.	80
Figure 4.6: Gap between Heat Sink and TEG Module.	81
Figure 4.7: Prototype of Design 6.	82
Figure 4.8: Measured Voltage of Each TEG Module.	83

Figure 4.9:	Prototype of Design 7.	84
Figure 4.10:	Experiment for Design 7.	85
Figure 4.11:	Measured Voltage of Each TEG Module.	85
Figure 4.12:	Prototype of Design 8.	86
Figure 4.13:	Experiment for Design 8.	87
Figure 4.14:	Graph of Voltage and Current Generated against Temperature Difference for First Trial.	88
Figure 4.15:	Graph of Power Output against Temperature Difference for First Trial.	88
Figure 4.16:	Graph of Voltage and Current Generated against Temperature Difference for Second Trial.	89
Figure 4.17:	Graph of Power Output against Temperature Difference for Second Trial.	89
Figure 4.18:	Graph of Voltage and Current Generated against Temperature Difference for Third Trial.	90
Figure 4.19:	Graph of Power Output against Temperature Difference for Third Trial.	90
Figure 4.20:	Graph of Voltage and Current Generated against Temperature Difference from Mean Data.	91
Figure 4.21:	Graph of Power Output against Temperature Difference from Mean Data.	91
Figure 4.22:	Set-up of Arduino Module.	95
Figure 4.23:	Dashboard of Ubidots showing Real-Time Data from ESP32 Arduino Board.	95

**LIST OF SYMBOLS / ABBREVIATIONS**

$V$	volt, V
$I$	current, A
$P$	power, W
$zT$	Fig. of Merit
$s$	compatibility factor
$u$	relative current density
IMDs	Implanted Medical Devices
IoT	Internet of Things
TEG	Thermoelectric Generator
TEC	Thermoelectric Cooler
WSN	Wireless Sensor Network
CFD	Computational Fluid Dynamics

**LIST OF APPENDICES**

Appendix A: Gantt Chart	105
Appendix B: Experimental Data for Design 8	106
Appendix C: Arduino Code for ESP32	109



## CHAPTER 1

### INTRODUCTION

#### 1.1 General Introduction

The world is facing the challenge of increasing population that leads to higher demands of resources. Therefore, higher supply is needed to cope with the consumption by boosting the production. Although this is a good development prospects in modernization to ensure linear path towards a developed industrial society, but the side effects of uncontrolled mass production have always been ignored which may cause more harm than good to the society. One of the major concerns of the side effect is the waste heat released from the industries to the atmosphere that is contributing to global warming (Bian, 2020).

Waste heat can be found in most of the industries including as oil and gas refining, food processing, steel and iron production and the regular practice of getting rid of it is releasing the heat into the atmosphere. For instance, internal combustion engine produces high temperature exhaust gases, cooling unit releases heat at the condenser and heat from the oven is vented to the surrounding.

As shown in Figure 1.1, based on the research, the recycling rate for low-temperature waste heat is significantly low which is less than 1% because of its low quality that restricts the potential for increasing the utilization rate of industrial waste heat (Xiao et al., 2022). This might be due to the small amount of heat is not useful or the power generated is not sufficient to power up other process in the industries. Furthermore, it is convenient to release it to the atmosphere rather than investing in costly waste heat recycling machine. Therefore, in the context of global warming, enormous amounts of waste heat that released from industrial activities have been introduced into the climate system without substantial consideration about the consequences.

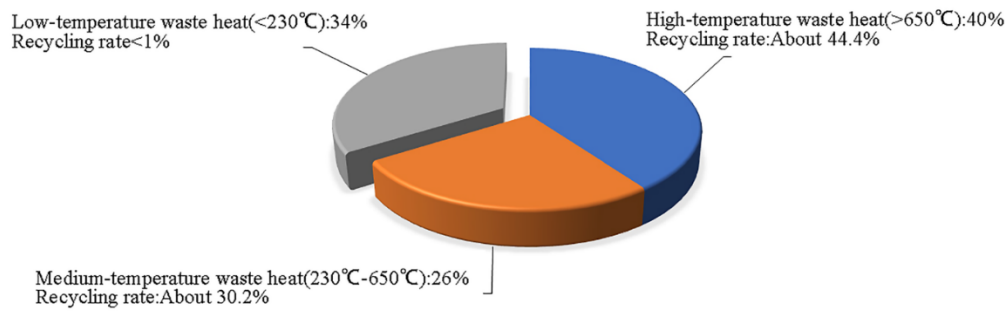


Figure 1.1: Distribution and Reuse of Waste Heat Resources (Xiao et al., 2022).

As stated in Sustainable Development Goal 11, in order to ensure sustainable growth, it refers to the methods of economic growth that aims for low emission, low consumption, high efficiency (United Nations Environment Programme (UNEP), n.d.). Therefore, it should be managed appropriately to reduce the waste heat from escaping into the atmosphere and leads to global warming.

In order to achieve this, thermoelectric generator (TEG) module can be used to recover low-temperature waste heat into usable energy for other purpose in the industries. TEG is also known as a Seebeck generator, it has the reverse process of thermoelectric cooler (TEC) that create temperature difference by supplying power to the module. For TEG, the waste heat from the surface of the machine is absorbed by the TEG at the hot side, then the heat is released from the cold side of TEG. This process creates a temperature difference between hot side and cold side of the TEG module and electricity is generated. More power is produced by the TEG when the temperature difference is larger.

## 1.2 Importance of the Study

The main purpose of the project is to recover low-temperature waste heat generated from the process of production lines from several industries into useful energy by using TEG. It is used to convert heat energy into electricity to power up small IoT devices that can be used to facilitate the overall production process of the industries such as wireless sensors and camera to monitor the production.

### **1.3 Problem Statement**

In most of the manufacturing industries, waste heat is being produced from the operation of the manufacturing process and it is released into the surrounding instead of recovering it due to the temperature is not high enough to perform any functional operation as mentioned above.

Subsequently, the effort and cost to set up additional devices for monitoring and controlling purpose in manufacturing industries by means of upgrading the system are considerably high. This is because the devices would require power source and the new power cables will need to be connected to the nearest power supply or the main switch if the power plug is not sufficient. As a result, in traditional way, the factory or plant will need to be shut down for system upgrading due to rewiring and restructuring of the whole system which is not economical. Most of the management team would refuse to perform this upgrade and remain as it is to avoid undesirable issue.

Other than that, when a large number of devices are installed, it is challenging to track down which cable leading to the device is having issue when bundle of cables is tied together. At the same time, wireless devices also eliminate the problem of cable disconnection and as a result, it has higher reliability and requires lesser maintenance.

### **1.4 Aim and Objectives**

The aim of the study is to develop an efficient TEG system that can function in most of the processes at the production lines of several industries. The TEG will eliminate the need for power source to power up the devices as it will generate electricity from the waste heat source of the production process. The study also aims to provides a better solution for the industries in waste heat recovery. The main focus of the study is to evaluate the designs of TEG system that can power up the small IoT device effectively. The specific objectives of this research are stated below:

1. To compare the power generated by different type of heat sink, thermal conductive paste, and TEG module.
2. To compare the configuration of the TEG to generate sufficient electricity to power small IoT device.

3. To develop a wireless sensor device powered up by the electricity generated by TEG.

### 1.5 Scope and Limitation of the Study

The study is divided into several scopes, and they are interrelated to each other to provide smoother process flow throughout the project. Table 1.1 shows the few scopes of the study together with the details.

Table 1.1: Details of Scopes of the Study.

Analyse the performance of TEG.	The output is to be measured from the series of TEG module and determine the quantity of TEG module needed to meet the minimum requirement for the following scope.
Fabricate a prototype of TEG.	Build the prototype with certain number of TEG modules that has been decided on earlier.
Build a prototype to power small IoT device	Connect the TEG modules with external module to stabilize the output and power up the loads.
Evaluate the performance of the prototype.	Verify if the prototype can power up small IoT devices such as Arduino with sensors. At the same time, evaluate the stability and sustainability of the device.
Modification and improvement.	Make certain changes on the prototype if the result does not meet the requirement or not able to power up the small IoT devices.

Subsequently, the limitation of the study is high atmospheric temperature. In Malaysia, the average atmospheric temperature in the daytime is around 30 °C (World Weather & Climate Information, n.d.). Therefore, the performance of TEG may not be at the peak as compared to the countries that are having lower average atmospheric temperature.

## **1.6 Contribution of the Study**

This study encourages the implementation of waste heat recovery focusing on low-temperature in the industries using TEG to produce electricity. Although the electricity produced is minimal, however, it is possible to power up small IoT devices such as camera and sensor to assist in the production process. At the same time, the electricity consumption from the power grid will remain unchanged with the installation of IoT devices as they are fully powered up by TEG system instead of power grid.

Furthermore, this study helps to increase the recycling rate of low-temperature waste heat due to its wide applications. When less waste heat is released into the atmosphere, the side effects mentioned above especially global warming can be suppressed or even reduced in long term. As a result, sustainable growth can be achieved and meeting the target of Sustainable Development Goal 11 to protect the environment.

Besides that, this study allows the industries to install additional devices to monitor production process more conveniently. It is cost-effective and user-friendly where the installation is as simple as placing the devices on the surface of waste heat source to power up. It can also be relocated as needed. These advantages increase the willingness of the management team of industries to invest in the smart IoT devices and recover waste heat concurrently.

## **1.7 Outline of the Report**

First and foremost, information about TEG was collected and analysed to understand the working principles of it. Then, the designs of the prototype were prepared based on the study of previous research and journals. Experiment on the TEGs were carried out to measure their performance and the designs of the prototype were modified accordingly. At the end, the data of the experiment were collected to discuss on the findings and further possible improvements were discussed to increase the efficiency of the prototype.

## CHAPTER 2

### LITERATURE REVIEW

#### 2.1 Introduction

The research and study done previously have to be fully utilised to develop a product, which is TEG system in this case, that has higher functionality and has the potential to benefit the industries.

This section will evaluate the TEG in terms of the working principle, configuration, working environment, and possible application. Previous research on the efficiency of TEG to produce electricity in various environment and the possible configuration of it must be done in order to provide clearer direction and valuable information for the product design to avoid repeating the same mistake in the product development. The set-up of the TEG is crucial because it affects the efficiency of the system as well as the amount of power generated by the system to supply power to the system as well as recharging the battery. Therefore, it is vital to gather information and research available to determine the best configuration to obtain the best result.

#### 2.2 Current Research Development on TEG

Due to the potential applications of TEG, a number of papers were published to discuss its performance, set-up, materials as well as applications and they are listed below with difference scopes. The effectiveness of the thermoelectric module was evaluated both experimentally and analytically (Casano and Piva, 2011). Waste heat to heat the thermoelectric generator and cooled by liquid and by air was investigated (Crane and Jackson, 2004). The applications of thermoelectric generator were compiled (Bell, 2008). The impact of the conditions that affecting the efficiency of thermoelectric generator was investigated (Niu, Yu and Wang, 2009). Several models of the parallel-plate heat exchanger on thermoelectric generator were assessed to determine its performance (Yu and Zhao, 2007). Application of thermoelectric generator for automobile was studied (Saqr, Mansour and Musa, 2008). The potential uses of thermoelectric devices were analysed (Riffat and Ma, 2003). The performance of power output from the thermoelectric module (TEG) was evaluated based on

the temperature, heat rates, mechanical loading conditions and electrical performance metrics (Sandoz-Rosado and Stevens, 2009). Experiment on thermoelectric generator (TEG) was conducted and output values in terms of voltage, current and power were obtained, where the temperature gradient of the module was also determined (Ubaidillah et al., 2014). Peltier effect and Seebeck effect were investigated about their relationship and a model was built to evaluate the Peltier-coefficient (Drebushchak, 2008).

### **2.3 Working Principle of TEG**

To make up a TEG, it consists of three main key components, which are TEG modules, heat exchanger and heat sink. The function of heat exchanger is to absorb the heat and transfer them to the TEG modules while the heat sink release extra heat from the other end of TEG modules. This creates a difference in temperature between two ends of the TEG modules and small amount of electricity is generated (Jouhara et al., 2021).

The amount of power generated by TEG is mainly determined by temperature gap between both sides of TEG module and in order to increase the voltage generated, the hotter end should be heat up further or the colder end should be cool down further or both at the same time. The hot face of the TEG module will be positively charge while the cooler side will be negatively charged due to the hot electrons move towards the cold face at faster rate than the cold electrons move towards the hot face (Jouhara et al., 2021). This is because the cold electrons have lower kinetic energy than the hot electrons (Jouhara et al., 2018).

#### **2.3.1 Seebeck Effect**

The thermoelectric effect is the name of this process where a temperature difference generates a voltage. When the different ends of the module that consist of different metallic conductors is being heated to different temperature, an electric current is produced. In addition, the amount of electric current produced increases linearly with the temperature gap and also affected by the material used (Seebeck, n.d.).

However, Seebeck inaccurately concluded that the transfer of heat produces the same effect as flowing energy because he was unable to convey

the actual explanation behind this process (Jouhara et al., 2021). Therefore, this process was further studied by Jean-Charles-Athanase Peltier, a French scientist, in 1832 followed by Willion Thomson in 1854.

### 2.3.2 Peltier Effect

It is found that the heat will be absorbed at one end and release at other end of the same circuit with different metals. This close the gap between the two materials' chemical structure capacity (Jouhara et al., 2021). It is known that Seebeck effect is the reverse of Peltier effect where Seebeck effect is used in generating power whereas Peltier effect is used in cooling mode as shown in Figure 2.1.

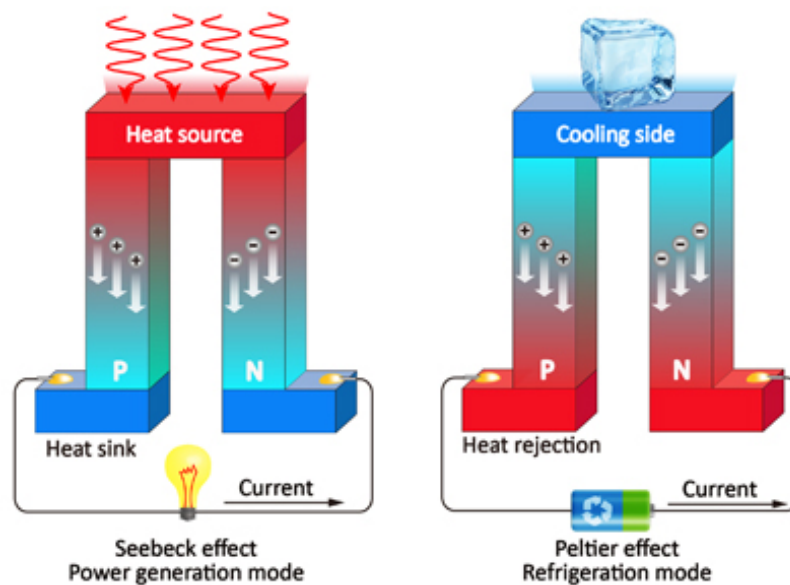


Figure 2.1: Graphical View of Seebeck Effect and Peltier Effect (Reardon Hazel, 2022).

### 2.4 Configuration of TEG

The material used and design of the TEG will directly affect the performance of it to produce electricity. Therefore, it is necessary to study and determine the optimum material and design for the TEG. Then, thermoelectric Fig. of Merit ( $zT$ ) is used to measure greatest effectiveness of the conversion of heat to thermoelectric energy (Jouhara et al., 2021).



### 2.4.1 Material of TEG

The TEG should possess the properties of adequate Seebeck coefficient, poor thermal conductivity and good electrical conductivity, in order to be effective. For high electrical conductivity, it minimises the Joule heating that the resistance of current flow causes the temperature to increase while good Seebeck coefficient will result in maximum conversion of heat to electric power. Then, lower thermal conductivity can reduce the thermal conduction to maintain the temperature gradient between both sides of the TEG (Jouhara et al., 2021).

Bismuth Telluride ( $\text{Bi}_2\text{Te}_3$ ), whereby the values of Fig. of Merit for n-type materials and p-type materials are 0.9 and 1.35 respectively, was the main material previously utilised in the industry to build TEG modules (Lan et al., 2010). Its performance is being limited by the deficient productivity of n-type material compared to p-type material (Han et al., 2017). Despite that, this material is still mainly used in refrigeration application as well as other devices that has working temperature of 180 to 450 K (Jouhara et al., 2021).

Apart from that, conventional material is divided into three groups according to their range of temperature at which performance is optimum. For example,  $\text{Bi}_2\text{Te}_3$  – based material is used when the operating temperature is below 150 °C while TAGS  $[\text{AgSbTe}_2]_{1-x}(\text{GeTe})_x$  is used for operating temperature of 150 to 500 °C and  $\text{SiGe}$  – based material is used for operating temperature of 500 °C and above (Zoui et al., 2020; Romanjek et al., 2015). In addition, Table 2.1 shows the categories of thermoelectric materials based on their working temperature with peak zT value.

Table 2.1: Categories of Thermoelectric Materials (Li et al., 2011; LaGrandeur et al., 2006; Espinosa et al., 2010).

Group	Material	Ideal Temperature Range (K)	Peak zT
<b>High Temperature (700 – 1000 K) (427 – 727 °C)</b>	CoSb <sub>3</sub> (n-type)	650 – 1100	0.9
	PbTe (n-type)	600 – 850	0.8
	SiGe (n-type)	> 1000	0.9
	Zn <sub>4</sub> Sb <sub>3</sub> (p-type)	> 600	1.4
	CeFe <sub>4</sub> Sb <sub>12</sub> (p-type)	> 850	1.5
	SiGe (p-type)	900 – 1300	0.5
	TAGS (p-type)	650 – 800	1.3
	CeFe <sub>3</sub> RuSb <sub>12</sub>	–	–
	Mg <sub>2</sub> Si (n-type)	645	1.1
<b>Medium Temperature (400 – 700 K) (127 – 427 °C)</b>	Tl <sub>9</sub> BiTe <sub>6</sub> (p-type)	> 400	1.3
<b>Low Temperature (300 – 400 K) (27 – 127 °C)</b>	Bi <sub>2</sub> Te <sub>3</sub> (n-type)	< 350	0.7
	Bi <sub>2</sub> Te <sub>3</sub> (p-type)	< 450	1.1
	(Bi, Sb) <sub>2</sub> Te <sub>3</sub> (p-type)	375	1

#### 2.4.2 Materials Arrangements of TEG

Due to the characteristics of thermoelectric materials that vary with the change of temperature, they typically exhibit the maximum zT in a particular range of temperatures. Thus, thermocouples with segmented materials were built to match with the temperature of heat source with specific operating temperature range while maximising the zT value (Ge et al., 2018; Tian et al., 2015; Shu et al., 2018). Figure 2.2 shows the thermocouple arrangements of conventional type and segmented type where the TE materials for layer one and layer two are chosen based on their ideal temperature range from Table 2.1. The TE material which is having lower operating temperature will be placed at layer one which is nearer to the heat sink while higher operating temperature TE material is placed at layer two that is nearer to the heat source.

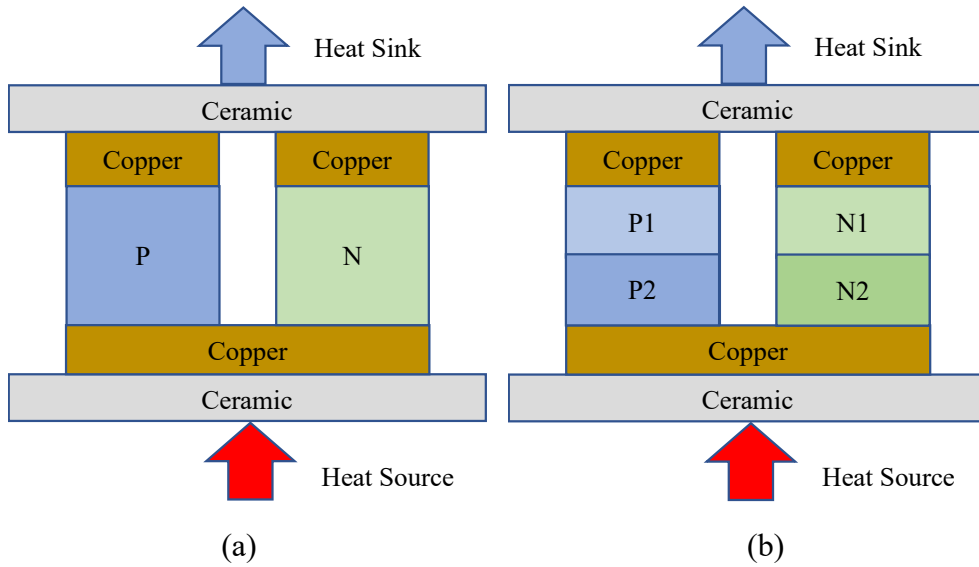


Figure 2.2: Arrangements of Peltier Module for (a) Standard Thermocouple, (b) Segmented Thermocouple.

However, when two materials with different mechanical properties are stacked together, there is a possibility that the two materials are incompatible and unable to produce maximum efficiency. The relative current density has to be same as the compatibility factor in order to achieve highest efficiency of the segmented TEG (Snyder, 2004; Snyder and Ursell, 2003). The compatibility factor,  $s$  is given by:

$$s = \frac{\sqrt{1+zT}-1}{\alpha T} \quad (2.1)$$

While the relative current density is given by:

$$u = \frac{J}{\lambda \nabla T} \quad (2.2)$$

To overcome this incompatibility problem, a cascaded arrangement of TE materials was used whereby the thermocouples was mounted parallelly as shown in Figure 2.3. The separation of the mechanical, thermal and electrical properties of the materials can increase the efficiency as the cascaded arrangement split them in stages and linked individually to the output circuit (Kanimba et al., 2017; Zhang et al., 2008; Shen et al., 2017).

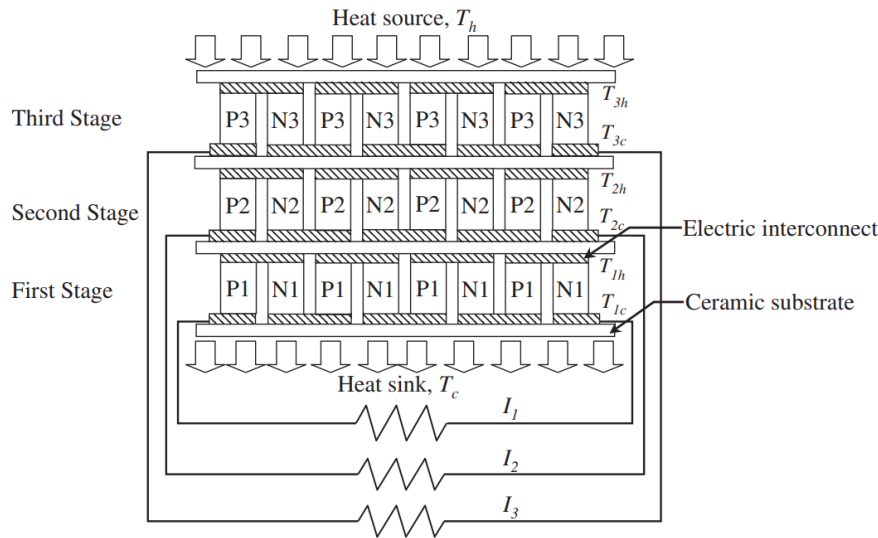


Figure 2.3: Schematic Diagram of Cascaded Three Stages TEG Modules  
(Zhang et al., 2008).

## 2.5 Waste Heat Recovery

Waste heat is commonly found in the industry from the several processes and part of the heat is recovered using Stirling engines, Rankine engines or steam turbines to convert them into electricity (Jouhara et al., 2021). Based on the finding from ceramic tile furnace at large industrial chimney that has a flue gas with mass flow rate of  $18,400 \text{ Nm}^3/\text{h}$  at  $187 \text{ }^\circ\text{C}$ , the theoretical output from the TEG prototype is found to be  $100 \text{ W/m}^2$  including the energy used to cool the TEG prototype (Aranguren, Astrain and Pérez, 2014).

Waste heat is categorised into three classifications which are low temperature (less than  $230 \text{ }^\circ\text{C}$ ), moderate temperature (from  $230 \text{ }^\circ\text{C}$  to  $650 \text{ }^\circ\text{C}$ ) and high temperature (more than  $650 \text{ }^\circ\text{C}$ ). Generally, high temperature waste heat can be obtained from operation of direct combustion, whereas for moderate temperature range, the waste heat is released at combustion units exhaust and low temperature waste heat is found from the equipment and products of process units (Brückner et al., 2015).

To date, several heat recovery machines are used to absorb and convert the waste heat to usable energy using heat exchanger. The systems primarily consist of air preheaters, regenerators, recuperators, regenerative burners, heat pipe heat exchanger, economisers, direct electrical conversion devices, plate heat exchanger and waste heat boilers.

Table 2.2 shows the amount of waste heat released from the industries in different regions. It is found that majority of the waste heat dissipated by United States region is low temperature while for China region, almost half of the waste heat released is low temperature of less than 150 °C from the chosen industries. As for European Union region, only approximate 30% of waste heat released is low temperature.

Table 2.2: Statistics of Waste Heat in US, China and EU (Xu, Wang and Yang, 2019).

<b>Region</b>	<b>Industries</b>	<b>Waste Heat Released</b>
<b>United State</b>	Metal, Aluminium, Glass, Cement, Iron and Ethylene.	1.56 EJ waste heat released every year. Approximate 60% of waste heat is less than 230 °C.
<b>China</b>	Glass, Iron and Cement.	1.8 GW, 2.9 GW and 41 GW waste heat released respectively. 0.8 GW, 1.9 GW and 20 GW of waste heat is with temperature below 150 °C.
<b>European Union</b>	Non-ferrous Metal, Chemical, Iron, Food and Beverages, Paper and Printing.	300 TWh of waste heat released every year. Approximate 30% of waste heat is less than 200 °C.

Table 2.3: Summary Table of Current Waste Heat Recovery Technologies (Jouhara et al., 2018).

<b>Technologies</b>	<b>Temperate Range</b>	<b>Usage/Benefits</b>
<b>Piezoelectric Power Generation</b>	Low	Generates electricity from ambient vibration from oscillatory gas expansion.
<b>Heat Pump</b>	Low, Medium	Improve energy efficiency of the system by recovering heat from several sources using heat sink.
<b>Economisers</b>	Low, Medium	Preheating liquids entering a system using heat from waste flue gas to increase the thermal efficiency.

<b>Rotary Regenerators</b>	Low, Medium	Provides high heat transfer efficiency.
<b>Recuperators</b>	Low, Medium, High	Preheating inlet air to the system to decrease energy demand.
<b>Thermo Photo Voltaic (TPV) Generator</b>	Low, Medium, High	Directly generate electricity from radiant energy with high efficiency.
<b>Waste Heat Boilers</b>	Medium, High	Generate steam from exhaust gases with moderate to high temperature.
<b>Regenerators</b>	Medium, High	Commonly used in coke ovens, furnaces and exhausts.
<b>Run around coil (RAC)</b>	Medium, High	Separate two flow sources and transfer heat from the source to recuperator.
<b>Plate Heat Exchanger</b>	Medium, High	Transfer heat through fluid without mixing.
<b>Heat Pipe Systems</b>	Medium, High	High thermal conductivities of the heat pipe reduce the temperature drop during heat transfer. Does not require maintenance due to passive operation. Operation costs is lower as compared to other heat exchangers.
<b>Direct Contact Condensation Recovery</b>	Medium, High	The transferring of heat is done using heat exchanger with direct. It acts as a filter to eliminate the mixing of flue gas and water from medium of solid – liquid or solid – gas and immiscible liquid – liquid.
<b>Indirect Contact Condensation Recovery</b>	Medium, High	Act as a filter of a process and avoid mixing of flue gas and water.
<b>Transport Membrane Condenser</b>	Medium, High	Capillary condensation channel is used to deliver hot water from exhaust gas to system feed water. Water is not obtained from flue gas directly so there is no mixing and filtering is not needed.

<b>Heat Recovery Steam Generator (HRSG)</b>	High	Steam is generated for heating process in power generation or factory from waste heat at the exhaust of manufacturing plant or power-station to increase the efficiencies.
<b>Thermionic Generator</b>	High	Generate electricity from difference in temperature between two mediums.
<b>Regenerative Burners</b>	High	Preheat the combustion air to save fuel and improve combustion efficiency.
<b>Recuperative Burners</b>	High	Increase the amount of heat at the nozzle by absorbing waste heat from burner nozzle's body.

### 2.5.1 Low Temperature Waste Heat

Waste heat of low temperature can be recaptured directly using recuperator, convection, waste heat boiler, passive air preheater, radiation, economizer and plate heat exchanger. It has lesser option as compared to higher temperature range of waste heat recovery and most common method of low temperature waste heat recovery is for the usage of domestic heating directly.

The utilisation of low-temperature waste heat recovery is constrained by low degree of temperature such as insufficient customer demand and low efficiency of the conversion of low-temperature waste heat into electricity.

In 2020, the food and beverage industry accounts for 11.9% of the overall energy consumption demand in Europe (Eurostat, 2020). Food and beverage industry is one of the largest manufacturing sectors in Europe where it consists of 294000 companies (FoodDrinkEurope, 2019). Low temperature waste heat is commonly found in food and beverage industry as most of the processes during production has temperature range between 40 – 120 °C excluding heat intensive process such as cooking and baking. Table 2.4 shows the list of typical processes along with their temperature ranges in food and beverage industry. There is a huge potential in recovering waste heat into valuable energy in this industry by using TEGs.

Table 2.4: Typical Processes and Temperature Ranges in Food and Beverage Industry (Fluch, Brunner and Grubbauer, 2017).

Waste Heat Sources	Temperature Range (°C)
Pasteurisation / Sterilization	70 - 120
Distillation	40 - 100
Drying	40 - 250
Evaporation	40 - 170

Figure 2.4 and Figure 2.5 show some examples of the hot surface of the machines where waste heat can be obtained. TEG can be placed on the surface to generate electricity from waste heat to power up small IoT device.



Figure 2.4: Cooker of Rice



Figure 2.5: Cooker of Instant Noodle.



### **2.5.2 High Temperature Waste Heat**

Because of high energy content, high-temperature waste heat is more manageable to recapture than low-temperature waste heat and able to satisfy customer need with a variety of temperature requirements. With existing technology including organic Rankine cycle or steam turbine, high-temperature waste heat has higher potential to be utilised to generate electricity.

## **2.6 Application**

There are various applications of TEG to convert waste heat into electrical energy in the industry including transportation, consumer products and production plant. The common usage of TEG in transportation is at the exhaust system of the automobile, aircraft and ships whereas for consumer products is watch that absorb the heat from human skin. Similarly, TEG is applicable to most of the industry where the waste heat is released as by-product from the operation of the production process.

TEG is essential to the evolution of Industry 4.0 and Internet of Things as it allows the smart devices to operate completely wireless. This unlocks the limitation to place smart devices in hard-to-reach area and facilitate the installation process that placing the devices on top of the hot surface will power up the devices.

### **2.6.1 Industry 4.0 and Internet of Things (IoT)**

Wireless devices such as sensors, RFID and wireless communication are the key components to build a powerful industrial system to increase the overall effectiveness of industry operation by sharing real-time data (Manavalan and Jayakrishna, 2019). Moreover, several manufacturing site can be connected together using internet and cloud to form a digital supply chain line (Hazen et al., 2016). In order to achieve seamless connectivity, wireless sensor networks (WSNs) that interlink all the sensors is a crucial technology to be implemented in the industry (Belli et al., 2019). This is because a wireless system provides better reliability and flexibility which is capable of supporting the emerging technologies of Industry 4.0 as well as IoT. In terms of reliability, wireless connectivity eliminates the need of cable which the cable may fail due to aging or disconnection of the wire and leads to interruptions of the operations. For the

flexibility, wireless devices can be relocated easily during reconfiguration, layout alterations of the factory floor plan and reduce the downtime significantly during the upgrade.

Industry 4.0 aims to build a more intelligent factory with self-learning machines that collect data from all the sensors and make improvements. As a result, the productivity of the factory will increase as the operations become more efficient and less resources are wasted. Therefore, large number of sensors as well as small devices will need to be installed at most of the spots around the machines to provide real-time data to the control centre for interpretation. Then, the control centre will send out command to adjust the operations of the machine accordingly.

Furthermore, sensors such as temperature sensor, vibration sensor, voltage sensor and current sensor can be installed to the machine to detect the early sign of malfunction. Unplanned downtime of a manufacturing production line due to broken machines is critical to the companies. The company may suffer big losses and endangered the workers from malfunctioned machines.

### **2.6.2 Medical Devices**

The heat released from humans' body is a continuous energy that can be effectively utilised in producing power for implanted medical devices (IMDs) as well as wearable devices, providing variety of applications including sports and fitness wearable devices, health monitoring and tracking system and more (Wahbah et al., 2014). These medical devices are used in hospital or at home to monitor the overall analysis of the patient and they are able to deliver stable connection as the power is generated from the heat of the body that ranges from 27 °C to 35 °C varying on the conditions of the body and environment (Proto et al., 2018). Especially for implanted medical devices (IMDs), TEG is the perfect replacement for the battery to eliminate the need for maintenance of the device, which is replacing old batteries that may consume time and cost for surgery. Additionally, when rechargeable batteries are used, it possesses a risk of battery failure which may harm the patient when battery malfunction. Figure 2.6 and Figure 2.7 shows the medical devices which can be integrated with TEG to produce electricity from using body heat.



Figure 2.6: Electroencephalography (EEG) Headband (CMP (Firm), Institute of Electrical and Electronics Engineers. and Components, 2009).



Figure 2.7: Electrocardiography (ECG) Shirt (Leonov, 2013).

### 2.6.3 Wearable Devices

The working principle of TEG powered watch is the same as the medical devices that use body heat to generate electricity. Figure 2.8 shows the end product of TEG powered smartwatch, named PowerWatch, is available on the market. The watch uses body heat and ambient light to generate power and it claims that it can last forever without charging (PowerWatch, n.d.). However, there is some limitation where the battery cannot charge from the body heat if the ambient temperature is above 32 °C. This is because the difference in temperature between ambient temperature and body heat is too small. Hence, it may not be suitable for consumers who stay at hot climate countries.



Figure 2.8: Matrix PowerWatch Powered by TEG and Body Heat (Tech4All, n.d.).

#### 2.6.4 Automotive

The automotive industries are looking for an alternative power source to increase the efficiency of internal combustion engine to reduce fuel energy cost. Therefore, TEG is attracting much interest from the manufacturers (Espinosa et al., 2010; Mostafavi and Mahmoudi, 2018; Crane and Lagrandeur, 2010; Sofyan et al., 2020; Cao, Luan and Wang, 2018a; Haidar and Ghajel, 2001; Yang, 2005; LaGrandeur et al., 2006). Based on the study, it is found that only 25% of the energy output from the engine is used to drive a passenger vehicle as well as accessories while 40% of the energy output is wasted in the form of exhaust gas (Espinosa et al., 2010; Crane and Lagrandeur, 2010; LaGrandeur et al., 2006). The temperature of the exhaust system ranges from 100 °C to 800 °C and it varies with the fuel category and vehicle speed (Yang, 2005). Due to this, a cascaded TEG was built that consist of two material which is  $\text{Bi}_2\text{Te}_3$  for temperature of 220 °C and  $\text{Mg}_2\text{Si}_{0.4}\text{Sn}_{0.6}/\text{MnSi}_{1.81}$  for temperature of 410 °C, and it managed to produce 2.5 kW of electrical power (Wilbrecht and Beitelschmidt, 2018). In addition, heat released from the radiator ranges from 90 °C to 105 °C and has the temperature difference of around 70 °C between the radiator and atmospheric air which is enough for TEG to produce electricity. It is found that with engine loads at 25%, the power produced by  $\text{Bi}_2\text{Te}_3$ -based TEG is over 1 kW (Crane, Jackson and Holloway, 2001). Figure 2.9 shows the set-up of TEG on automobile exhaust.



Figure 2.9: Heat Exchanger Subassemblies of Automobile Exhaust (Meisner, 2010).

### 2.6.5 Aerospace

Structural health monitoring (SHM) systems involve in wireless data transmission between sensors nodes and central base station are being used in an aircraft. The sensor nodes can be powered up by both piezoelectric transducers and TEG from the vibration and thermal gradients respectively. The study found that with peak temperature differential of  $10\text{ }^{\circ}\text{C}$  to  $40\text{ }^{\circ}\text{C}$ , peak power of  $5.46\text{ mW}$  to  $30.06\text{ mW}$  was obtained at several locations of the aircraft (Pearson et al., 2012). Figure 2.10 shows the potential locations of TEG to be used in an aircraft.

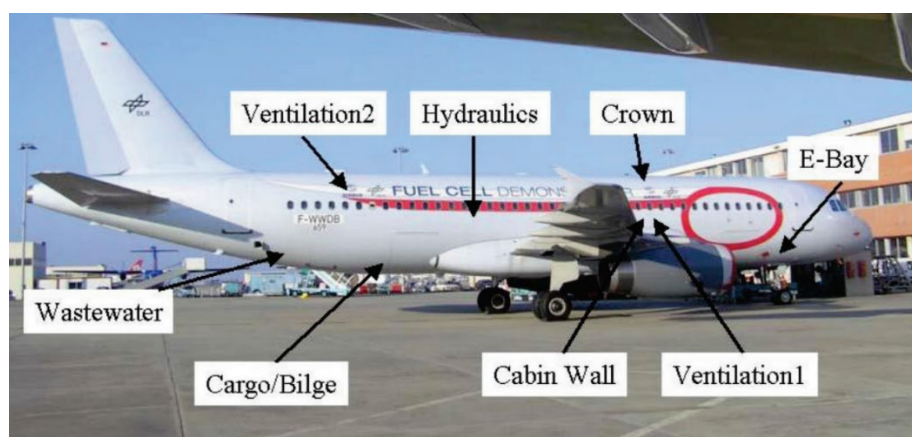


Figure 2.10: Locations of TEG Used on an Aircraft (Pearson et al., 2012).

Moreover, TEGs are used in Radioisotope Thermoelectric Generators (RTGs) to generate electricity from the heat produce by natural decay of radioactive materials. It is commonly used in space crafts, space probes, and satellites where combustion is not possible due to limited oxygen at the space.

## 2.7 Heat Sink

Heat sink is used to dissipate the heat from the cold side of TEG module and the thermal performance is crucial to cool down the TEG module as much as possible to achieve maximum temperature gradient. There are various type of heat sinks available with different geometry and all of them have different cooling efficiency. It was found that the heat transfer rate of the heat sink with thinner base is higher. The minimum temperature achieved is decreasing when the fins height of the heat sink is increasing. It was also found that aluminium heat sink dissipate heat faster than copper heat sink despite copper has higher thermal conductivity (Ekpu et al., 2011).

## 2.8 Efficiency of TEG

The efficiency of the TEG system used in automobiles range from 5.35% to 1.03% and the details are listed in Table 2.5. The cold side of the TEGs were cooled by the wind from the moving of vehicles. When the vehicles are moving at higher speed, the TEGs can be cooled down more effectively and thus, increasing the efficiency. For this application, different method was used to cool down the TEG modules as compared to this project. Therefore, the data are not suitable to be benchmarked with the experiment in this study. However, the data can be used as a reference.

Table 2.5: Efficiency of Waste Heat Recovery System in Automobiles using TEG.

Authors	Number of TEGs	Type of TEG	Efficiency, $\eta$ (%)
Liu et al., 2016	96	$\text{Bi}_2\text{Te}_3$	5.35
Quan et al., 2018	240	$\text{Bi}_2\text{Te}_3$	1.03
Cao, Luan and Wang, 2018	36	$\text{Bi}_2\text{Te}_3$	2.58

## **2.9 Air Flow of Fan**

Air flow of the fan is important to ensure equal cooling effect on all of the heat sinks. Simulation on the air flow of the fan can be done to analyse the direction of the air flow coming out of the fan. Further modification on the fan can be done to improve the air flow of the fan such as using guide fins to alter the directions of the air. According to previous study, the air flow of the axial fan has increased up to 6.3% with the use of guide vane (Saeidi and Taheri, 2020). The total efficiency of the fan has been increased with the reduction of swirl energy as well as the improvement on static pressure. Computational Fluid Dynamics (CFD) software can be used to simulate the air flow of the fan and make improvement accordingly. Some examples of CFD software are Ansys Fluent and SolidWorks Flow Simulation.

## **2.10 Summary**

To sum up, TEG has been evolving rapidly for the past few years as the global industries is approaching to Industry 4.0 that focus on automation and IoT 4.0. The current development progress of TEG was discussed along with the working principles. TEG can be categories into 3 group which are low temperature, medium temperature and high temperature. Each group works on different temperature ranges based on the applications of TEG to be used in.

The type of waste heat to be recovered was also analysed to discover possible application of TEG. As mentioned above, the current rate of waste heat recovery especially for low-temperature is relatively low and has limited recovery options due to low grade heat energy. Further research can be carried out to improve the situation and apply TEG into the industries with its wide temperature range of applications.

TEG has been applied widely in several industries mentioned above including manufacturing, medical, consumer products, automotive, and aerospace industry. This is because it has the potential to replace the battery and generating electricity from heat source which leads to lower maintenance cost and higher reliability.

## CHAPTER 3

### METHODOLOGY AND WORK PLAN

#### 3.1 Introduction

This chapter discussed about the design of the prototype and the approach to build and construct it. Several trials were expected to determine the final configuration of the prototype to ensure that the power generated by TEG was sufficient to power up the small IoT device which is an Arduino module.

A flowchart as shown in Figure 3.1 was developed to visualise the overall activities in sequential order to ensure smooth progress throughout the project flow. Problem statements were identified and research was carried out before planning of the project. At planning stage, theoretical calculation was done to design the prototype. After planning, experiment 1 was carried out to measure the efficiency of the equipment and materials used. If the result for experiment 1 was satisfied, the prototype is built and tested in experiment 2. Else, the process starts over at the planning stage to substitute with a better equipment or material. Then, the data from the result were collected by measuring the power output from the prototype. If the result was not satisfying, the process starts over at planning stage to collect more information and improve the design of the prototype until the result is satisfied. Lastly, overall results were collected to carry out the discussion. Conclusion of the project was documented together with recommendation to suggest further improvements on the project for future works.



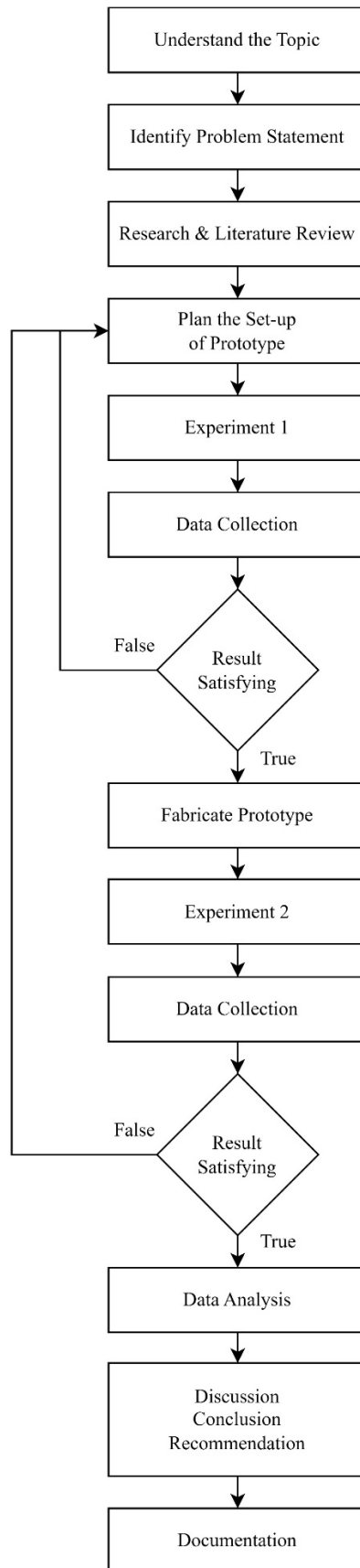


Figure 3.1: Flowchart of the Building of Prototype.

## 3.2 Equipment and Material

The Table 3.1 and Table 3.2 shows the required equipment and materials to build the prototype as well as to conduct the experiments.

Table 3.1: Equipment Required for the Experiment.

Equipment	Qty
TEG Module	16
Heatsinks	16
Fan	1
Step-down Power Module	1
Arduino Module	1
DHT11 Humidity and Temperature Sensor	1
Heating Bed	1
Soldering Iron Pen	1
Soldering Iron Stand	1
Thermocouple Thermometer	1
Temperature Controller	1
Multimeter	2

Table 3.2: Materials Required for the Experiment.

Material	Qty
Soldering Iron Wire	1
Thermal Conductive Paste	4
Wire	1
Aluminium Plate	1

Subsections below discuss the types of equipment and materials used and the reasons for each selection. Several types of TEG module, heat sink and thermal conductive paste were listed out and were compared in experiment 1 to verify their efficiency.

### 3.2.1 Thermoelectric Generator (TEG) Module

TEG module is the main component of the prototype that can produce electricity from the temperature difference between two faces of the module. Three types of TEG modules were used in this project to compare their efficiency and power output. Three of them are having same type of semiconductor material which is

Bismuth Telluride alloy-based, best material for thermoelectric generation at low to medium temperature to date (Goldsmid, 2014). However, their performance is varied by the surface material, density of semiconductor inside the TEG module as well as the manufacturing process. Moreover, they have different maximum operating temperature from various construction of the module such as soldering material.

The first TEG module used was SP1848-27145 as shown in Figure 3.2. The surface material is made up of Aluminium Oxide ceramics that is thermally conductive on both sides of the module. It can withstand maximum temperature of up to 120 °C. This model is designed dedicated for power generation that the gap between hot side and cold side is sealed for maximum Seebeck effect as well as moisture protection. The dimension for this model is 40 mm × 40 mm in width and length respectively with thickness of 4 mm.

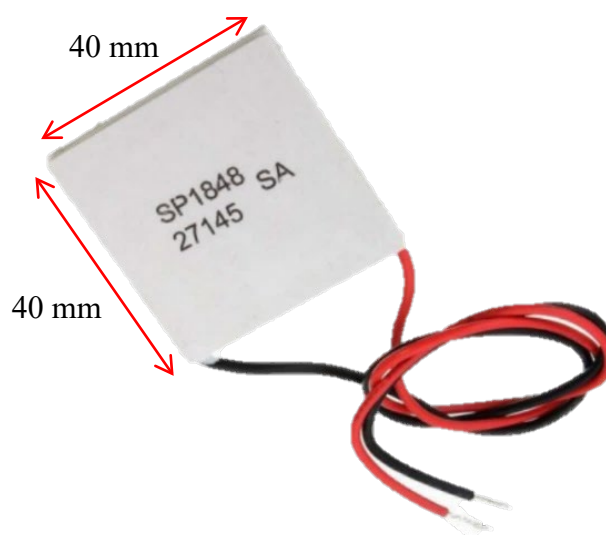


Figure 3.2: SP1848-27145 TEG Module.

The second TEG module used was TEC1-12730 as shown in Figure 3.3. The surface material is made up of Aluminium Oxide ceramics that is thermally conductive on both sides of the module. It can withstand maximum temperature of up to 150 °C. Although this model is designed for refrigeration, it can be used as TEG module to generate electricity using similar method. Similarly, the gap is sealed for maximum Seebeck effect as well as moisture

protection. The dimension for this model is 62 mm × 62 mm in width and length respectively with thickness of 3.9 mm.

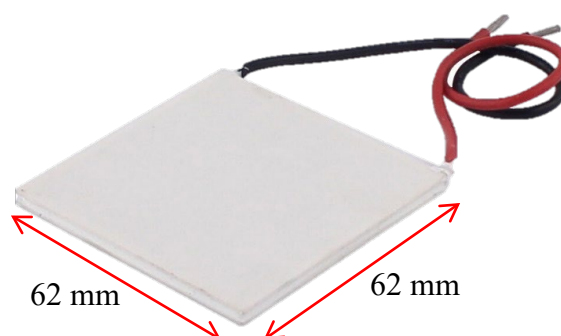


Figure 3.3: TEC1-12730 TEC Module.

The third TEG module used was TEG-127-3.5-2.8T250D as shown in Figure 3.4. The surface material is made up of graphite that has higher thermal conductivity on both sides of the module. It can withstand maximum temperature of up to 200 °C. The gap between the cold side and hot side is not sealed to protect against thermal bridging. The dimension for this model is 40 mm × 40 mm in width and length respectively with thickness of 4 mm.

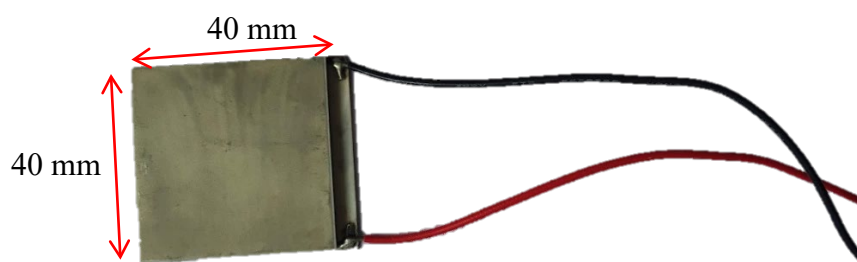


Figure 3.4: TEG-127-3.5-2.8T250D TEG Module.

### 3.2.2 Heat Sink

The material used was aluminium due to its good thermal conductivity to transfer heat than iron or steel. Although copper has better thermal conductivity than aluminium, aluminium is more cost effective, and it can dissipate heat considerably well. Heat sink with higher and more fins was selected. This is because the surface area can be increased to release heat at a faster rate.

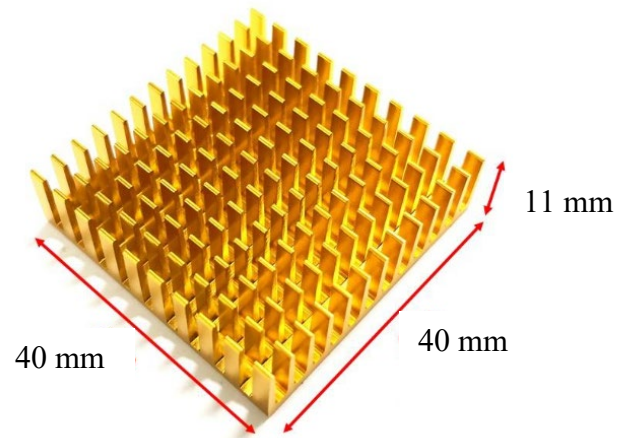


Figure 3.5: Aluminium Heat Sink With 11 mm Fins.

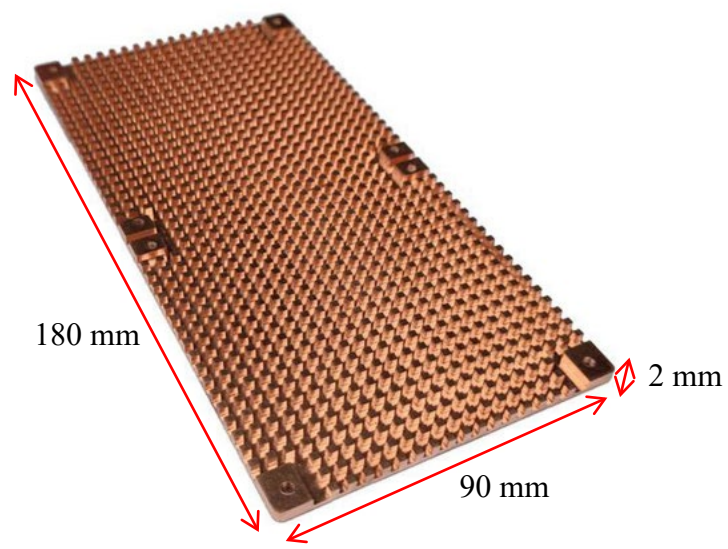


Figure 3.6: Copper Heat Sink With 2 mm Fins.

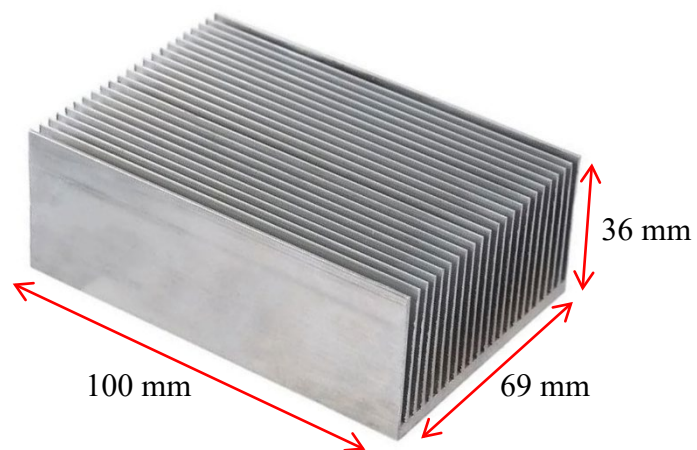


Figure 3.7: Aluminium Heat Sink With 36 mm Fins.

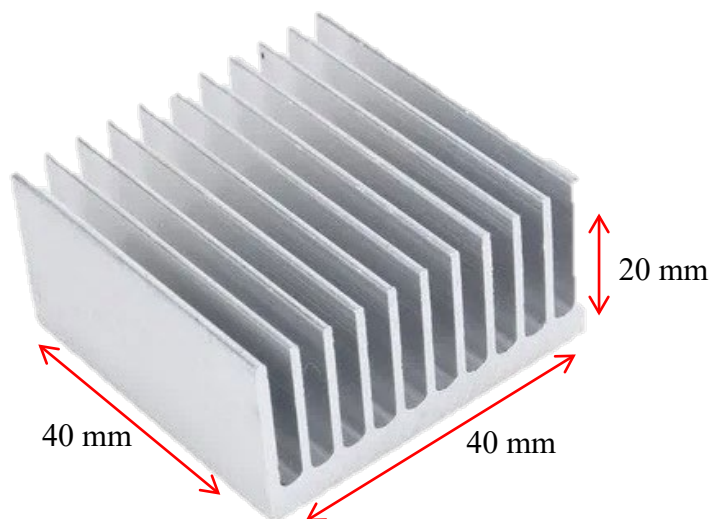


Figure 3.8: Aluminium Heat Sink With 20 mm Fins.

### 3.2.3 Electric Fan

Active cooling was used to cool down the heat sinks. Fan was introduced to create forced air flow onto the heat sinks to increase the heat dissipation. However, the power consumed by the fan was the load of TEG and additional TEG modules were needed to overcome the extra load.

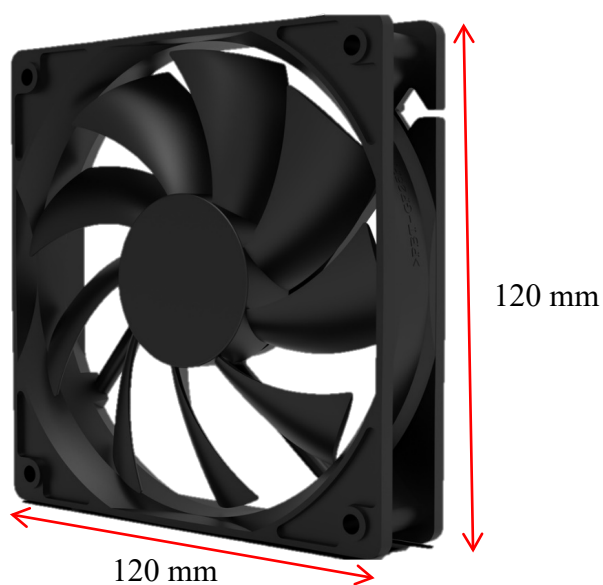


Figure 3.9: Electric Fan 5 V 0.15 A.

### 3.2.4 Aluminium Plate

Aluminium plate was used as the heat exchanger to transfer heat from the heating element to the TEG modules evenly. Aluminium is an excellent thermal conductor and able to transfer heat at a faster rate than iron or steel. The thickness of the aluminium plate used was 2 mm as it can be heated up rapidly and withstand the load of TEG modules and heat sink without bending.

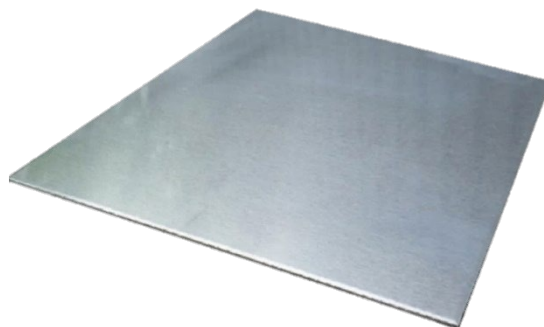


Figure 3.10: Aluminium Plate.

### 3.2.5 Thermal Conductive Paste

Thermal Conductive Paste was used to improve the thermal coupling between two metal components to allow efficient heat transfer by filling the air gaps between the two surfaces. This is because these metal plates have microscopic imperfections which can cause the two metals to not entirely in contact with each other and cause poor heat transfer. It is preferred to select the thermal conductive paste with higher thermal conductivity in order to ensure maximum heat transfer rate between the two surfaces. However, there is a trade-off for high thermal conductivity which is liquidity where most of the thermal conductive paste with high thermal conductivity has low liquidity. Low liquidity increases the difficulty to apply the thermal conductive paste and tends to create air bubbles which can negatively affects the thermal conductivity.



Figure 3.11: Ice Fusion V2 Thermal Paste With 5 W/m-K Thermal Conductivity.



Figure 3.12: HY510 Thermal Paste With 1.93 W/m-K Thermal Conductivity.





Figure 3.13: HTK-002 Thermal Paste With 0.8 W/m-K Thermal Conductivity.



Figure 3.14: Frost X25 Thermal Paste With 10.5 W/m-K Thermal Conductivity.

### 3.2.6 Insulation

Thermal insulation between cold and hot faces is crucial to create maximum temperature gradient on the TEG module. Therefore, more power is generated from the TEG modules. Metal plate has high thermal conductivity and the heat will be transferred to the cold face of the TEG if the gaps between the TEG modules are not insulated. Table 3.3 shows the type of materials used for insulation. Material with lower thermal conductivity is preferred because it has lower heat transfer rate.

Table 3.3: Insulation Material With Respective Thermal Conductivity.

Material	Thermal Conductivity (W/mK)
PVC Board	0.310
Cork Sheet	0.043
Ethylene Vinyl Acetate (EVA) Foam	0.038



Figure 3.15: PVC Board.



Figure 3.16: Cork Sheet.



Figure 3.17: Ethylene Vinyl Acetate (EVA) Foam.

### 3.2.7 Step-Down Power Module

Figure 3.18 shows DC-DC step-down power module that was used to convert high output voltage from the TEG module to a stable usable voltage of 5 V. It operates in constant frequency and is dedicated for low power devices such as LCD Bias Supply, set-top boxed, networking cards powered from PCI and battery-powered equipment.

The specific module board used has output voltage of 5 V with maximum current load of 5 A whereas the input voltage range from 7 V to 30 V. Both fan and Arduino board are requiring voltage input of 5 V while the voltage generated by the TEG module fluctuates to a great extent around 0 – 20 V depending on the temperature difference. Therefore, this step-down power module is the perfect fit to stabilize the power generated by the TEG module to a constant output voltage of 5 V.



Figure 3.18: DC-DC Step-Down Power Module.

### 3.2.8 ESP32 Arduino Module

Figure 3.19 shows the ESP32 Arduino Module equipped with Wi-Fi and Bluetooth was used as the load that was connected to the output of step-down power module. This module has relatively low power consumption with the input voltage of 5 V.

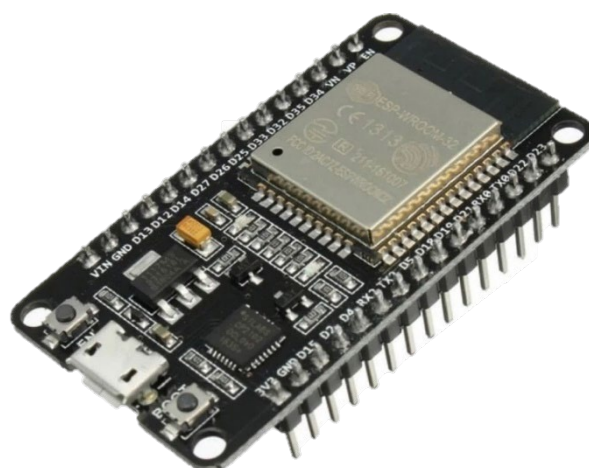


Figure 3.19: ESP32 Arduino Module With Wi-Fi and Bluetooth.

It is a microcontroller with built-in Wi-Fi and Bluetooth with dual mode support as it supports Bluetooth Classic and Bluetooth Low Energy (BLE). It can be operated in extremely low power consumption with the features of power saving such as clock synchronization and different modes of operation. It can be integrated with various sensors including temperature sensor, humidity sensor, infrared sensor, microphone sensor, light sensor, gas sensor and camera depending on the purpose and usage. With these features, IoT system can be implemented by integrating all the sensors and upload the data of the sensors to the cloud.

### 3.2.9 DHT11 Humidity and Temperature Sensor Module

Figure 3.20 shows the DHT11 Humidity and Temperature Sensor Module that was connected to the Arduino module. This sensor has a dedicated negative temperature coefficient (NTC) thermistor to measure the temperature and humidity with an accuracy of 1 °C and 1%. It consists of an 8-bit microprocessor to generate the output data of temperature and humidity which can be read by

the Arduino module. This device was calibrated during production; therefore, it can be used directly by connecting it to the Arduino module.

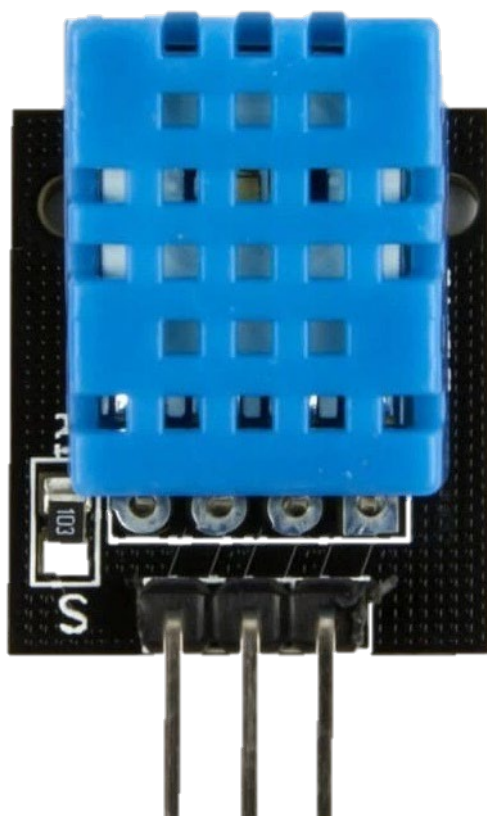


Figure 3.20: DHT11 Temperature and Humidity Sensor Module.

### 3.3 Theoretical Analysis of TEG Module and Load

This section shows the expected power output from a single TEG module and the expected power required by the load. The data of power output by a single TEG module will be used in experiment 2 section to design an appropriate prototype in order to generate sufficient power output as required by the loads.

#### 3.3.1 Theoretical Output of SP1848-27145 TEG Module

Table 3.4 shows the thermoelectric parameter of a single TEG module SP1848-27145 obtained from product datasheet. The output of voltage, current and power are expected from the temperature gradient between both sides of TEG module.

Table 3.4: Thermoelectric Parameter for a Single SP1848-27145TEG Module.

Temperature Difference, $\Delta T$ (°C)	Voltage (V)	Current (mA)	Power (mW)
20	0.97	0.225	0.21825
40	1.8	0.368	0.6624
60	2.4	0.469	1.1256
80	3.6	0.558	2.0088
100	4.8	0.669	3.2112

Figure 3.21 shows the graph of thermoelectric parameter for SP1848-27145 plotted based on the values in Table 3.4. It can be seen that the voltage and current generated increased linearly with temperature difference. Trendlines were added to illustrate the voltage and current produced from temperature difference between 0 to 100 °C. The voltage and current will be produced by the TEG module as soon as there is temperature difference between the cold side and hot side.

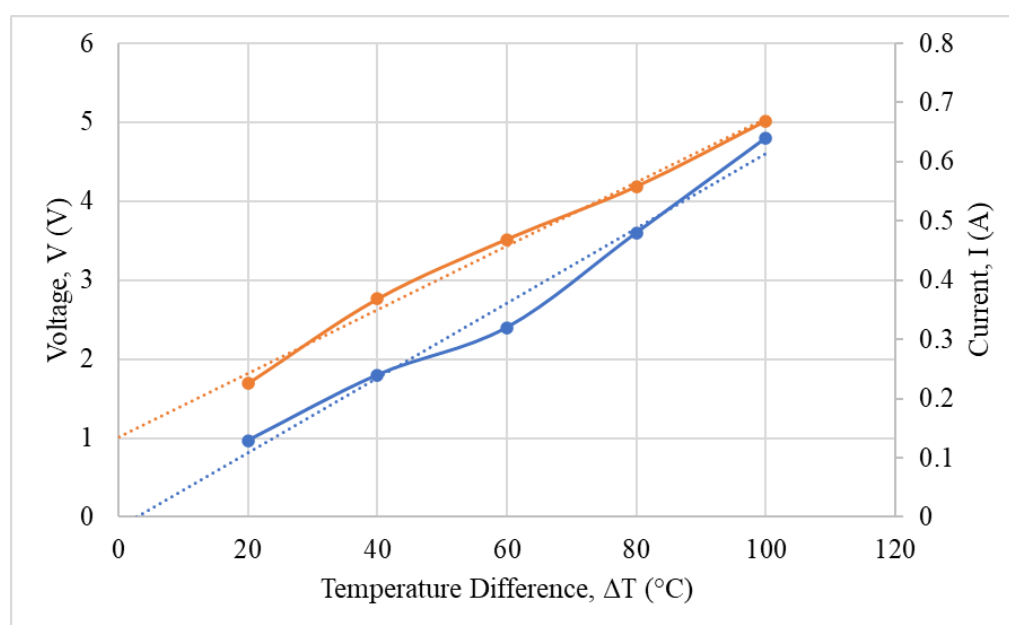


Figure 3.21: Graph of Voltage and Current Produced from Temperature Difference of a Single SP1848-27145 TEG Module.

### 3.3.2 Theoretical Output of TEC1-12730 TEC Module

Since TEC1-12730 is a TEC module which is used for refrigeration instead of power generation, there is no data on expected output when there is temperature

gradient on both sides of the module. Therefore, the experimental data obtained were compared with other TEG modules to analyse the power generation efficiency in experiment 1.

### 3.3.3 Theoretical Output of TEG-127-3.5-2.8T250D TEG Module

Table 3.5 shows the thermoelectric parameter of a single TEG module TEG-127-3.5-2.8T250D. The output of voltage, current and power are expected from the temperature gradient on both sides of the TEG module.

Table 3.5: Thermoelectric Parameter for a Single TEG-127-3.5-2.8T250D TEG Module.

Temperature Difference (°C)	Voltage (V)	Current (mA)	Power (mW)
20	1.7	0.10	0.168
40	2.8	0.18	0.504
60	3.7	0.27	0.999
80	4.5	0.35	1.575
100	5.3	0.43	2.279

Figure 3.22 shows the graph of thermoelectric parameter for TEG-127-3.5-2.8T250D plotted based on the values in Table 3.5. It can be seen that the voltage and current generated increased linearly with temperature difference. Trendlines were added to illustrate the voltage and current produced from temperature difference between 0 to 100 °C. The voltage and current will be produced by the TEG module as soon as there is temperature difference between the cold side and hot side.

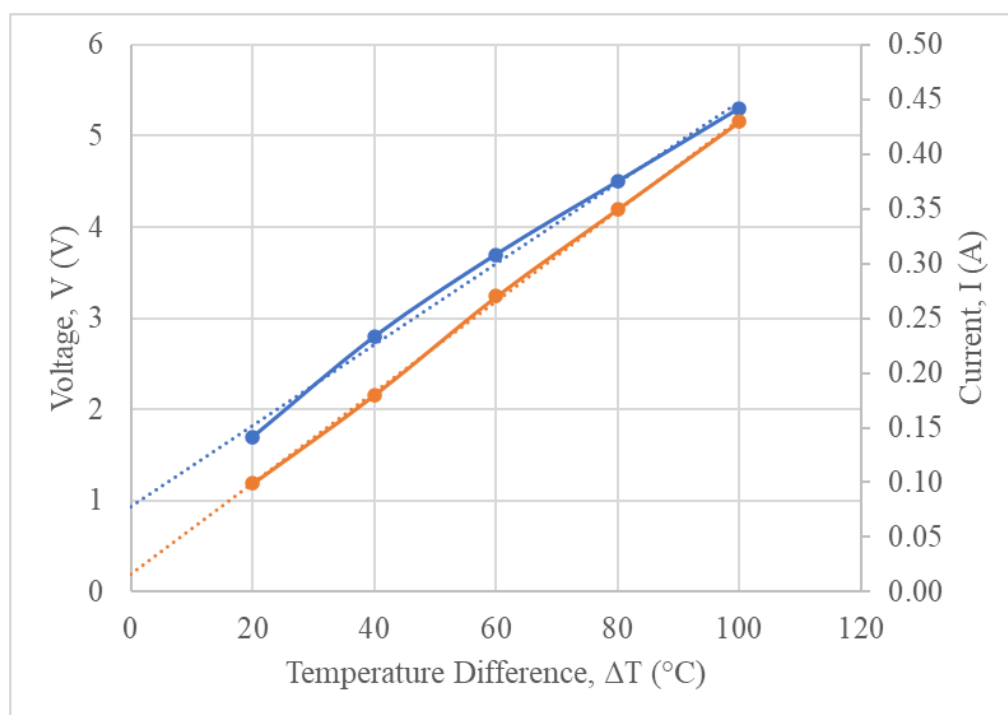


Figure 3.22: Graph of Voltage and Current Produced from Temperature Difference of a Single TEG-127-3.5-2.8T250D TEG Module.

### 3.3.4 Theoretical Loads

The loads that connect to the output of step-down power modules were calculated to determine the power required. The voltage and rated current draw from the fan and ESP32 Arduino Board are listed in Table 3.6 according to the specification sheet of the product. Then, power for each load was calculated and by summing up both power, total power consumption obtained was 1750 mW.

Table 3.6: Calculation of Loads.

Load	Voltage (V)	Current (A)	Power (W)
Fan	5	0.15	0.75
ESP32	5	0.20	1

## 3.4 Methodology

This section discusses about the set-up of the prototype to perform the experiments. The placement of TEG modules and heat sink on the aluminium plate were explained. Moreover, analysis on the air flow by the cooling fan was done to solve the problem encountered during the experiment. Experiment procedures show the steps to build the prototype for experiment 2 while some



of the steps are applicable to experiment 1 which will be discussed in the following section.

### 3.4.1 Methods of Data Collection

Figure 3.23 is the set-up of the TEG module prototype in Solidworks drawing. This was the set-up with only one TEG module and the aluminium plate act as a heat exchanger to transfer heat from heating element to the TEG module evenly. Heating element will be representing the waste heat source in the experiment to heat up the TEG modules. Opposingly, the heat sinks cool down another face of TEG module and create a temperature gradient between two faces of the TEG module. Then, output of voltage and ampere were measured.

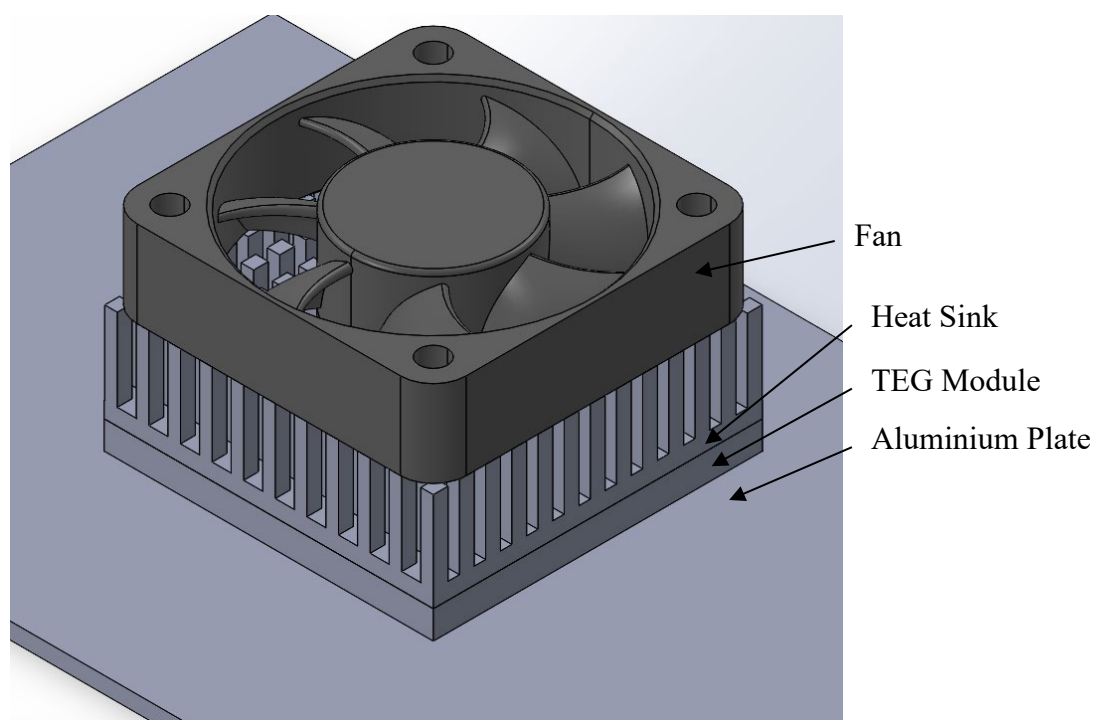


Figure 3.23: Set-up of Single TEG Module.

Subsequently, the number of TEG modules was added for each trial, and they were connected to each other in series to add up the voltage produced by all TEG modules until output power is sufficient to power up the loads. The set-up of multiple TEG Module is shown in Figure 3.24.

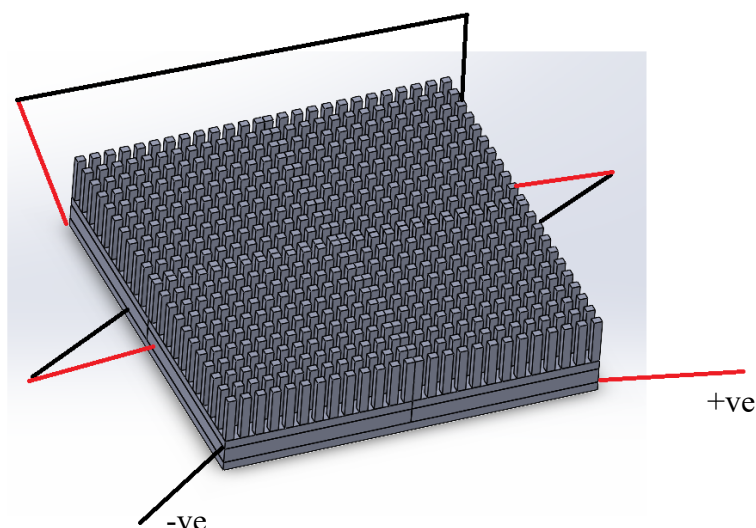


Figure 3.24: Set-up of Multiple TEG Module.

For experiment 1 and experiment 2, the TEG will be heated up until the certain temperature and maintain for 10 minutes before taking the reading of the measurements. This is to ensure that the temperature of the whole prototype has reached equilibrium state. Because the specific heat capacity of each heat sink used is different and may leads to inaccurate result.

### 3.4.2 Air Flow

The air flow produced by the fan is crucial to ensure maximum cooling effect on the heat sink. As shown in Figure 3.25, simulation was done to analyse the direction of air flow coming out of the fan. Due to the design of the fan, the direction of air flow is spreading away from the centre instead of focusing on the centre. Furthermore, there is backflow of air at the centre due to low pressure region created at the centre as there is no air flow coming out from the centre of the fan.

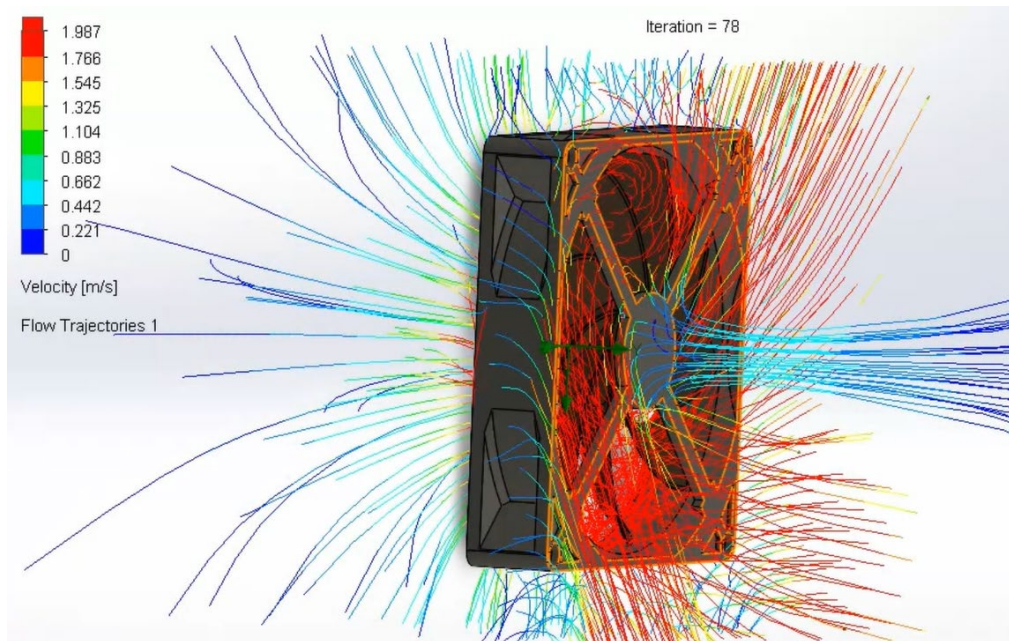


Figure 3.25: Air Flow Simulation of Fan Without Fins.

In order to overcome this problem, curved fins were designed as shown in Figure 3.26 and mounted on the outlet of the fan as shown in Figure 3.27. The fins will guide the direction of the air flow out of the fan to become straight and the curve design will draw some air flow towards the centre of the fan. Therefore, the direction of the air flow is focusing on the centre and creating equal air flow to cool down the heat sink effectively.

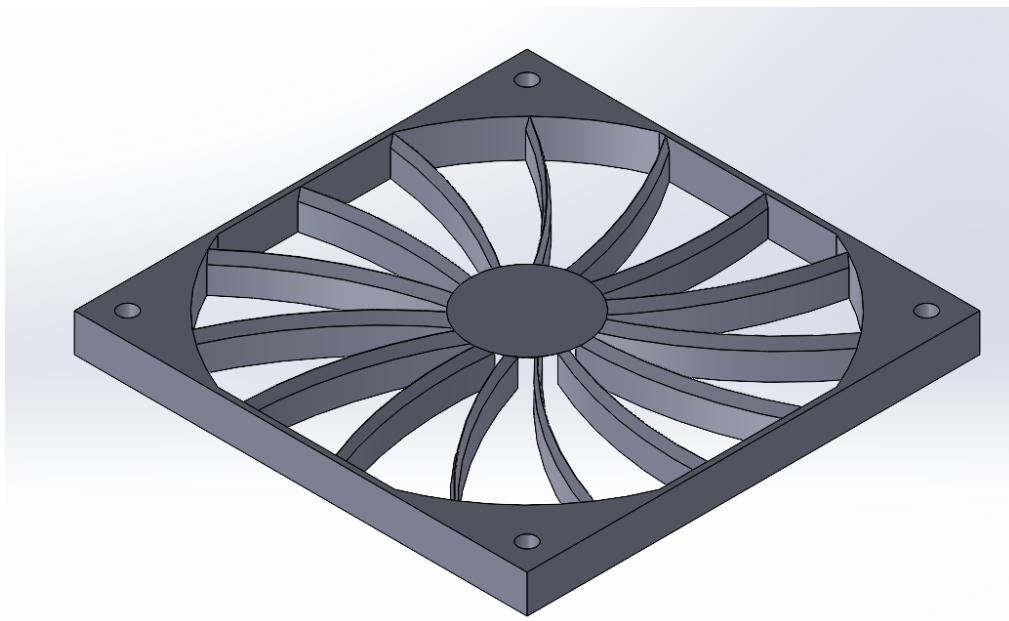


Figure 3.26: Fins for Fan.

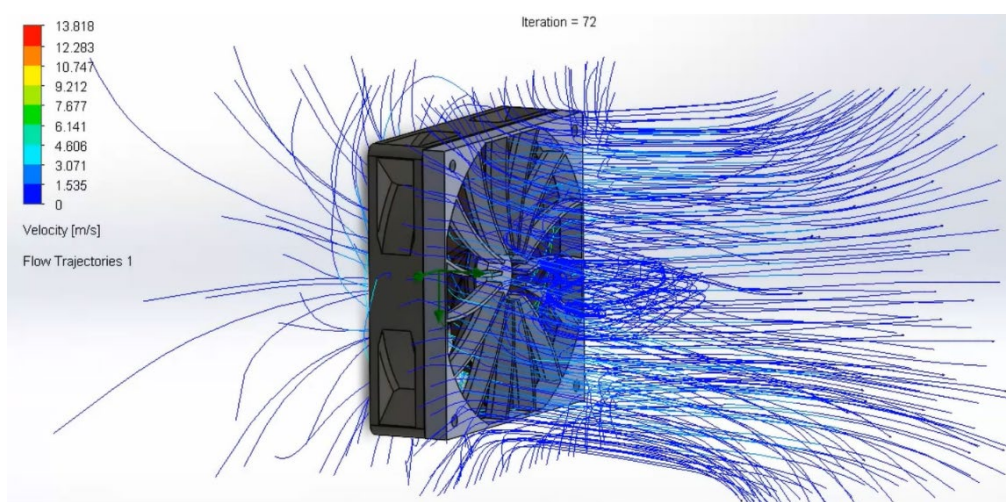


Figure 3.27: Air Flow Simulation of Fan with Fins.

### 3.4.3 Experimental Procedure

This subsection discusses the procedure to build the prototype for each design for experiment 2 in the following section. Firstly, the prototype was designed using SolidWorks. Then, the parts such as clamp and aluminium plate were fabricated in the workshop while the case was printed using 3D printer. Aluminium plate was sanded and degreased to create a smooth surface. Next, thermal conductive paste was applied on the aluminium plate evenly. TEG modules were placed on the metal plate accordingly. Thermal conductive paste was applied on the cold side of TEG modules. Heat sinks were then placed on the TEG modules. Subsequently, the fan was assembled to the case. Thermocouples were placed on the hot side as well as the cold side to measure the temperature respectively. Insulation board was cut and placed on the exposed area of metal plate. Case assembly was placed on top of the heat sink. Afterwards, all TEG modules were soldered together to create a good connection. Step-down power module was soldered to TEG modules, fan and Arduino module. Lastly, ammeter and voltmeter were connected to the circuit. To carry out the experiment, metal plate was heated up to 120 °C. After 10 minutes, the reading of ammeter, voltmeter and temperature were recorded. Figure 3.28 to Figure 3.44 shows the procedures to build the prototype step by step.

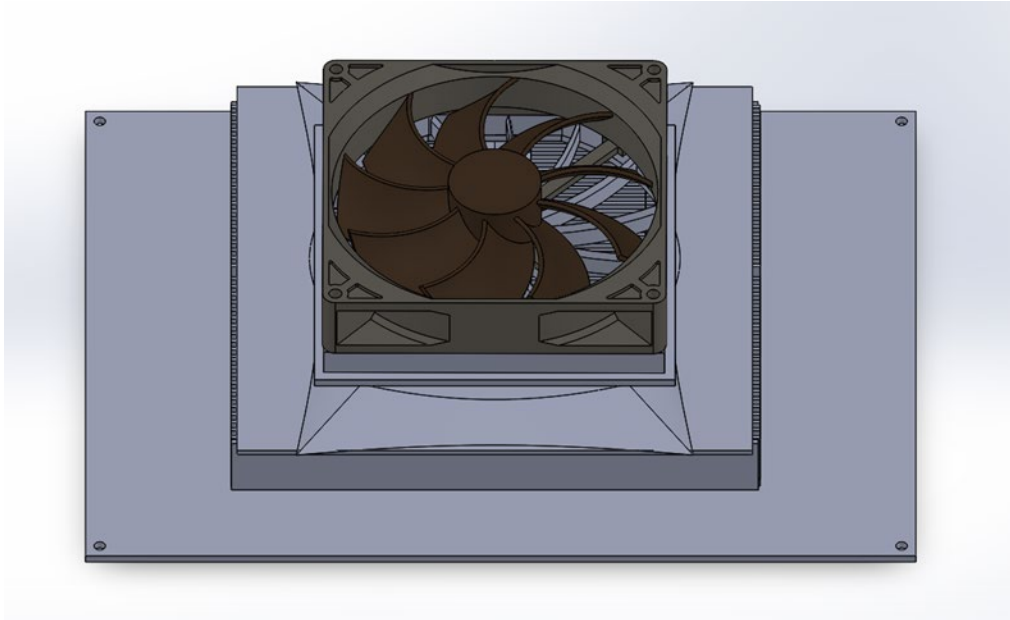


Figure 3.28: Prototype Design in SolidWorks.



Figure 3.29: Fabrication of Metal Plate.



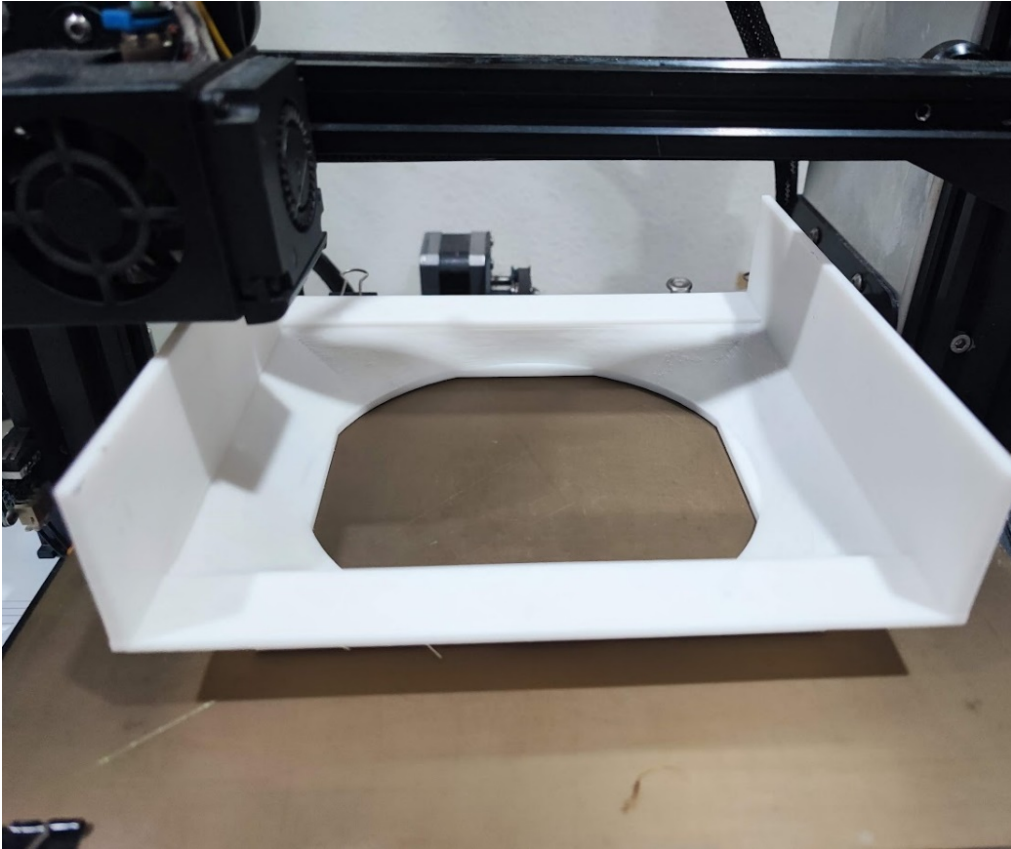


Figure 3.30: 3D Printing of Case.

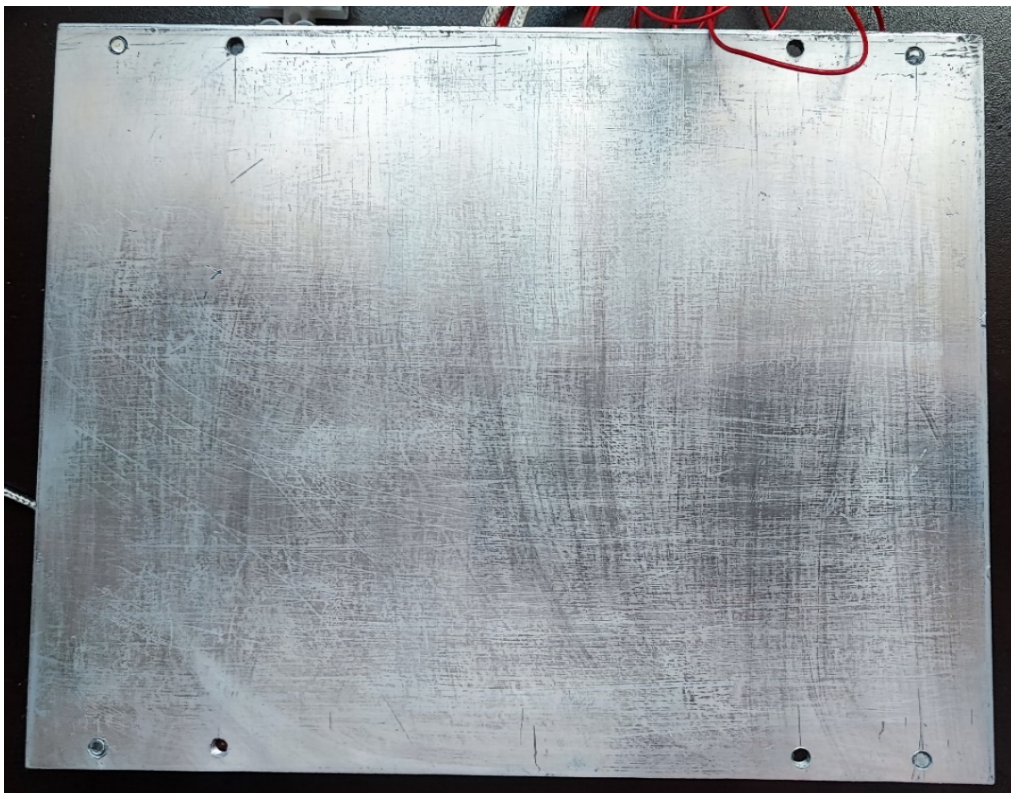


Figure 3.31: Prepared Surface of Aluminium Plate.



Figure 3.32: Aluminium Plate with Thermal Conductive Paste.

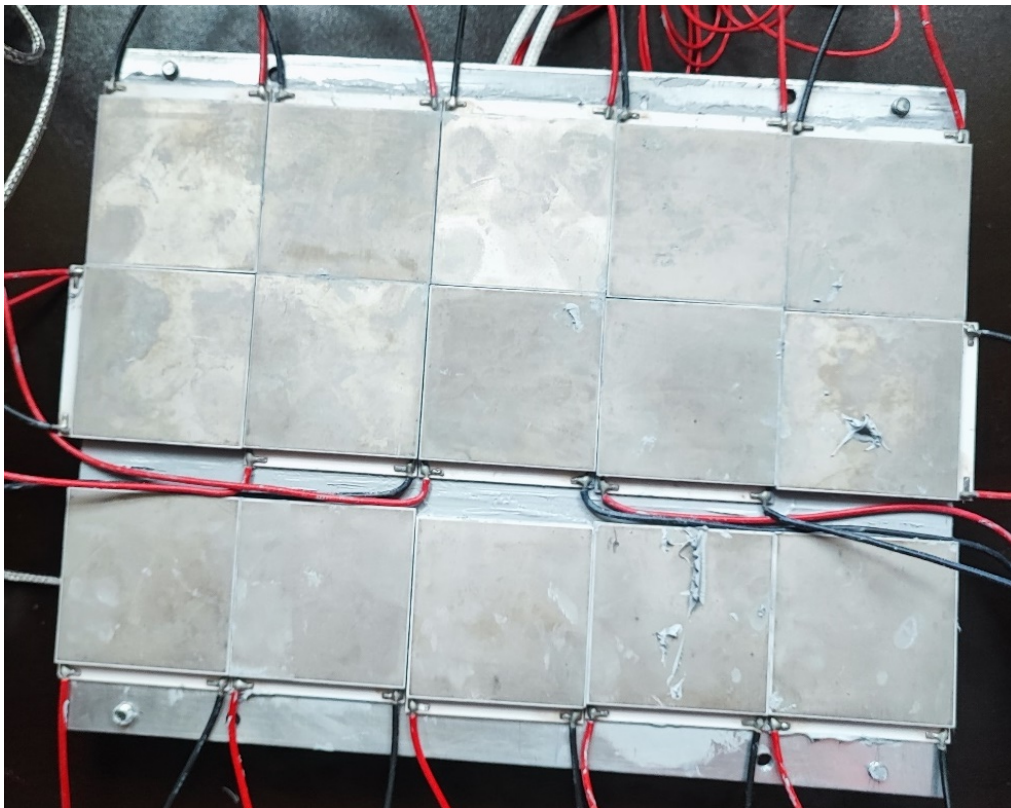


Figure 3.33: TEG Modules on Aluminium Plate.



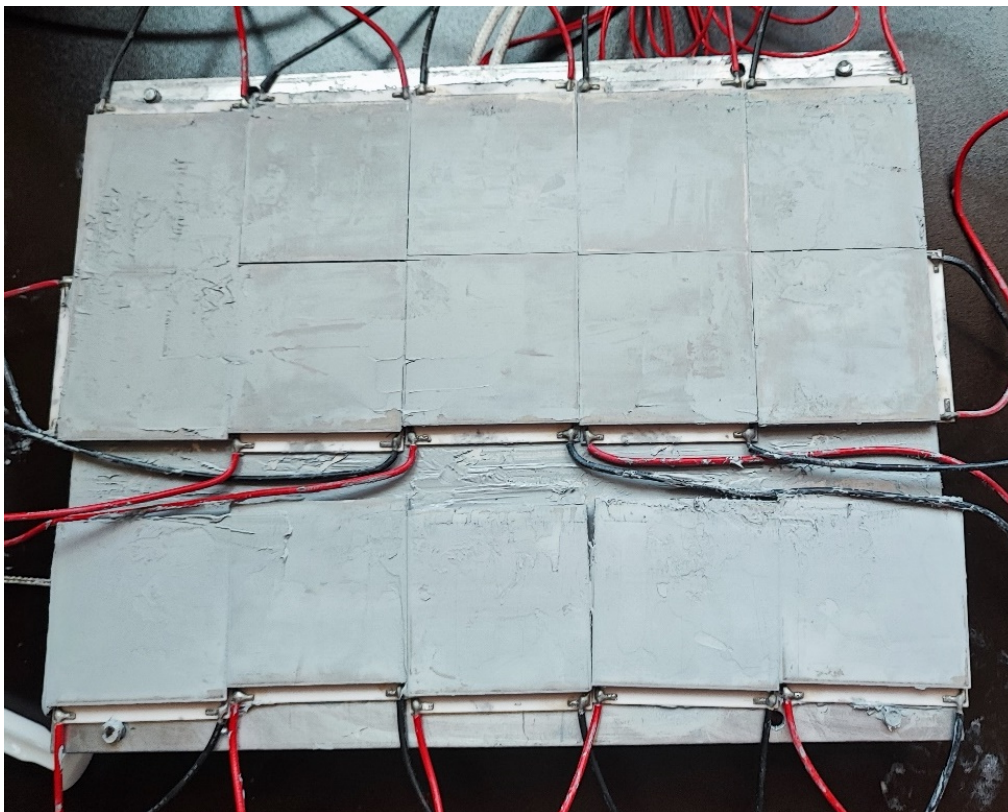


Figure 3.34: TEG Modules with Thermal Conductive Paste on the Cold Side.

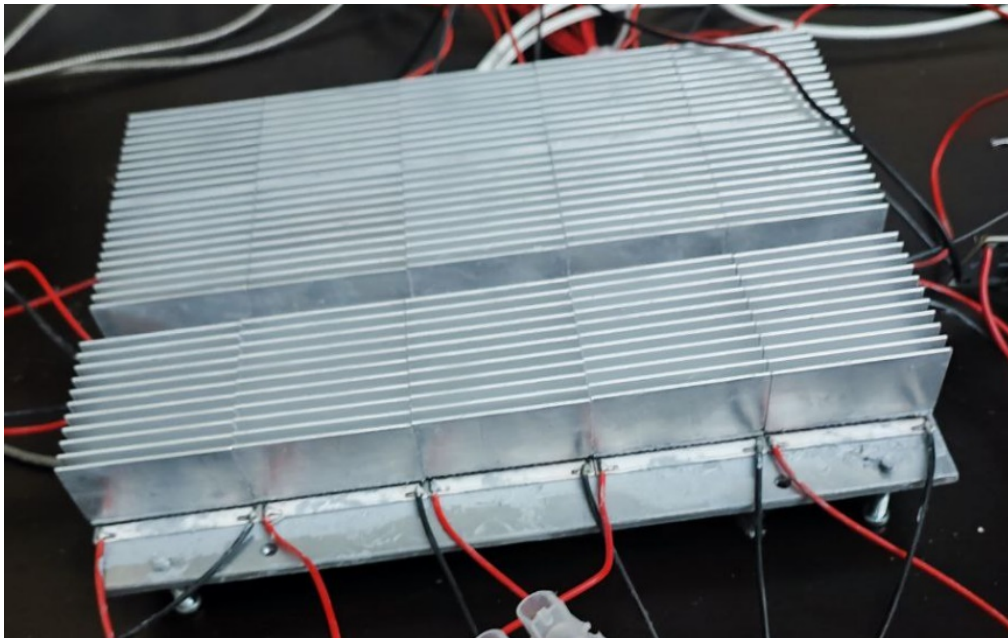


Figure 3.35: Heat Sink Placed on TEG Modules.





Figure 3.36: Case Assembled with Fan.

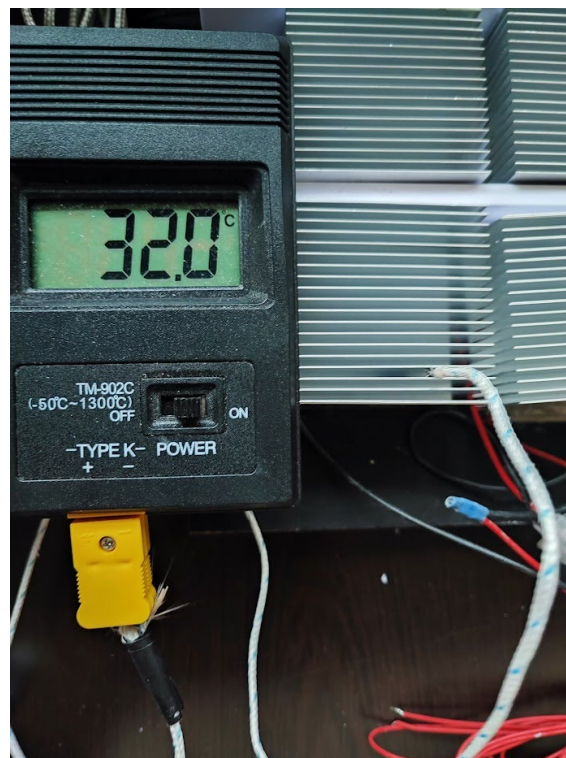


Figure 3.37: Placing of Thermocouples on the Heat Sink.



Figure 3.38: Insulation Board.



Figure 3.39: Fully Assembled Prototype.

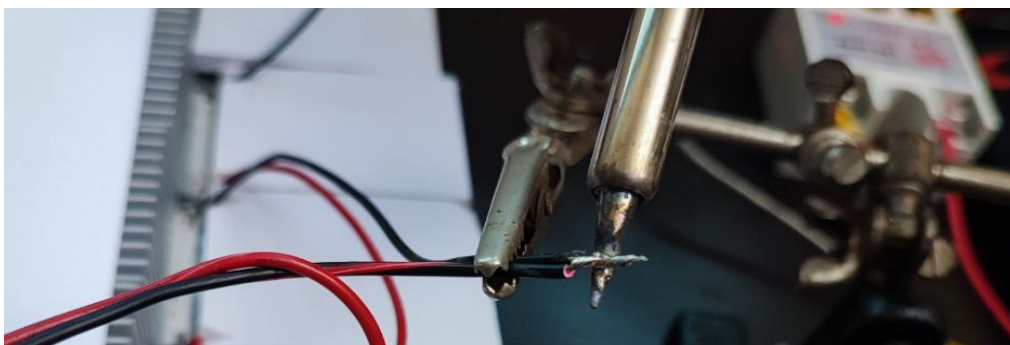


Figure 3.40: Soldering of the Connection of TEG Modules.

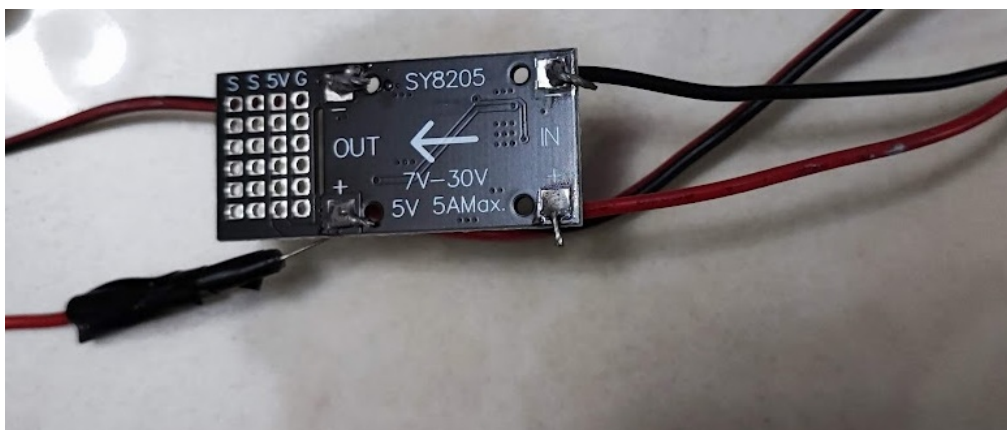


Figure 3.41: Soldering of the Connection of Step-Down Power Module.

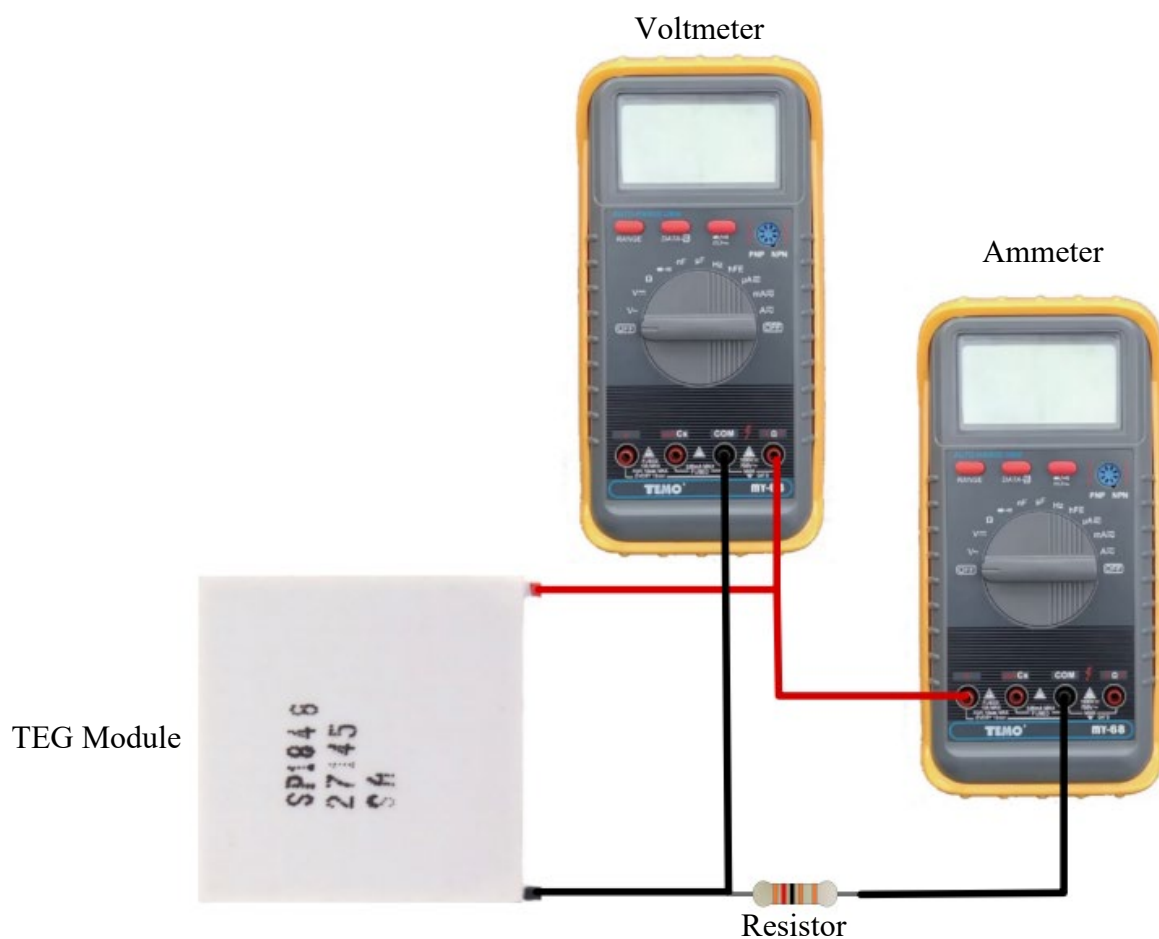


Figure 3.42: Connection of Voltmeter and Ammeter.

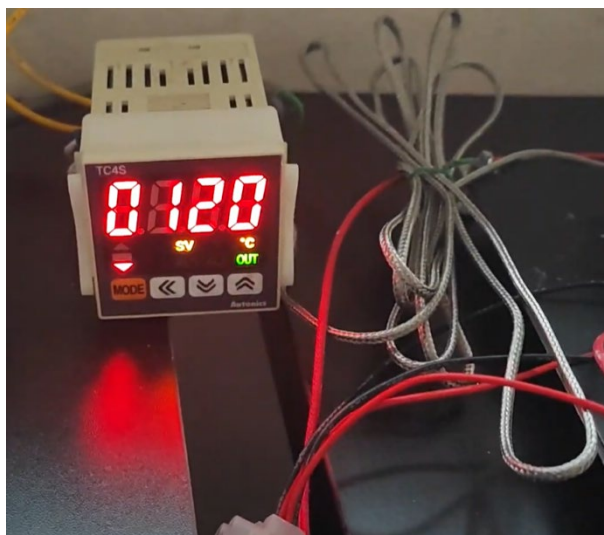


Figure 3.43: Temperature Setting of Heater.



Figure 3.44: Prototype Testing in Experiment 2.

### 3.5 Experiment 1 – Compare Different Type of Heat Sink, Thermal Conductive Paste and TEG Module

This experiment was conducted based on single TEG module set-up as shown in Figure 3.45. The types of heat sink, thermal conductive paste and TEG module were swapped accordingly on each run. The procedures to build the prototype was similar to the steps shown above. The aluminium plate was fabricated and prepared. Then, thermal conductive paste was applied on the both side of TEG module. TEG module was placed on the aluminium plate, followed by the heat sink. A fan was powered from external power source to cool down



the heat sink. The temperature of the heater was set to 80 °C. After 10 minutes, the output voltage of the TEG module was measured and recorded.

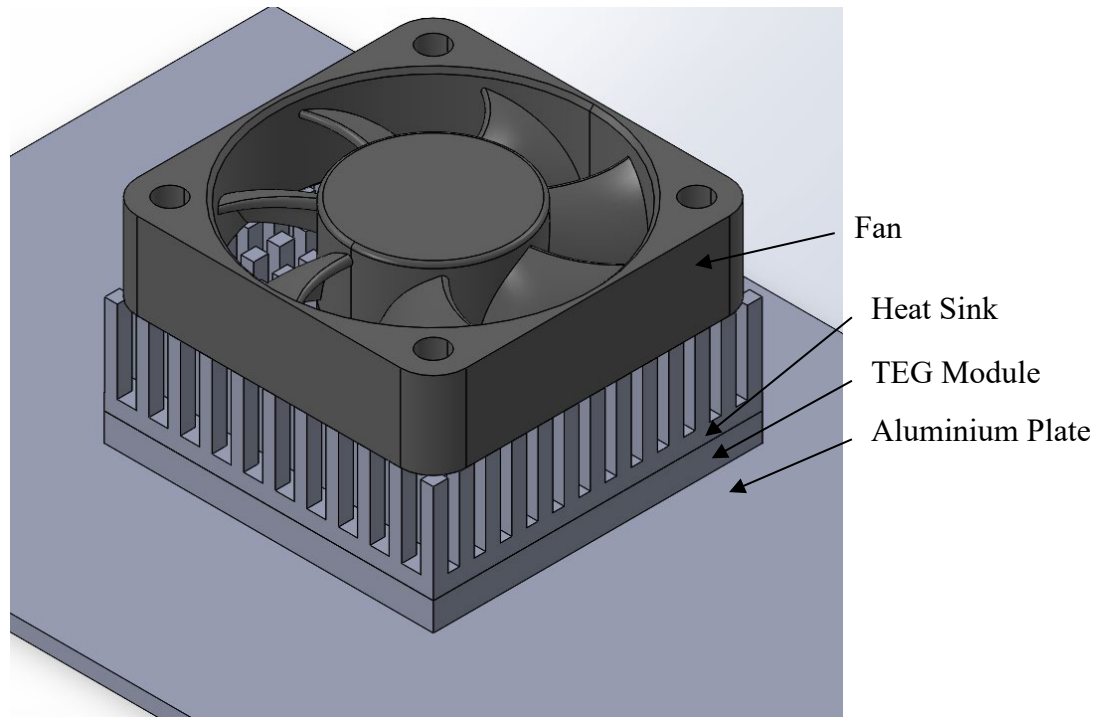


Figure 3.45: Set-up of Single TEG Module.

For the comparison of heat sink and thermal conductive paste, the type of TEG module used was remain unchanged. The open circuit voltage,  $V_{OC}$  between the two terminals of TEG module was used to indicate the efficiency. This is because the voltage generated increases linearly with the temperature difference, therefore the type of heat sink and thermal conductive paste that managed to create most significant temperature difference have the best efficiency in terms of heat dissipation and heat transfer rate. Hence, the type of heat sink and thermal conductive paste that generated the highest open circuit voltage,  $V_{OC}$  was selected to build the prototype.

For the comparison of TEG module, a load resistor with resistance of  $470 \Omega$  was connected to the TEG module as shown in Figure 3.46. The voltmeter and ammeter were connected to the circuit in parallel and in series respectively to measure the voltage,  $V$  and current,  $I$  generated. Then, power,  $P$  was calculated using Ohm's law and is given by:

$$P = VI \quad (3.1)$$

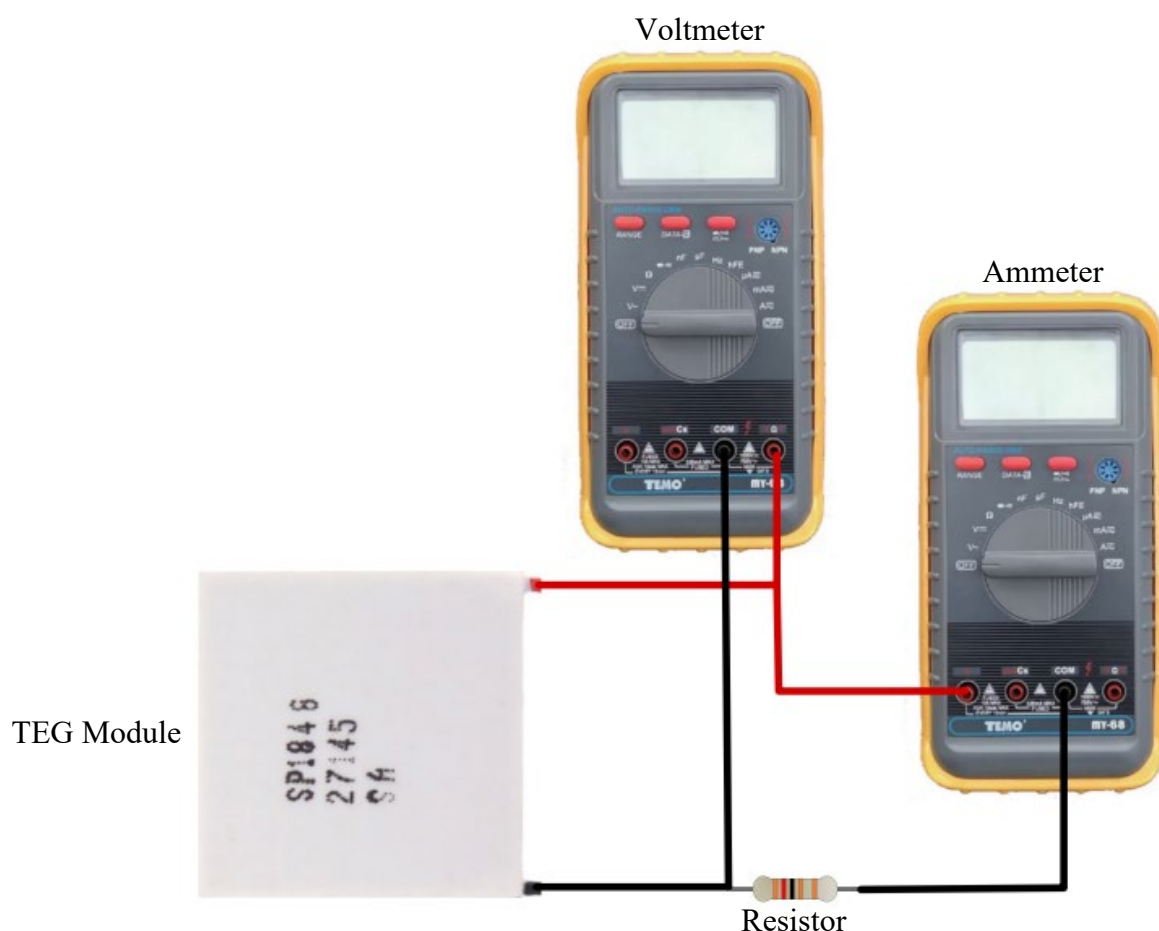


Figure 3.46: Connection of Voltmeter and Ammeter.

### 3.6 Experiment 2 – Compare the Configuration of TEG Module

Few designs of the TEG prototype were prepared to evaluate their effectiveness as well as assessing the power generated whether it is sufficient to power up the loads. This include altering the air flow using 3D printed case, arrangements of the TEG modules, different size of fan and gaps between TEG modules.

The method used in this experiment was trial and error. The process was divided into four stages: design, build, test and analyse. A viable prototype was designed based on the research done previously. Then, the prototype was fabricated. Experiment was carried out on the prototype to test the functionality. Lastly, data were collected and analysed to identify the problems encountered. This concludes the one cycle of the process. The cycle was repeated until the result is satisfying. The prototype will be improved on each cycle where the prototype is designed based on the findings from previous cycle.

### 3.6.1 Design 1

For design 1, the TEG module used was TEG-127-3.5-2.8T250D and four TEG modules were joined together in series as shown in Figure 3.47. The heat sink used in this design is 40 mm × 40 mm aluminium which has the same size as TEG module. The fins height of the heat sink is 10 mm. The aluminium plate with dimension of 80 mm × 80 mm was fabricated and it was able to fit four TEG modules perfectly. This is to ensure that no excessive surface is exposed to the surrounding of TEG modules that may eventually heats up the cold side of TEG modules. An 80 mm × 80 mm fan that has the same size with the design was used to cool down the heat sink.

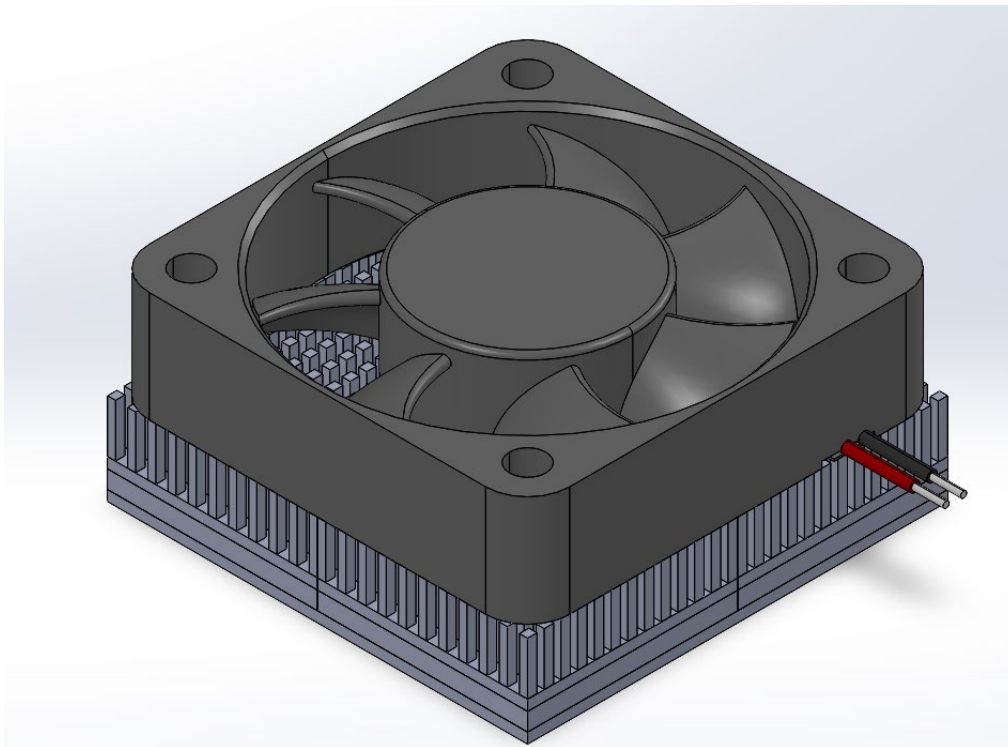


Figure 3.47: Set-up of Four TEG Modules Connecting in Series with Fan.

Table 3.7 shows the calculated theoretical power output for design 1 at different temperature difference where the connection of TEG modules was based on the circuit diagram as shown in Figure 3.48.

Table 3.7: Theoretical Output for Design 1.

Temperature Difference, $\Delta T$ ( $^{\circ}\text{C}$ )	Voltage, V (V)	Current, I (A)	Power, P (W)
20	6.8	0.10	0.673
40	11.2	0.18	2.016

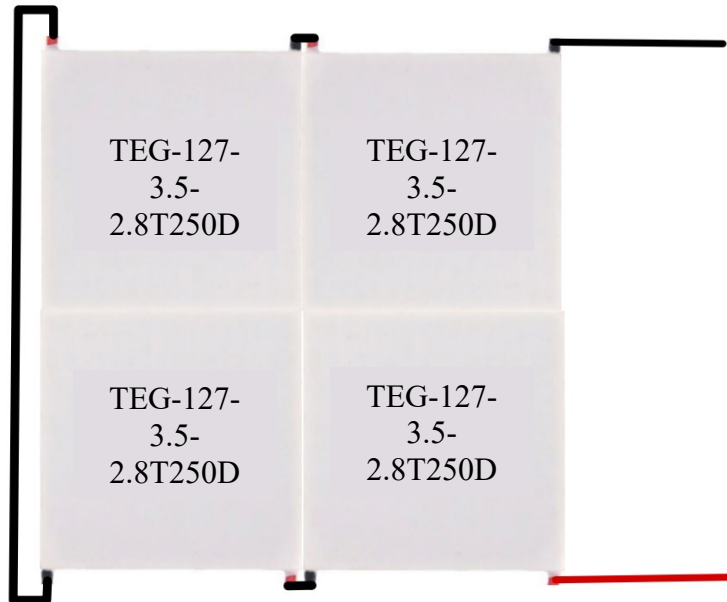


Figure 3.48: Circuit Diagram of Four TEG Modules.

### 3.6.2 Design 2

For design 2 as shown in Figure 3.49, six TEG-127-3.5-2.8T250D TEG modules were used while the other parts remain unchanged from design 1. The heat sink and fan used were similar to design 1. The aluminium plate with dimension of  $120\text{ mm} \times 80\text{ mm}$  was fabricated and it was able to fit six TEG modules perfectly. This is to ensure that no excessive surface is exposed to the surrounding of TEG modules that may eventually heats up the cold side of TEG modules.



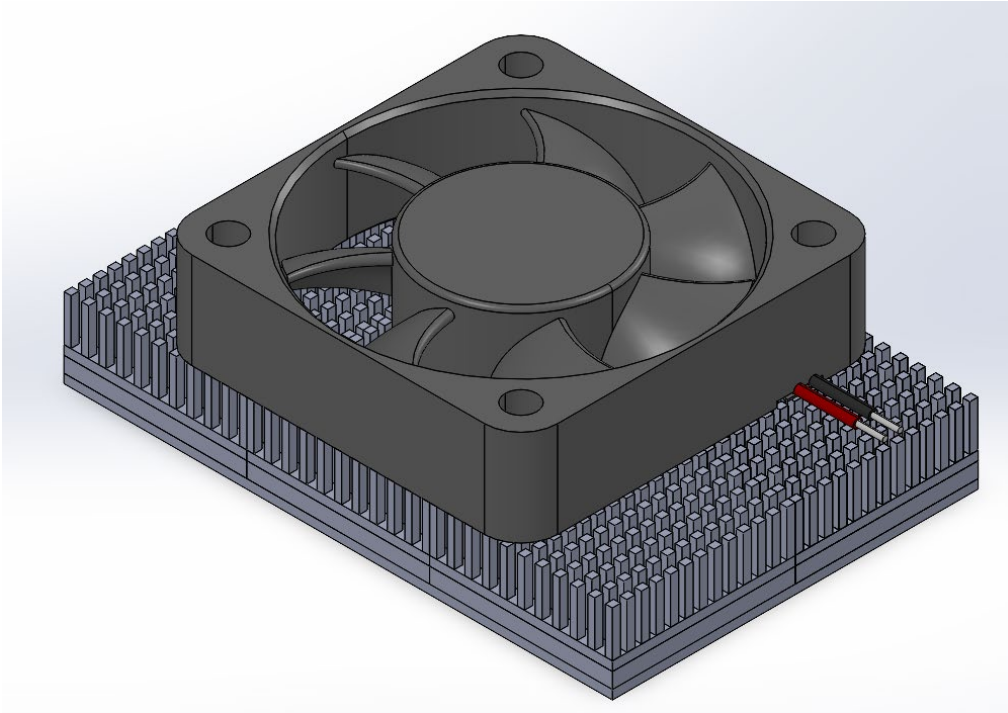


Figure 3.49: Set-up of Six TEG Modules Connecting in Series and Parallel with Fan.

Table 3.8 shows the calculated theoretical power output for design 2 at different temperature difference where the connection of TEG modules was based on the circuit diagram as shown in Figure 3.50. Two sets of three TEG modules in series were connected parallelly.

Table 3.8: Theoretical Output for Design 2.

Temperature Difference, $\Delta T$ (°C)	Voltage, V (V)	Current, I (A)	Power, P (W)
20	5.1	0.20	1.010
40	8.4	0.36	3.024

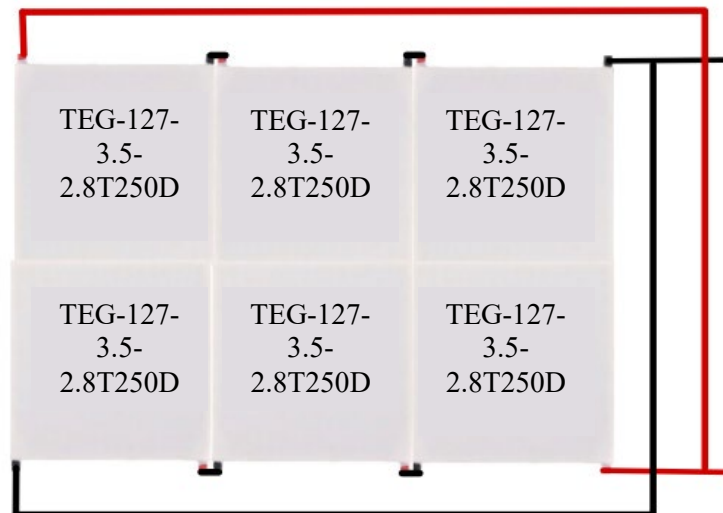


Figure 3.50: Circuit Diagram of Six TEG Modules.

### 3.6.3 Design 3

For design 3 as shown in Figure 3.51, the TEG module used was SP1848-27145 and nine TEG modules were joined together in series. The heat sink used in this design was 40 mm × 40 mm aluminium which has the same size as TEG module. The fins height of the heat sink is 10 mm. The aluminium plate with dimension of 120 mm × 180 mm was fabricated and it was able to fit nine TEG modules. Additional surface at the two sides was used by the clamp to hold down the heat sink and TEG modules on the aluminium plate tightly. An 80 mm × 80 mm fan was used to cool down the heat sink.

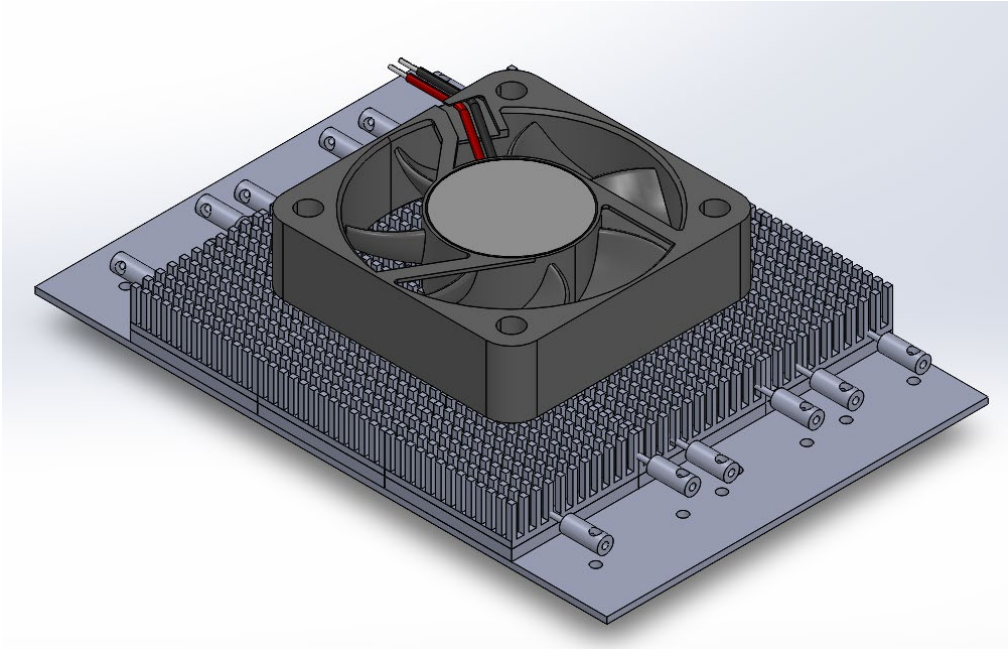


Figure 3.51: Set-up of Nine TEG Modules Connecting in Series with Fan.

Table 3.9 shows the calculated theoretical power output for design 3 at different temperature difference where the connection of TEG modules was based on the circuit diagram as shown in Figure 3.52.

Table 3.9: Theoretical Output for Design 3.

Temperature Difference, $\Delta T$ ( $^{\circ}\text{C}$ )	Voltage, V (V)	Current, I (A)	Power, P (W)
20	8.73	0.23	1.964
40	16.2	0.37	5.962

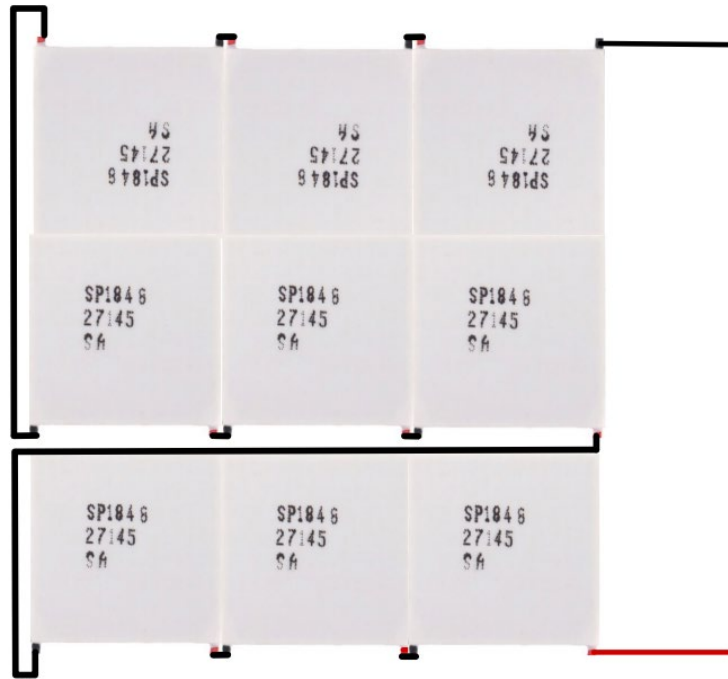


Figure 3.52: Circuit Diagram of Nine TEG Modules.

#### 3.6.4 Design 4

For design 4 as shown in Figure 3.53, the TEG module used was SP1848-27145 and eight TEG modules were joined together in series. The heat sink used in this design was 90 mm × 180 mm copper which is sufficient to cover up to eight TEG modules with total surface area of 80 mm × 160 mm. The fins height of heat sink is 2 mm. Aluminium plate with dimension of 100 mm × 190 mm was fabricated and it was able to fit eight TEG modules. Additional borders allow the heat sink to be screwed on the plate to hold down the heat sink and TEG modules on the aluminium plate tightly. An 80 mm × 80 mm fan was used to cool down the heat sink.

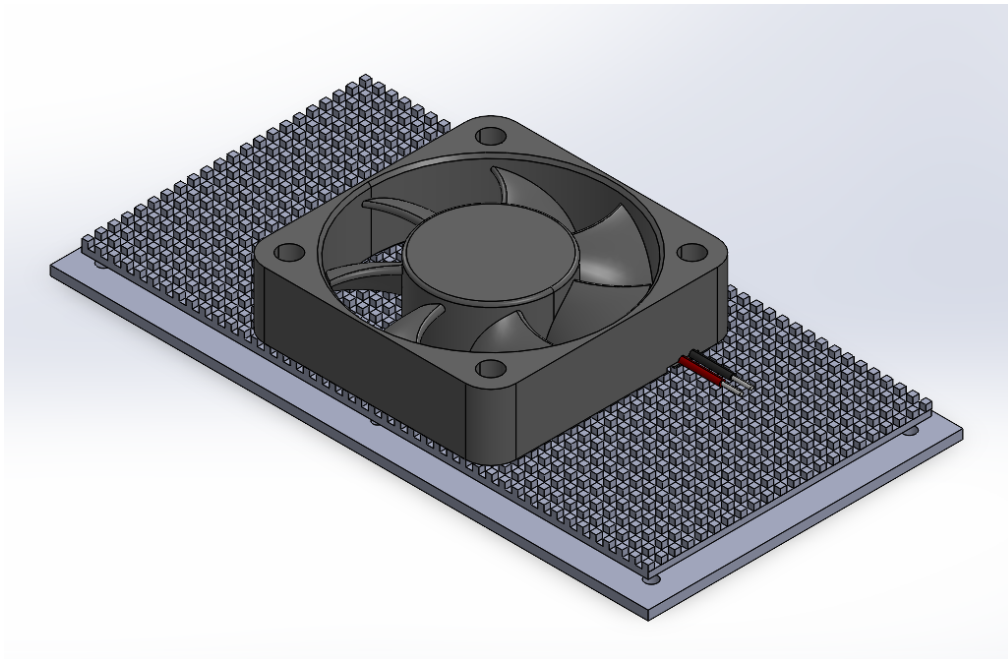


Figure 3.53: Set-up of Eight TEG Modules Connecting in Series with Fan.

Table 3.10 shows the calculated theoretical power output for design 4 at different temperature difference where the connection of TEG modules was based on the circuit diagram as shown in Figure 3.54.

Table 3.10: Theoretical Output for Design 4.

Temperature Difference, $\Delta T$ ( $^{\circ}\text{C}$ )	Voltage, V (V)	Current, I (A)	Power, P (W)
20	7.76	0.23	1.746
40	14.4	0.37	5.299

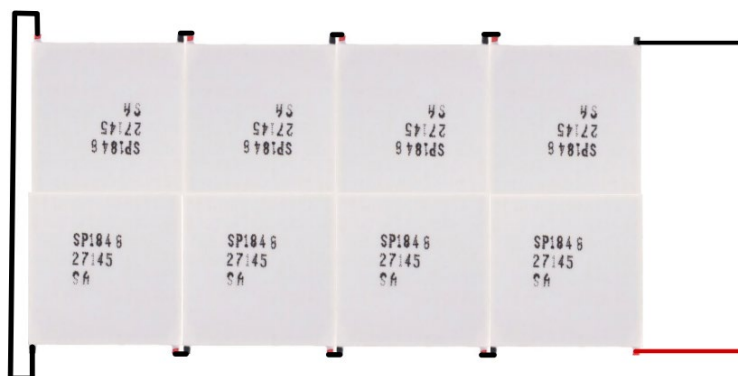


Figure 3.54: Circuit Diagram of Eight TEG Modules.

### 3.6.5 Design 5

For design 5 as shown in Figure 3.55, the TEG module used was changed back to TEG-127-3.5-2.8T250D due to it has higher power output and 15 TEG modules were joined together in series. The heat sink used in this design was 69 mm × 100 mm aluminium and 4 pieces of heat sink were used to cover 15 TEG modules. The fins height of the heat sink is 36 mm and the air flow is flowing in one direction where the heat sink at the two ends can be cooled down equally. The aluminium plate with dimension of 160 mm × 200 mm was fabricated and it was able to fit 15 TEG modules. Additional surface at the two sides was used by the clamp to hold down the heat sink and TEG modules on the aluminium plate tightly. An aluminium plate on the top was fabricated to clamp on the heat sink as well as to force the air flow to pass through all the heat sink towards to end. A 120 mm × 120 mm fan was used to cool down the heat sink.

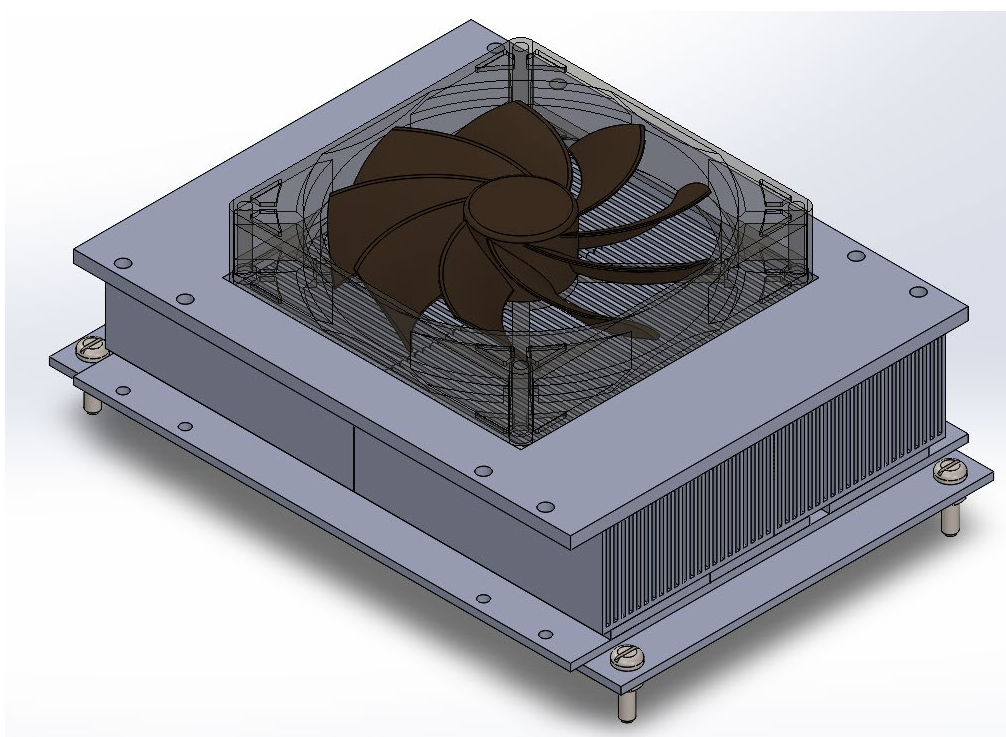


Figure 3.55: Set-up of 15 TEG Modules Connecting in Series with Fan.

Table 3.11 shows the calculated theoretical power output for design 5 at different temperature difference where the connection of TEG modules was based on the circuit diagram as shown in Figure 3.56.

Table 3.11: Theoretical Output for Design 5.

Temperature Difference, $\Delta T$ ( $^{\circ}\text{C}$ )	Voltage, V (V)	Current, I (A)	Power, P (W)
20	25.5	0.10	2.525
40	42	0.18	7.560

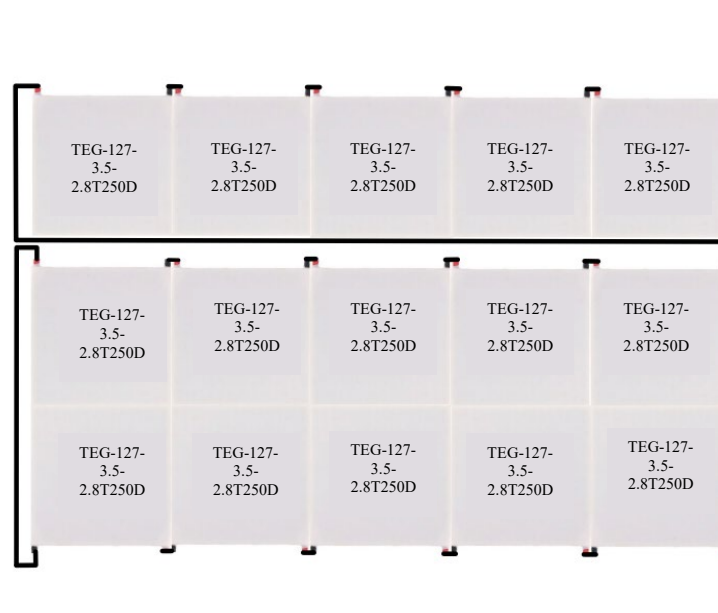


Figure 3.56: Circuit Diagram of 15 TEG Modules.

### 3.6.6 Design 6

For design 6 as shown in Figure 3.57, the TEG module used was TEG-127-3.5-2.8T250D and 16 TEG modules were joined together in series and parallel. This configuration has square shape to make sure the air flow is equal from the square shape of the fan. The heat sink used in this design was 40 mm  $\times$  40 mm aluminium which has the same size as TEG module to eliminate the gap between the heat sink and TEG module. The 20 mm fins height of the heat sink create larger surface area to dissipate heat at a faster rate. The aluminium plate with dimension of 220 mm  $\times$  290 mm was fabricated and it was able to fit 16 TEG modules. Clamp was removed from the design as it did not show any significant improvement on the temperature difference. A 120 mm  $\times$  120 mm fan was used to cool down the heat sink as shown in Figure 3.58. A case was designed and 3D printed to create a distance between the fan and heat sink. This forces the air flow towards all the heat sinks equally. Fins were designed based on the air flow

analysis done in the previous section and mounted on the fan to create an equal air flow. Hence, heat sinks can be cooled down effectively to create a more significant temperature difference.

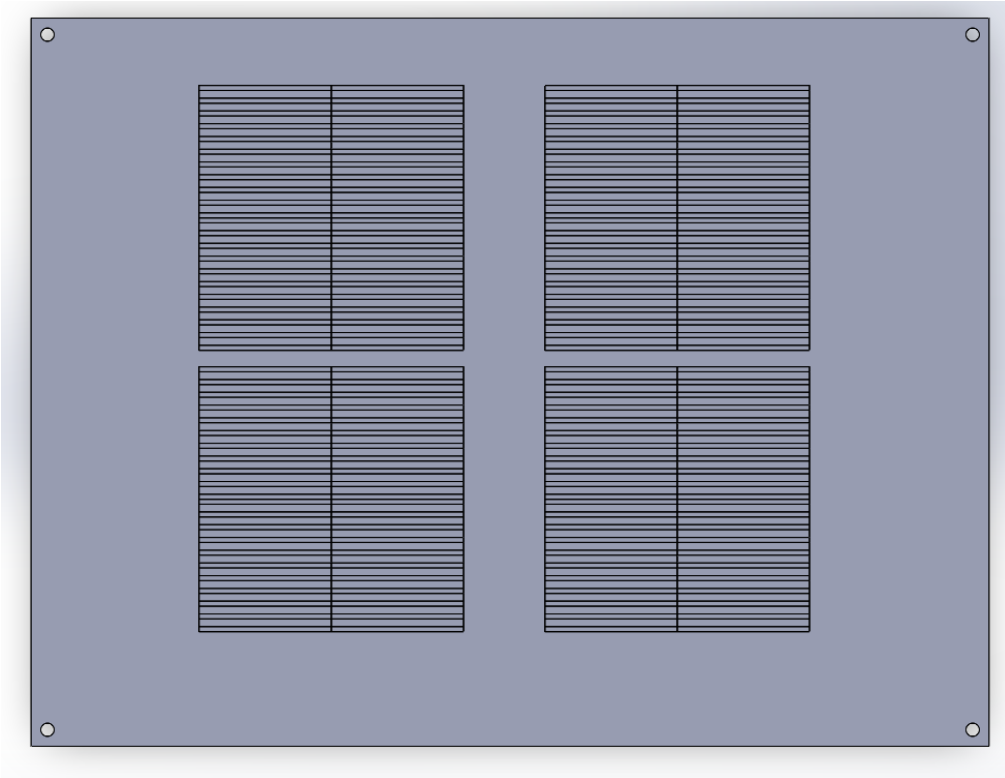


Figure 3.57: Set-up of 16 TEG Modules Connecting in Series and Parallel.

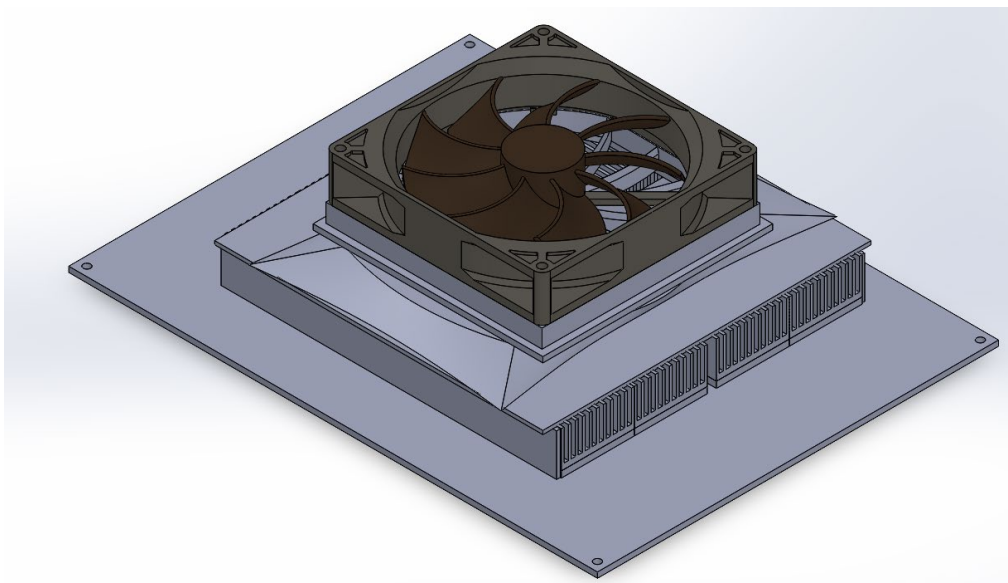


Figure 3.58: Set-up of 16 TEG Modules Connecting in Series and Parallel with Case and Fan.



Table 3.12 shows the calculated theoretical power output for design 6 at different temperature difference where the connection of TEG modules was based on the circuit diagram as shown in Figure 3.59. Two sets of eight TEG modules in series were connected parallelly.

Table 3.12: Theoretical Output for Design 6.

Temperature Difference, $\Delta T$ (°C)	Voltage, V (V)	Current, I (A)	Power, P (W)
20	13.6	0.20	2.693
40	22.4	0.36	8.064

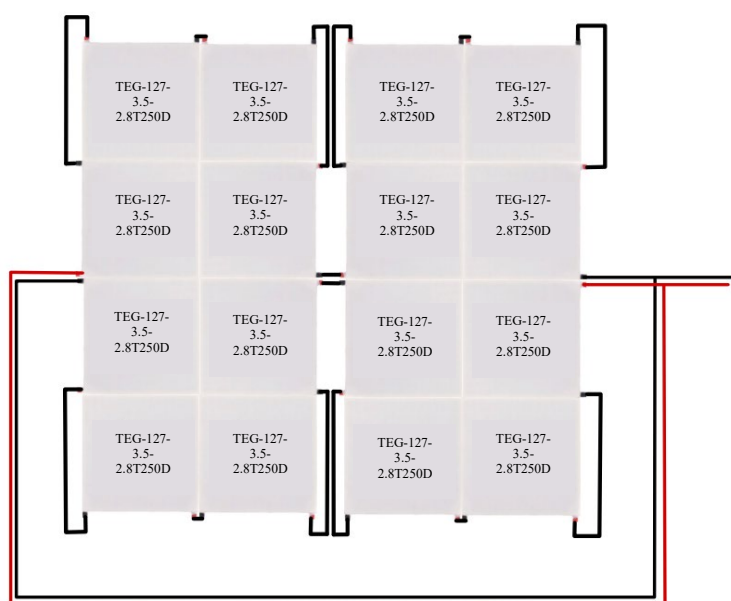


Figure 3.59: Circuit Diagram of 16 TEG Modules.

### 3.6.7 Design 7

For design 7 as shown in Figure 3.60, the TEG module used was TEG-127-3.5-2.8T250D and nine TEG modules were joined together in series. The heat sinks and TEG modules were separated with a small gap of 50 mm instead of sticking next to each other. This is to prevent the heat from concentrated at the centre and increasing the temperature on the cold side. The heat sink chosen in this design was 45 mm × 50 mm aluminium which has slightly larger size than the TEG module to increase the rate of heat dissipation. The fins height of the heat sink is 36 mm. The aluminium plate with dimension of 220 mm × 300 mm was fabricated and it was able to fit nine TEG modules with a small gap between

each TEG modules. A 120 mm  $\times$  120 mm fan was used to cool down the heat sink.

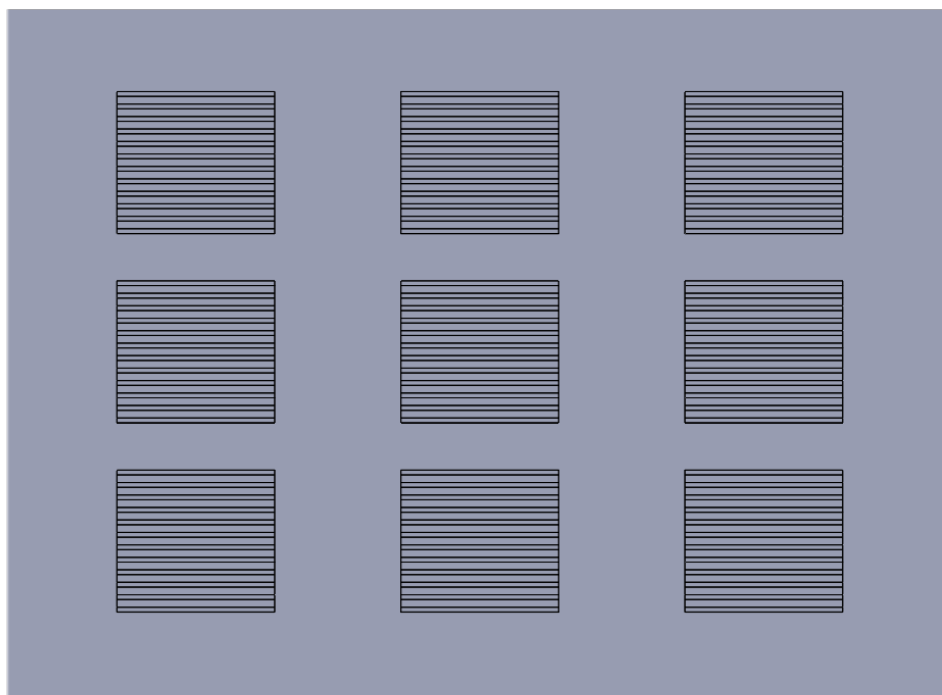


Figure 3.60: Set-up of Nine TEG Modules Connecting in Series.

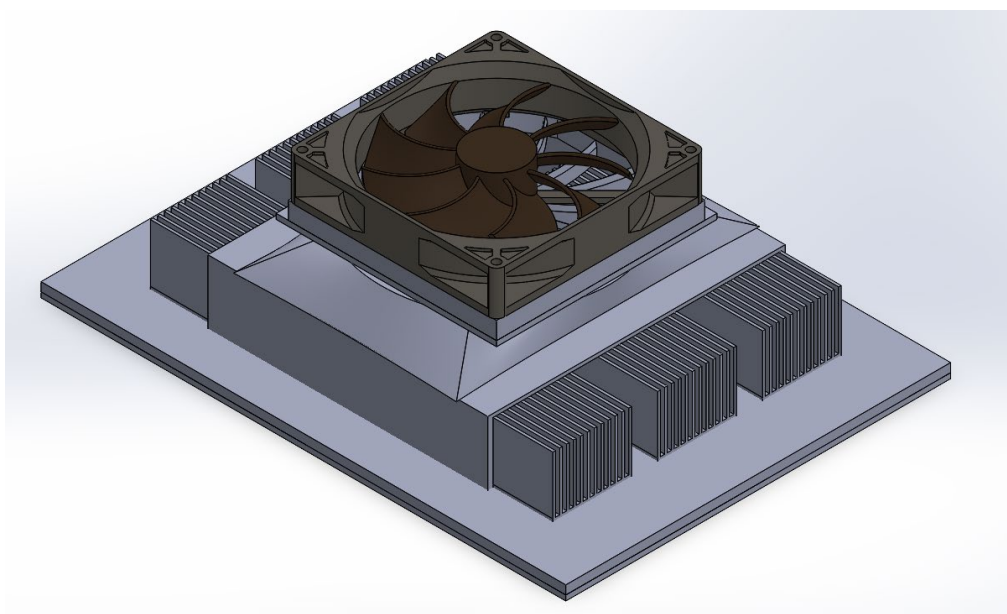


Figure 3.61: Set-up of Nine TEG Modules Connecting in Series with Case and Fan.

Table 3.13 shows the calculated theoretical power output for design 7 at different temperature difference where the connection of TEG modules was based on the circuit diagram as shown in Figure 3.62.

Table 3.13: Theoretical Output for Design 7.

Temperature Difference, $\Delta T$ (°C)	Voltage, V (V)	Current, I (A)	Power, P (W)
20	15.3	0.10	1.515
40	25.2	0.18	4.536

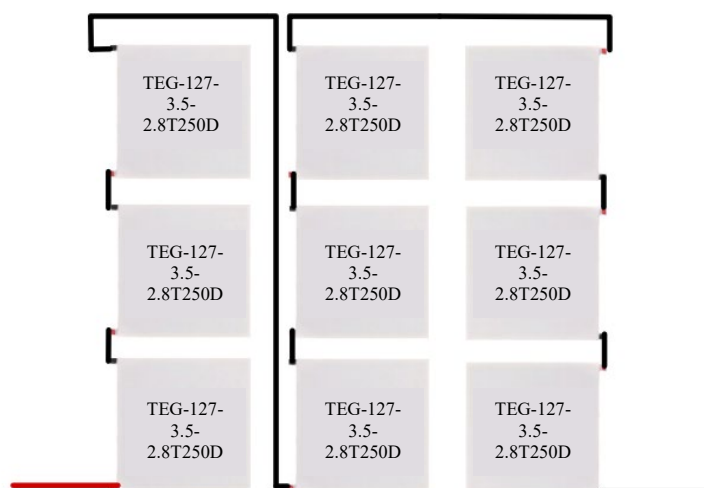


Figure 3.62: Circuit Diagram of Nine TEG Modules.

### 3.6.8 Design 8

For design 8 as shown in Figure 3.64, the TEG module used was TEG-127-3.5-2.8T250D. This design is similar to design 7 except that the gaps between heat sinks and TEG modules were decreased to 10 mm and the number of TEG modules was increased to 12 pieces connecting in series and parallel. This size of the fan is 120 mm × 120 mm and by decreasing the gaps, the heat sinks were brought closer towards the fan to allow the air flow of the fan to blow directly on the heat sinks.

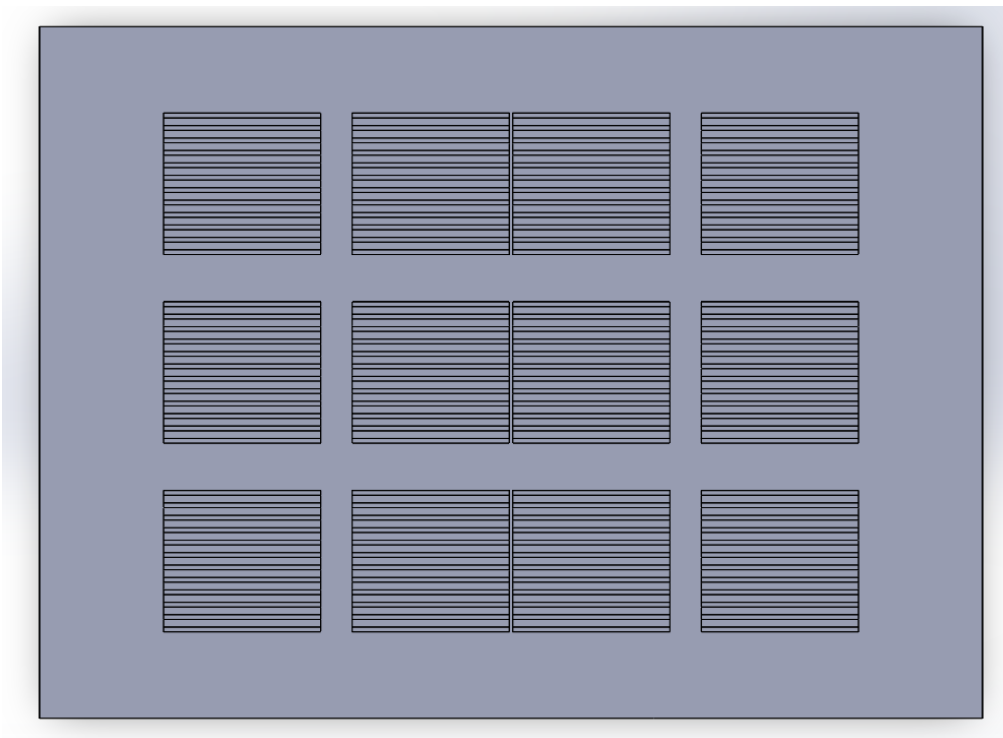


Figure 3.63: Set-up of 12 TEG Modules Connecting in Series and Parallel.

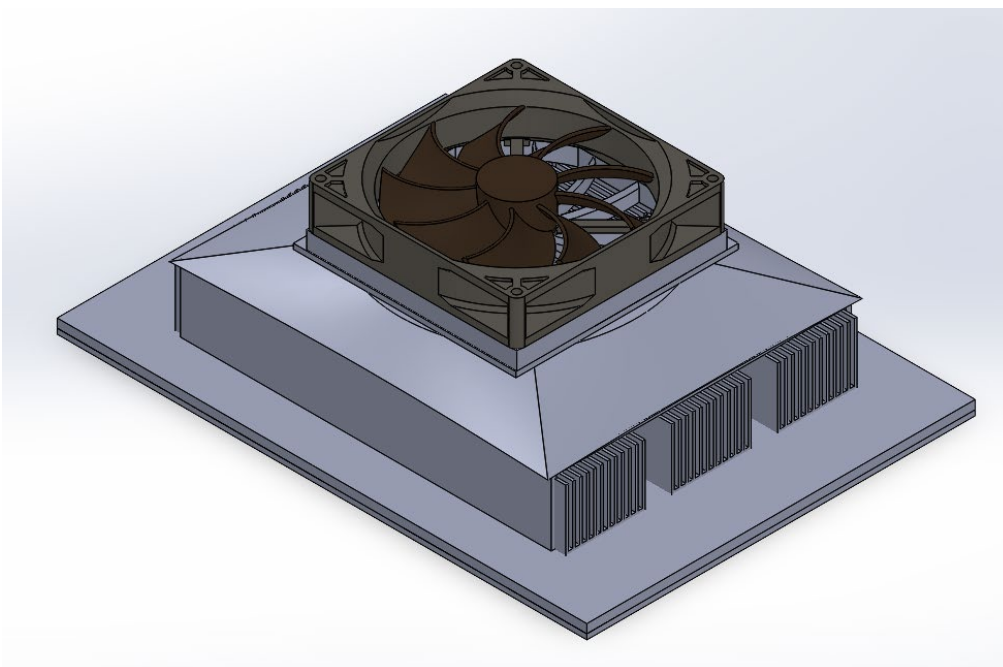


Figure 3.64: Set-up of 12 TEG Modules Connecting in Series and Parallel with Case and Fan.

Table 3.14 shows the calculated theoretical power output for design 8 at different temperature difference where the connection of TEG modules was

based on the circuit diagram as shown in Figure 3.65. Two sets of six TEG modules in series were connected parallelly.

Table 3.14: Theoretical Output for Design 8.

Temperature Difference, $\Delta T$ ( $^{\circ}\text{C}$ )	Voltage, V (V)	Current, I (A)	Power, P (W)
20	10.2	0.20	2.020
40	16.8	0.36	6.048

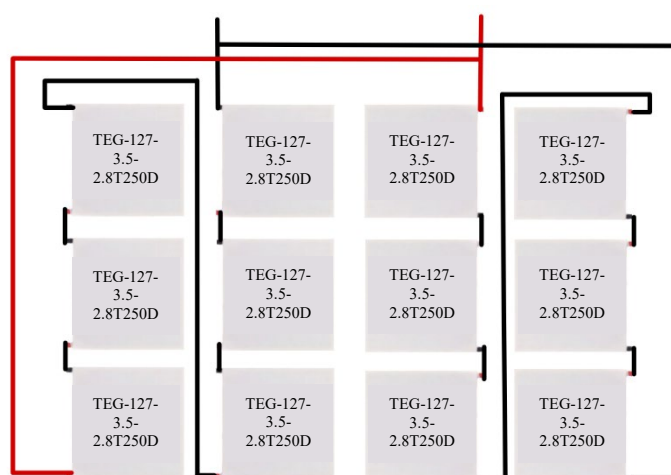


Figure 3.65: Circuit Diagram of 12 TEG Modules.

### 3.7 Develop Arduino Module – Wireless Device

The purpose of Arduino module is to validate the power produced by TEG prototype is sufficient to power up a small IoT device which is ESP32 Arduino module in this case. The ESP32 Arduino module with built-in Wi-Fi was connected to the internet and data received from the sensor was sent to the cloud. Therefore, the data of all the sensors from multiple area can be view in the dashboard of the cloud.

Figure 3.66 shows the schematic diagram of the entire prototype. TEG modules were connected to the step-down power module at the IN+ and IN- terminal according to the polarity. The ESP32 Arduino module and fan which were the loads and they were connected to the OUT+ and OUT- terminals of the step-down power module.

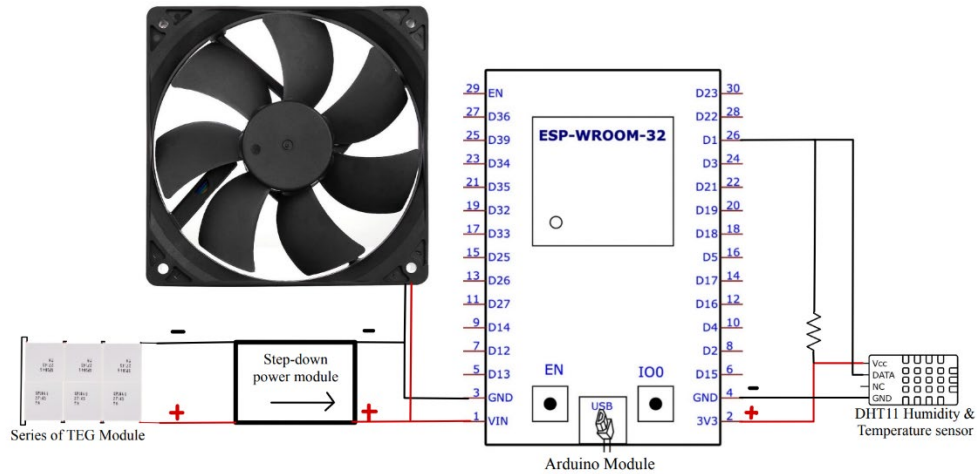


Figure 3.66: Schematic Diagram of Prototype.

The cloud service provider used was Ubidots where the ESP32 Arduino board can publish and subscribe data to or from the cloud using MQTT. The ESP32 Arduino board was programmed and connect to the local Wi-Fi network to access the internet. Then, it was connected to Ubidots server using unique API key. After successful connection, data were sent to the cloud by the ESP32 module to be displayed.

### 3.8 Summary

The chapter sums up the work plan before beginning the development of the prototype together with a flowchart to sort out the tasks in sequence. Materials and equipment required for the project were listed out and to be prepared before building the prototype. Solidworks drawings were prepared to fabricate the prototype and schematic diagrams were drawn to illustrate each module used. Further research was done on the parts used in order to ensure they have the best compatibility and functionality in the whole system. The procedures on the experiments were planned out to facilitate the overall development process and to obtain desire results.

## CHAPTER 4

### RESULTS AND DISCUSSION

#### 4.1 Introduction

Prototype was built based on the work plan in previous chapter and experiment on the prototype was done. Data were collected and compared in this chapter to discuss the deviation between each result. In this project, experiment 1 and experiment 2 were carried out simultaneously to investigate the best configuration of the prototype. Total of 8 designs were built and modifications were done on each design to improve the prototype. The modifications done on the design includes changing the number of TEG modules used, substituting different type of TEG module, heat sink, thermal conductive paste, insulation material, using different design of case, size of fan as well as the arrangement of TEG modules. Problems were identified on each design and were solve accordingly in the following design until the prototype was able to power up the Arduino board and fan successfully.

#### 4.2 Experiment 1 - Compare Different Type of Heat Sink, Thermal Conductive Paste and TEG Module

This experiment was divided into three subsections, relating to the type of heat sink, thermal conductive paste and TEG module respectively. At the end of the experiment, best type from each subsection was selected and was used in the final design of experiment 2 to build the prototype.

##### 4.2.1 Comparison of Heat Sink

Initially, the heat sink used for experiment 2 was the first one as shown in Table 4.1. The dimensions of the heat sink are 40 mm × 40 mm × 10 mm in terms of width, length and height respectively. From the result of the experiment, it did not provide sufficient cooling effect. Therefore, copper heat sink was used in the following experiment as copper has higher thermal conductivity than aluminium (Gabrian, n.d.). However, the height of the fins for copper heat sink is only 2 mm due to cost limitation. Thus, it did not provide sufficient cooling effect in the experiment. Next, a large aluminium heat sink with the dimensions

of  $100 \text{ mm} \times 69 \text{ mm} \times 36 \text{ mm}$  in terms of width, length and height respectively was used to replace the previous heat sink. This heat sink has the highest fins height among other heat sinks. Although it has excellent heat dissipation rate, but the large surface area covering few TEG modules with one heat sink creates gap at the contact area between heat sink and TEG modules. For that reason, it was replaced with another heat sink that has the same surface area with the TEG modules which is  $40 \text{ mm} \times 40 \text{ mm}$ . It has higher fins height which is 20 mm that is higher than the first heat sink which has 10 mm fins height.

Table 4.1: Data Obtained from Experiment 1.

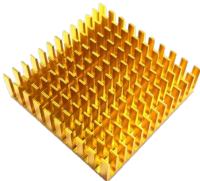



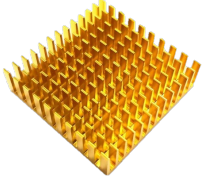



Type of Heat Sink	Fins Height (mm)	Voltage Generated (V)
 1. Aluminium	10	1.23
 2. Copper	2	1.3
 3. Aluminium	36	1.49
 4. Aluminium	20	1.24

Table 4.2 shows the comparison between the heat sinks in terms of respective advantages and disadvantages.



Table 4.2: Comparison of Heat Sink.

Type of Heat Sink	Advantage	Disadvantage
 1. Aluminium	The air flow is flowing in two directions which could increase the rate of heat dissipation.	The fins are the shortest among other aluminium heat sinks, therefore, the rate of heat dissipation is the slowest.
 2. Copper	It has better cooling effect than first and fourth heat sink with single TEG module in experiment 1. This is because the surface area is large compared to other heat sinks. The high thermal conductivity of copper leads to faster heat dissipation.	While only one TEG module was used in experiment 1. Therefore, the result of the experiment for this heat sink was considered as invalid. This was because when more TEG modules were being used in experiment 2, it was unable to provide sufficient cooling effect.
 3. Aluminium	It has the highest fins height among other heat sinks. The thickness of the fins is thinner than other first and fourth heat sink. This increases the number of fins and increasing the surface area to dissipate heat at a faster rate.	The surface area is relatively large and must be used with few TEG modules. This creates a problem of the contact between heat sink and TEG modules to transfer heat effectively.
 4. Aluminium	It has slightly higher fins but the voltage generated was similar to the first heat sink with 10 mm fins height.	The air flow of this heat sink is in one direction which reduces the cooling effect.

The outcome of this comparison is that the third heat sink was machined into the size of 45 mm × 50 mm in terms of length and width. This has overcome the problem stated at the disadvantage of third heat sink.




Therefore, the machined heat sinks can be used with individual TEG module instead of sticking with a few TEG modules.


As compared with previous study, aluminium heat sink has better cooling efficiency than copper heat sink. The fins height of the heat sink also has significant effect on the cooling efficiency where higher fins height is able to dissipate heat at a faster rate (Ekpu et al., 2011).

#### 4.2.2 Comparison of Thermal Conductive Paste

Table 4.3 shows the comparison of thermal conductive paste that was used to fill the gap between two surfaces to ensure maximum heat transfer.

Table 4.3: Comparison of Thermal Conductive Paste.

Type of Thermal Paste	Thermal Conductivity (W/m-K)	Voltage Generated (V)	Explanation
 1. HTK-002	0.80	2.10	It has the highest liquidity and it was the easiest to apply among other thermal conductive paste.
 2. HY510	1.93	2.11	It has moderate liquidity with higher thermal conductivity as compared to the first thermal conductive paste.
 3. Ice Fusion V2	5.00	2.10	It has lower liquidity and challenging to apply. The paste applied on the surface may not be smooth and flat. It tends to create air gaps between the contact surfaces which lower heat transfer rate.



	10.50	2.19	It has similar liquidity to the third thermal conductive paste. However, with higher thermal conductivity, it was able to transfer heat effectively.
4. Frost X25			

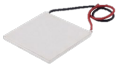
To sum up this comparison, the thermal conductivity did not have significant impact on the heat transfer rate between the contact surfaces. Whereas the condition of the paste applied on the surface was contributing to the heat transfer rate. If the applied paste is too thick, the efficacy of the paste will be reduced as the contact surfaces are far apart (Intel, n.d.). If the applied paste is too thin, the gap between the contact surfaces is not filled evenly. Effort was needed to create a perfect applied paste on the surface to ensure maximum heat transfer rate.

#### 4.2.3 Comparison of Thermoelectric Generator (TEG) Module

Table 4.4 shows the comparison of TEG modules that was used to generate electricity from the temperature difference between two sides.

Table 4.4: Comparison of TEG Modules.

Type of TEG Module	Voltage Generated (V)	Current Generated (A)	Power Generated (W)	Explanation
 TEG-127-3.5-2.8T250 D	2.190	0.0045	0.00986	It has highest power output among other TEG modules. It was used in most of the designs of experiment 2.
 SP1848-27145	1.502	0.0031	0.00466	It has moderate power output among other TEG modules. It was used in design 3 and design 4 in experiment 2 to test the efficiency.

	TEC1-12730	0.796	0.0016	0.00127	The power generated was too low and was excluded from experiment 2 to build the prototype.
---	------------	-------	--------	---------	--

The first TEG module, TEG-127-3.5-2.8T250D, was used in design 1, 2, 5, 6, 7, 8 to build the prototype due to it has highest power output as compared to other TEG modules at similar temperature difference.

### 4.3 Experiment 2 - Compare the Configuration of TEG

Experiment was carried out on the prototype to analyse the power output of each design. Result and problems were discussed for each design and the problems were solved accordingly in the following design until the prototype is functionable.

#### 4.3.1 Design 1

The experiment was conducted and data were collected as shown in Table 4.5. The total power generated was 1.654 W from the temperature difference of 30 °C. This design with four TEG modules was not able to provide sufficient power to power up the loads. Therefore, more TEG modules were added in design 2.



Figure 4.1: Prototype of Design 1.

Table 4.5: Experimental Data for Design 1.

Temperature Difference, $\Delta T$ (°C)	Voltage, V (V)	Current, I (A)	Power, P (W)
30	8.27	0.20	1.654

### 4.3.2 Design 2

For design 2, the data were collected as shown in Table 4.6. The total power generated was 1.201 W from the temperature difference of 21 °C. The temperature difference for design 2 was 21 °C which is lower than design 1 that has 30 °C temperature difference. This may be due to the contact between the heat sink and TEG module was not good and heat transfer rate was reduced.

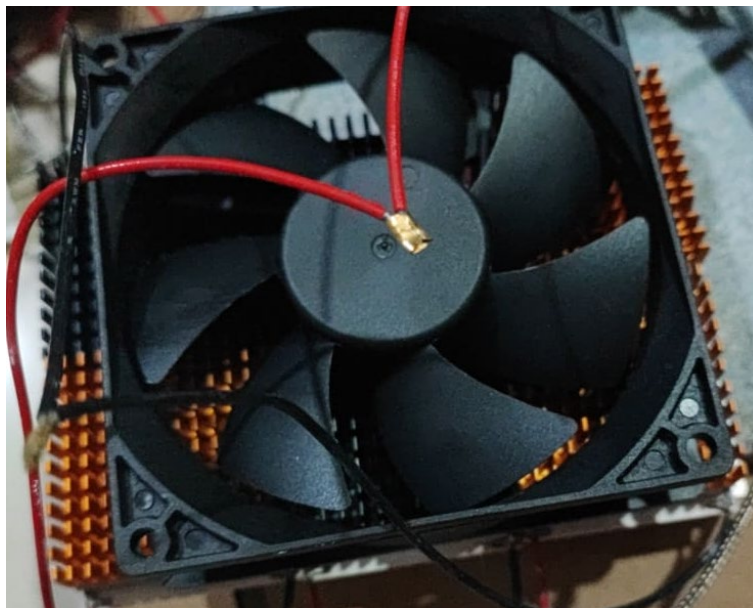


Figure 4.2: Prototype of Design 2.

Table 4.6: Experimental Data for Design 2.

Temperature Difference, $\Delta T$ (°C)	Voltage, V (V)	Current, I (A)	Power, P (W)
21	4.73	0.25	1.201

For the following design, a clamp was added to clamp the heat sinks and TEG modules tightly on the aluminium plate to ensure maximum contact between the two surfaces. At the same time, the number of TEG modules was increased to 9 pieces to increase the power output.

### 4.3.3 Design 3

From the data collected in Table 4.7, the total power generated was 1.376 W from temperature difference of 21 °C. However, the diameter of the rods used were only 2 mm which was limited by the spacing of the fins on the heat sink. Therefore, the rod was not rigid and tends to bend when force is applied to clamp on the heat sink.

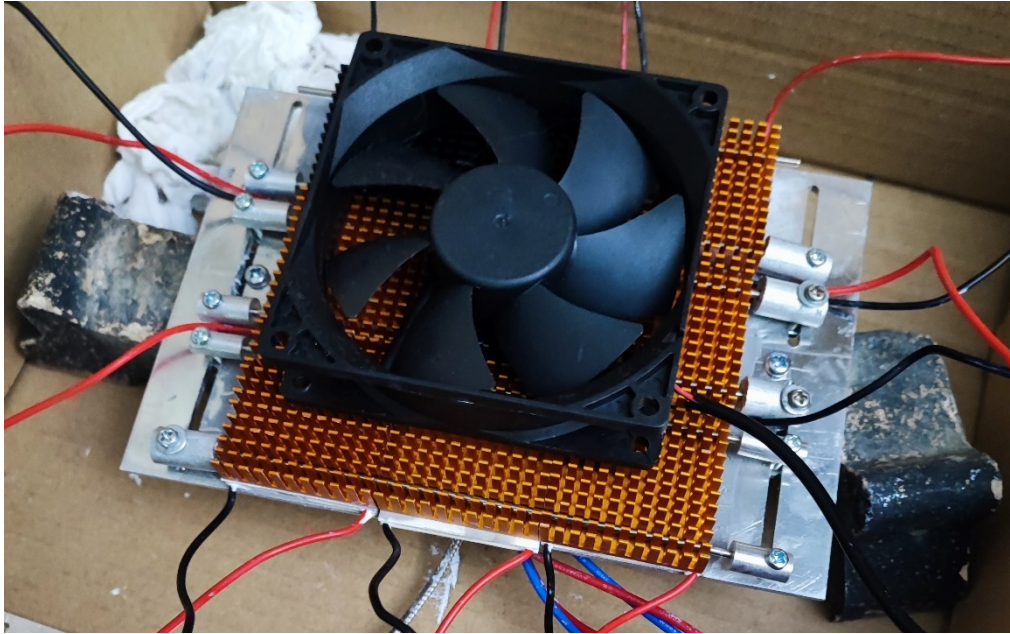


Figure 4.3: Prototype of Design 3.

Table 4.7: Experimental Data for Design 3.

Temperature Difference, $\Delta T$ (°C)	Voltage, V (V)	Current, I (A)	Power, P (W)
21	8.60	0.16	1.376

For the following design, the heat sinks were replaced with a copper heat sink that has six screw holes. The copper heat sink was used to clamp the TEG modules on the aluminium plate to ensure maximum contact.

### 4.3.4 Design 4

From the data collected in Table 4.8, the total power generated by eight TEG modules was 0.915 W from a temperature difference of 18 °C. A copper heat sink with 90 mm width and 180 mm length is used in this design to cool the cold



face of TEG modules. However, heat sink with 2 mm fins were too short and it was unable to dissipate heat effectively despite copper has high thermal conductivity.

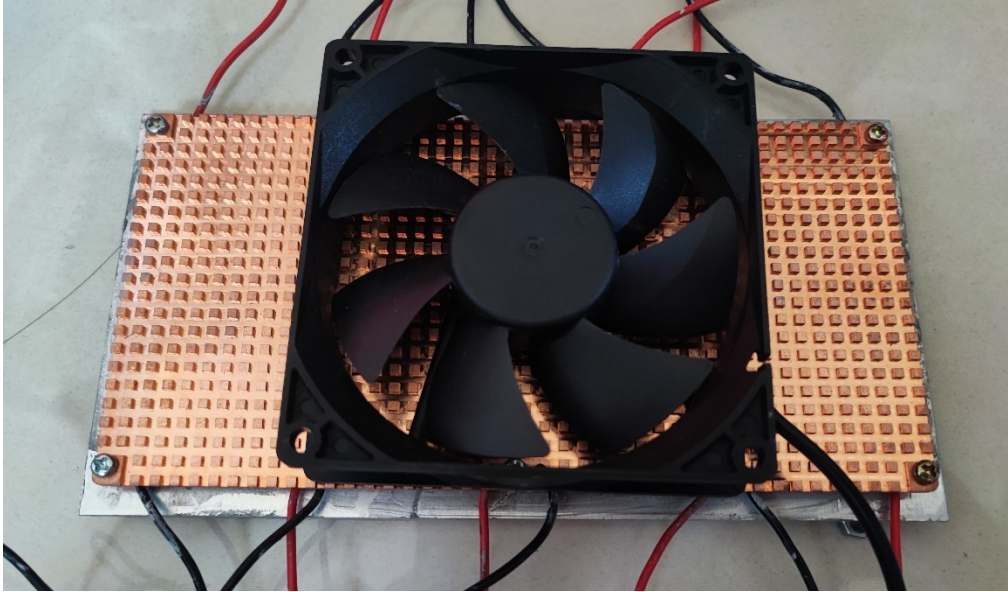


Figure 4.4: Prototype of Design 4.

Table 4.8: Experimental Data for Design 4.

Temperature Difference, $\Delta T$ ( $^{\circ}\text{C}$ )	Voltage, V (V)	Current, I (A)	Power, P (W)
18	7.04	0.13	0.915

For the following design, an aluminium heat sink with high fins was used to replace the copper heat sink. A clamp was design to clamp the heat sinks and TEG modules on the aluminium plate. The number of TEG modules used was increased to 15 pieces.

#### 4.3.5 Design 5

From the data collected in Table 4.9, the total power generated was 1.231 W from temperature difference of 17  $^{\circ}\text{C}$ . In this design, aluminium heat sink with 36 mm long fins was used to dissipate the heat at a faster rate. Another metal plate was placed on top of the heat sink to clamp the TEG modules and heat sink onto the metal plate to ensure maximum contact. However, the length and width of the heat sink is 100 mm and 69 mm respectively while the length and width

of the TEG module is 40 mm only. Therefore, one heat sink was placed on top of six TEG modules. This caused some gaps in between the heat sink and TEG module due to the uneven thickness of TEG modules as shown in Figure 4.6. Hence, TEG modules with gaps were underperforming as heat was not dissipated appropriately to cool down the cold side.

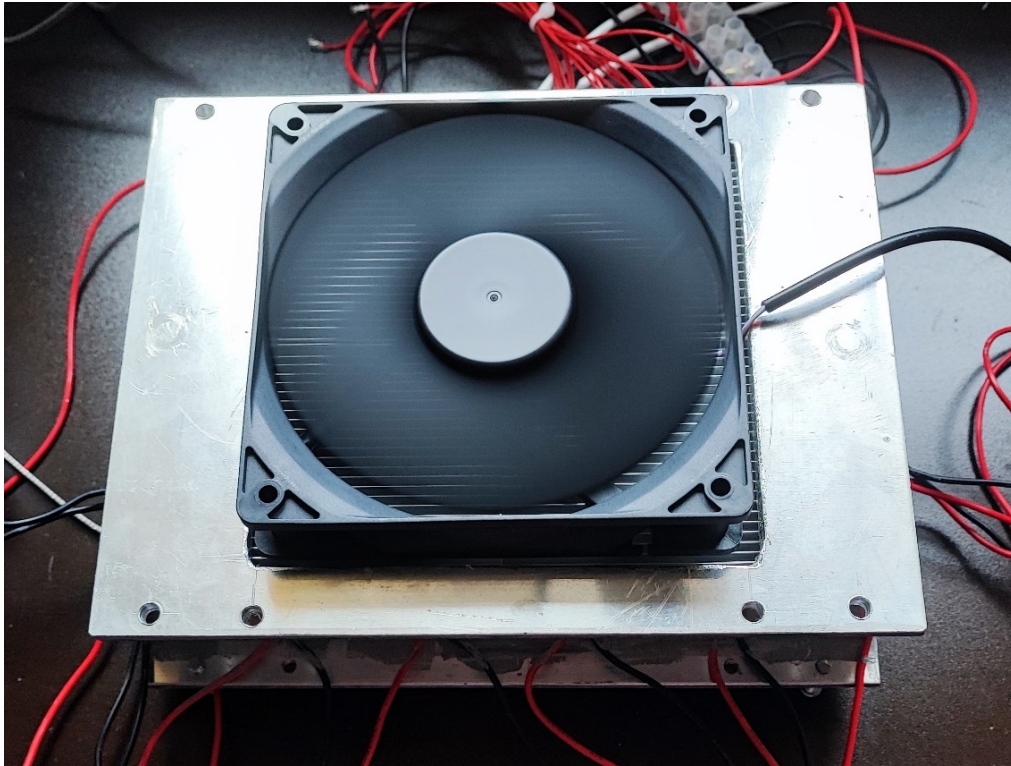


Figure 4.5: Prototype of Design 5.



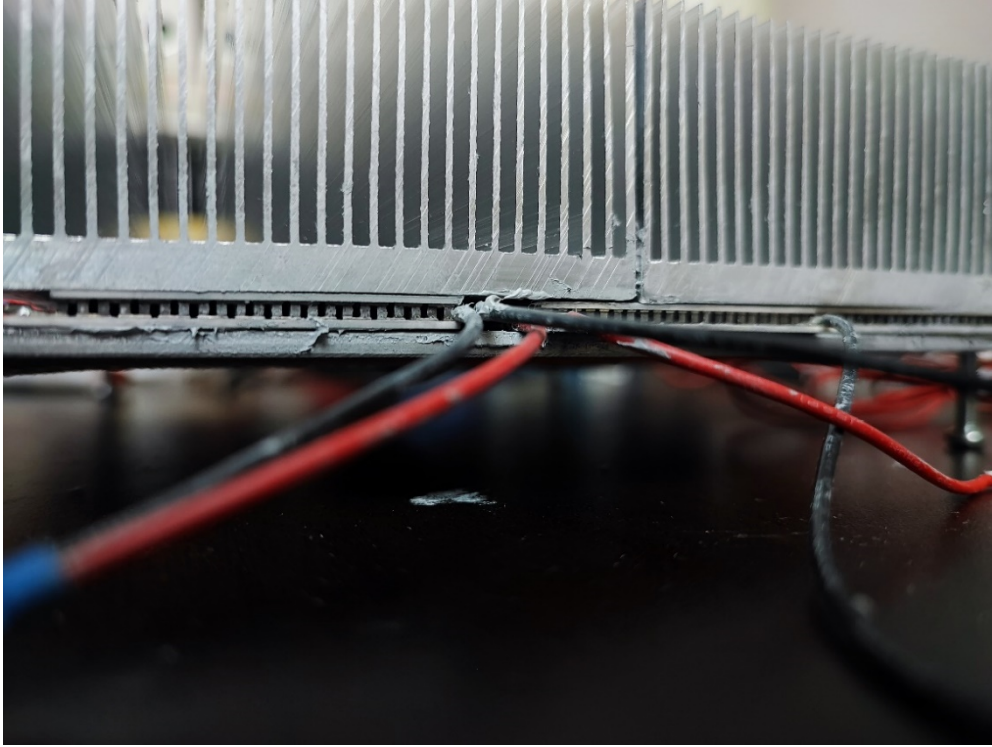


Figure 4.6: Gap between Heat Sink and TEG Module.

Table 4.9: Experimental Data for Design 5.

Temperature Difference, $\Delta T$ ( $^{\circ}\text{C}$ )	Voltage, V (V)	Current, I (A)	Power, P (W)
17	13.68	0.09	1.231

For the following design, aluminium heat sink that has the same size as TEG module was used to replace this heat sink. Clamp was removed from the design to identify the effectiveness. This is because the results for the designs with clamps were not satisfying. It was found that the air flow from the fan was blowing away from the centre. Therefore, there was no air flow at the centre of the fan. Therefore, the heat sink placed under the centre of the fan was not cooled down and caused the TEG module to underperform. In order to solve these issues, a case and fins for the fan were designed to create an equal air flow towards the heat sinks. Moreover, insulation was added on the exposed surface of aluminium plate in next design to isolate cold side. The number of TEG modules used was increased to 16 pieces.

### 4.3.6 Design 6

From the data collected in Table 4.10, the total power generated was 3.127 W from temperature difference of 25 °C. There was a significant improve on the power as compared to previous design where the power output was doubled. Although the power output was sufficient to power up the loads, but it was not able to sustain for one minute. On the other hand, it was concluded that clamping on the heat sinks did not have notable improvement on the efficiency of the prototype.



Figure 4.7: Prototype of Design 6.

Table 4.10: Experimental Data for Design 6.

Temperature Difference, $\Delta T$ (°C)	Voltage, V (V)	Current, I (A)	Power, P (W)
25	16.46	0.19	3.127

To further investigate the problem, the voltage across each TEG module was measured as shown in Figure 4.8. The measured voltage for the TEG modules at the four corners were between 0.4 V to 0.5 V which is less than half of the highest measured voltage of TEG module at the centre. There is significant deviation between the highest and lowest values of the voltage

generated by TEG modules. This means that the heat sinks at the corners were not cooled down effectively and caused temperature imbalance on the whole prototype. Power generated by the TEG modules at the centre were limited by the TEG modules at the corners which were underperformed. This is because they were connected in series and the power output of each TEG module was equal to the lowest power output among the TEG modules. Temperature mismatch can have significant impact on the performance of a thermoelectric system (Faiz and V.K. Maurya, 2017). Therefore, further modification was done to improve on this design.

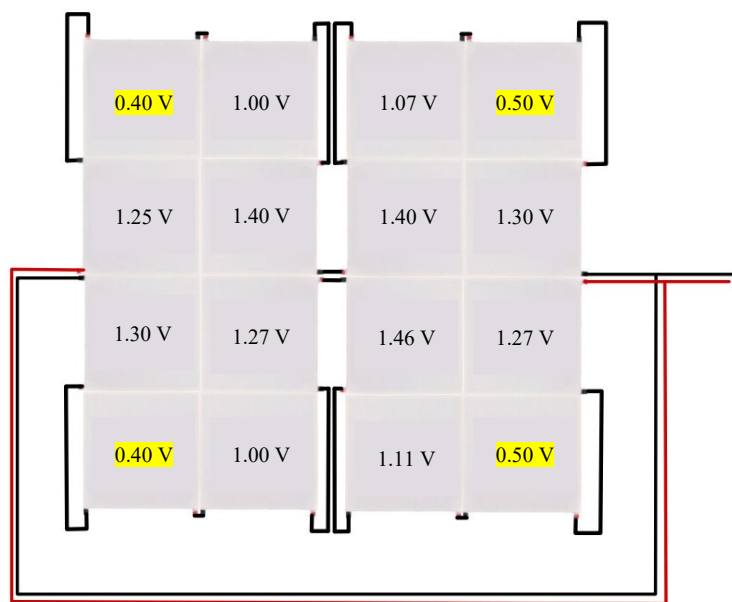


Figure 4.8: Measured Voltage of Each TEG Module.

This design has concentrated heat at the centre and the air became warm before it passed through the heat sinks at the corners. Thus, lesser heat was dissipated from the heat sinks at the corners and led to lower temperature gradient. For the next design to overcome this issue, the number of TEG modules was reduced to nine pieces and the arrangement of TEG modules were separated with a gap in between. Moreover, the heat sinks were replaced with the machined aluminium heat sinks with 36 mm fins height.

#### 4.3.7 Design 7

From the data collected in Table 4.11, the total power generated was 3.237 W from temperature difference of 35 °C. It has slight improvement as compared to previous design. The heat sinks with 36 mm fins height were able to achieve temperature difference of 35 °C which is 10 °C higher than the previous heat sinks. However, this design was not able to sustain for one minute despite power generated was sufficient for the loads. This is because the fan was not operating at full speed when it was powered by the TEG modules, this led to decrease cooling effect on the heat sinks. Hence, the temperature difference was decreasing and reducing the power output of the TEG modules. Eventually, the whole prototype stopped working until the fan is powered up by external power source.

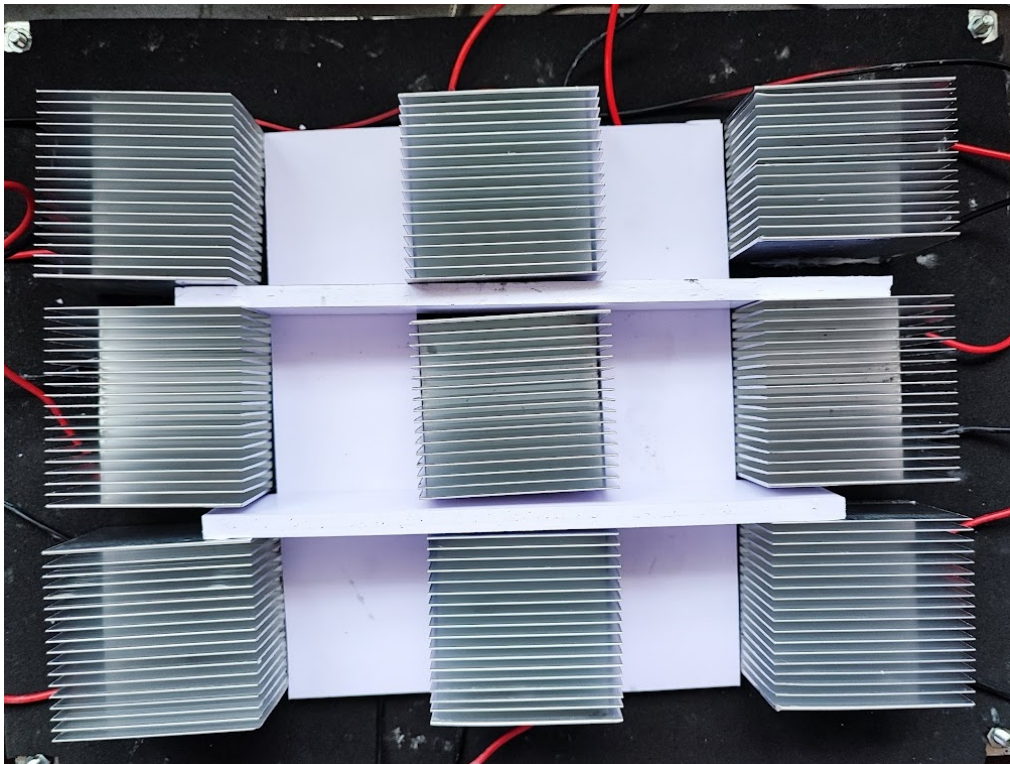


Figure 4.9: Prototype of Design 7.



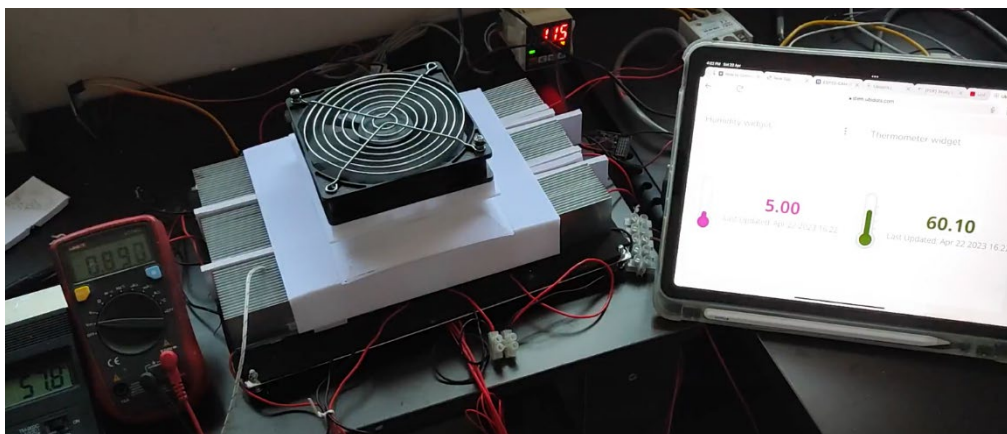


Figure 4.10: Experiment for Design 7.

Table 4.11: Experimental Data for Design 7.

Temperature Difference, $\Delta T$ ( $^{\circ}\text{C}$ )	Voltage, V (V)	Current, I (A)	Power, P (W)
35	20.23	0.16	3.237

To further investigate the problem, the voltage across each TEG module was measured as shown in Figure 4.11. The measured voltage for the TEG modules at the two sides were between 1.8 V to 2.2 V, slightly less than the TEG module at the centre. This is due to the fan was not blowing directly on the heat sinks at the two sides. Instead, the air was blown towards the centre before passing through the heat sinks at the sides and the air has become warm beforehand.

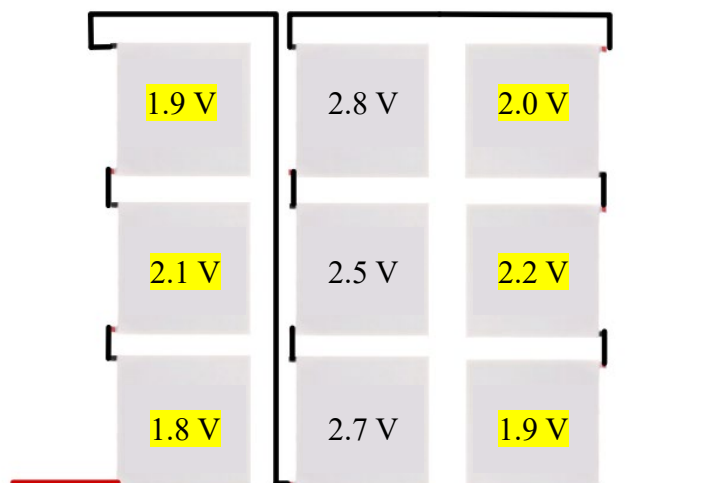


Figure 4.11: Measured Voltage of Each TEG Module.

For this design, the gaps between heat sinks and TEG modules were too far and the fan was unable to blow evenly on all the heat sinks. For the following design, the gaps were reduced to 10 mm and the number of TEG modules were increased to 12 pieces.

#### 4.3.8 Design 8

From the data collected in Table 4.12, the total power generated was 4.591 W from temperature difference of 39.8 °C. This design was able to power up the loads and sustain continuously as long as heat is supplied to the aluminium plate. For this design, the fan was able to blow evenly on all heat sinks to create equal temperature difference among all TEG modules.

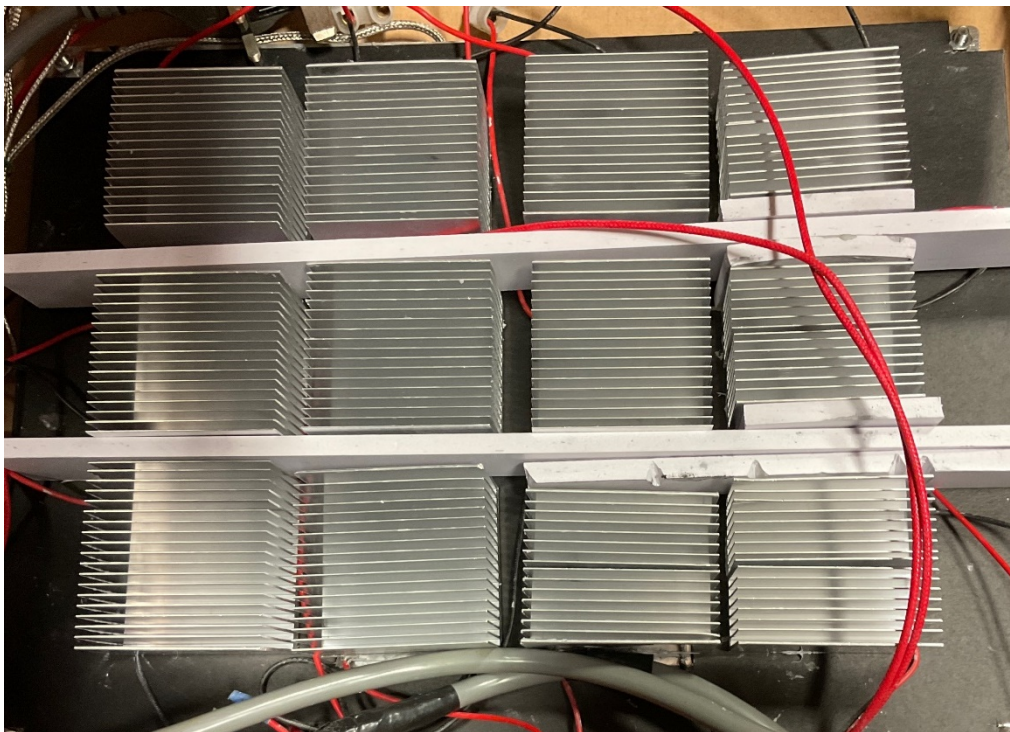


Figure 4.12: Prototype of Design 8.



Figure 4.13: Experiment for Design 8.

Table 4.12: Experimental Data for Design 8.

Temperature Difference, $\Delta T$ ( $^{\circ}\text{C}$ )	Voltage, V (V)	Current, I (A)	Power, P (W)
39.8	18.74	0.25	4.591

#### 4.3.9 Design 8 Under Load

Experiment 2 was repeated for design 8 with the loads to further analyse the performance of the prototype and the uncertainty of the experiment. Three trials were done to measure the consistency of the results as well as increasing the reliability of the measured data.

As shown in Figure 4.14 and Figure 4.15, graphs were plotted based on the data collected for first trial from Table B-1. Figure 4.14 shows the graph of voltage and current generated against temperature difference while Figure 4.15 shows the graph of power generated against temperature difference. The fan was turned on at temperature difference of  $23^{\circ}\text{C}$ , while the Arduino module was turned on at temperature difference of  $37.9^{\circ}\text{C}$ . Measurements recorded were based on the power consumed by the fan and Arduino module. The prototype was able to generate higher power output for other loads, where the maximum power output generated is shown in Table 4.12. As shown from the graph, the power output increased linearly with the temperature difference.

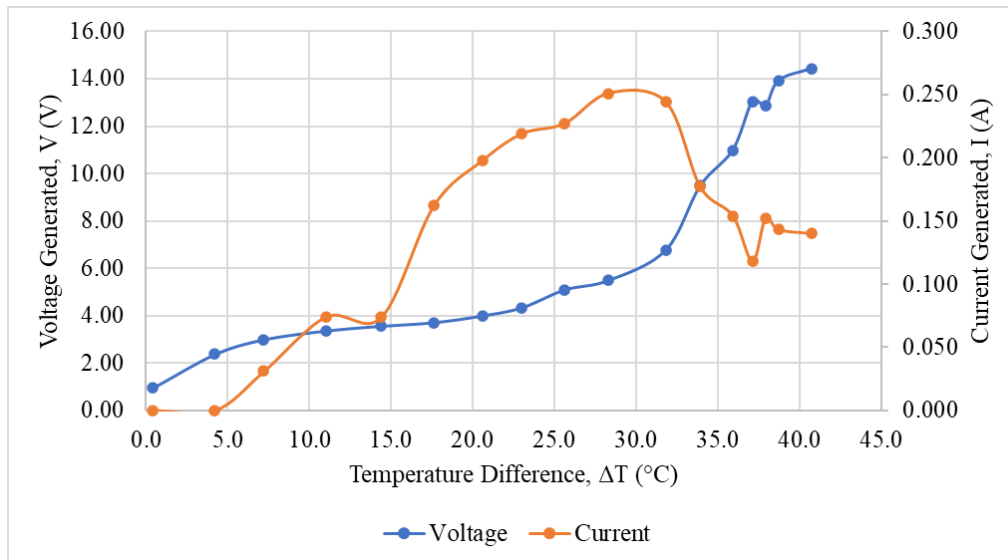


Figure 4.14: Graph of Voltage and Current Generated against Temperature Difference for First Trial.

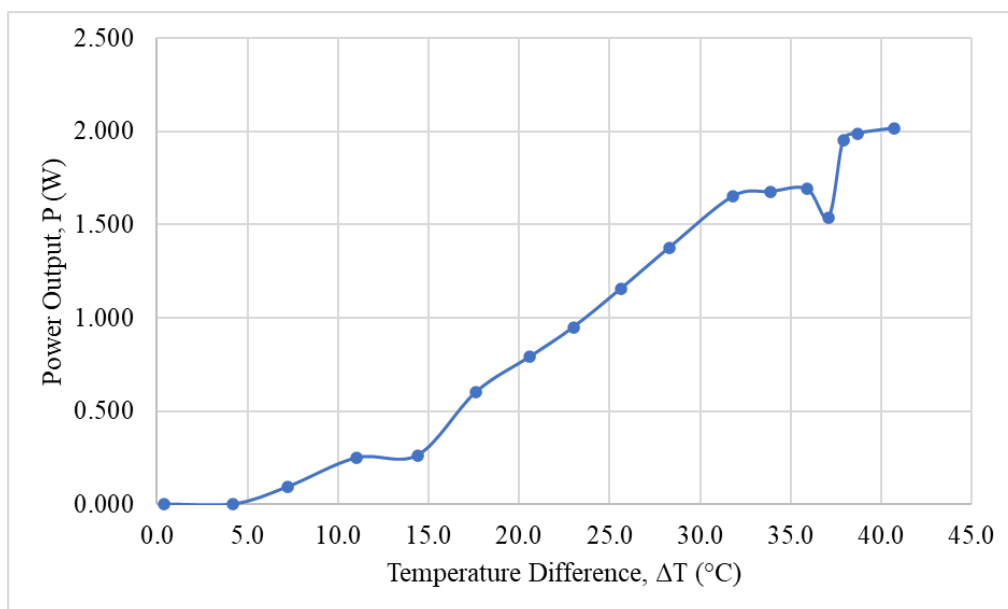


Figure 4.15: Graph of Power Output against Temperature Difference for First Trial.

For second trial, Figure 4.16 shows the graph of voltage and current generated against temperature difference while Figure 4.17 shows the graph of power generated against temperature difference.



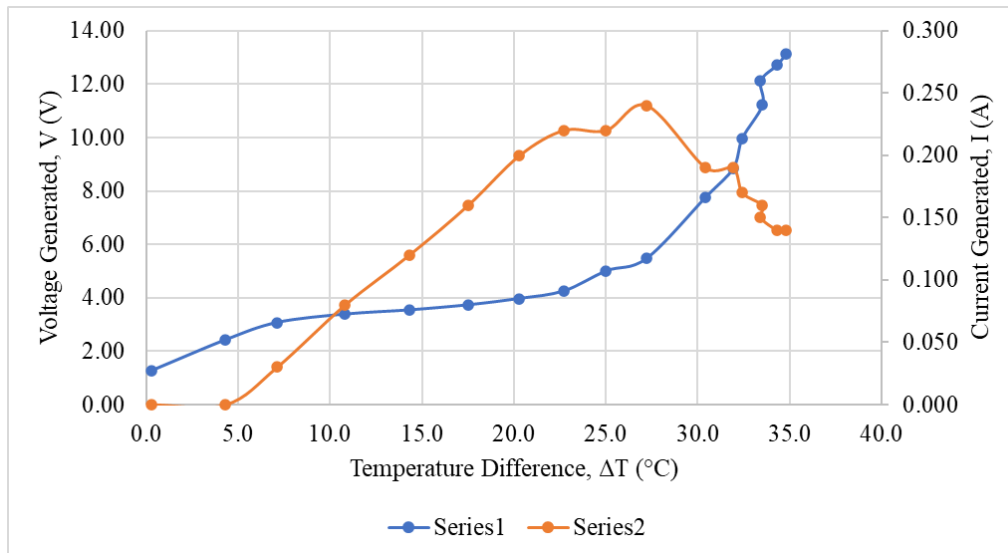


Figure 4.16: Graph of Voltage and Current Generated against Temperature Difference for Second Trial.

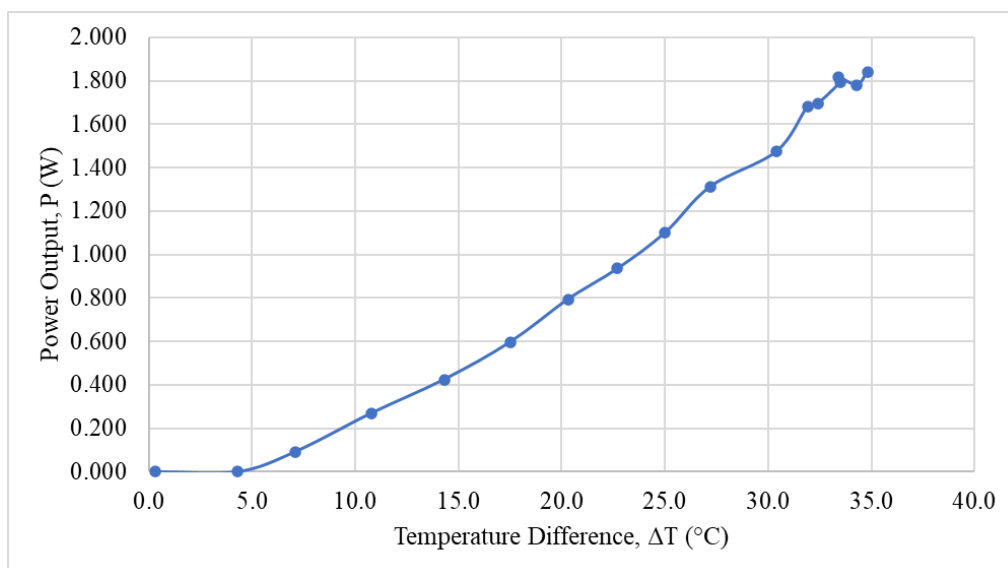


Figure 4.17: Graph of Power Output against Temperature Difference for Second Trial.

For third trial, Figure 4.18 shows the graph of voltage and current generated against temperature difference while Figure 4.19 shows the graph of power generated against temperature difference.

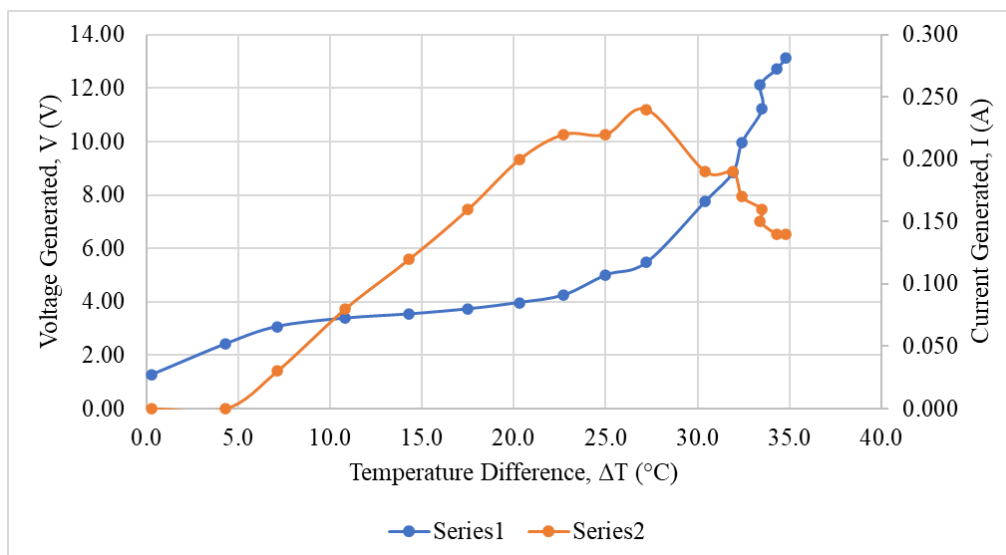


Figure 4.18: Graph of Voltage and Current Generated against Temperature Difference for Third Trial.

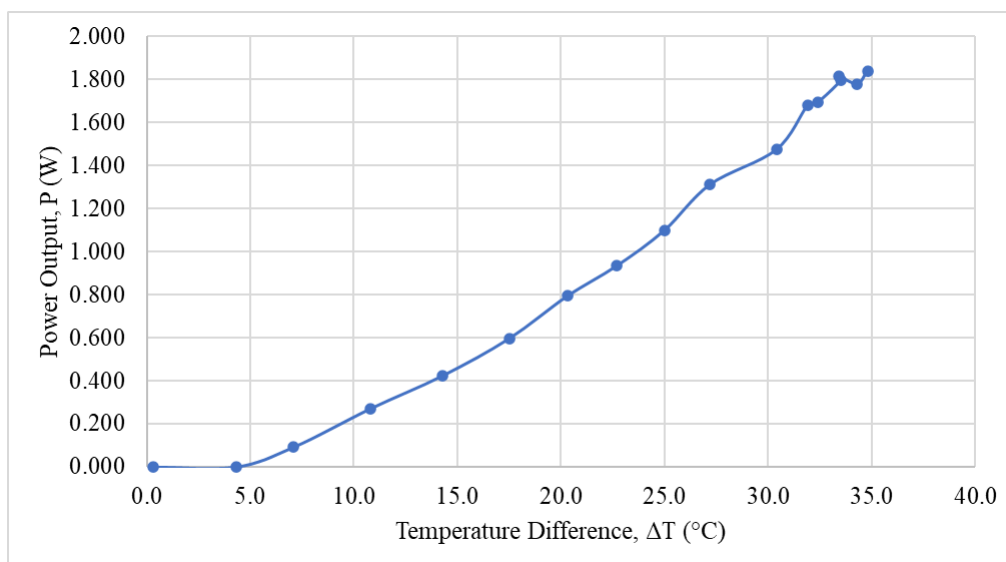


Figure 4.19: Graph of Power Output against Temperature Difference for Third Trial.

Then, mean data were calculated from the data of all trials and graphs were plotted. Figure 4.20 shows the graph of voltage and current generated against temperature difference while Figure 4.21 shows the graph of power generated against temperature difference.

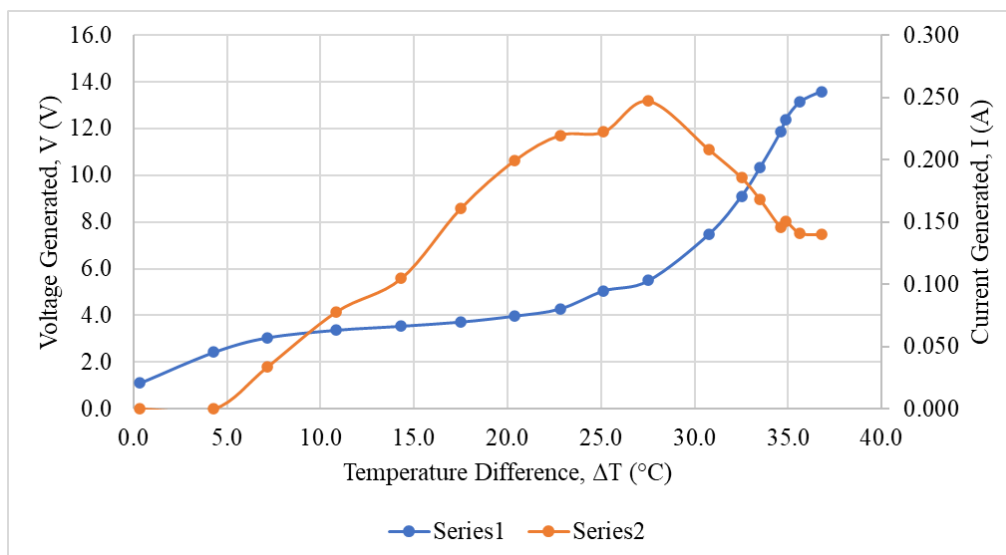


Figure 4.20: Graph of Voltage and Current Generated against Temperature Difference from Mean Data.

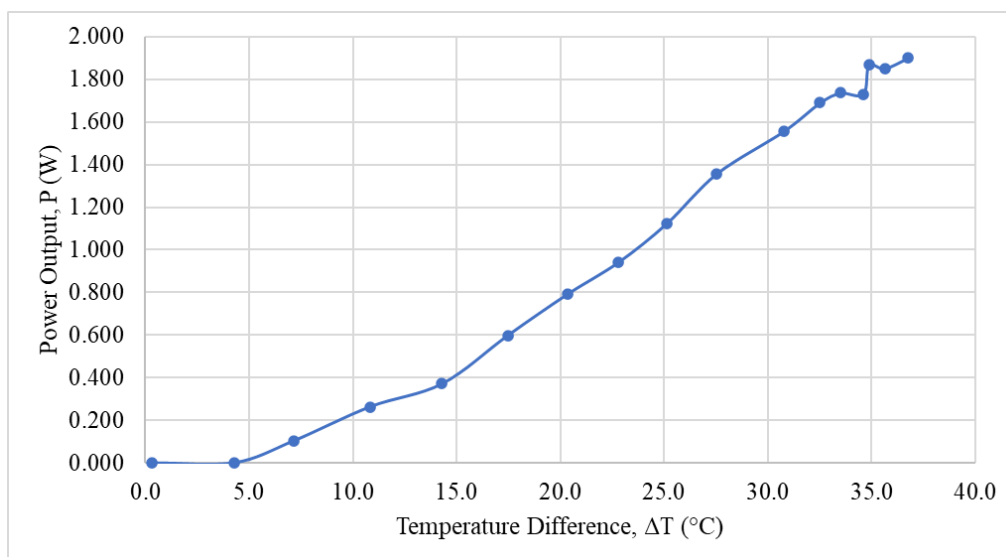


Figure 4.21: Graph of Power Output against Temperature Difference from Mean Data.

Subsequently, standard deviation which is one of the measures of dispersion was calculated to measure the spread of data from the mean as shown in Table 4.13. The average standard deviation obtained is 0.049 W which is acceptable. The deviation of the measurements may be due to other external factors such as atmospheric temperature and wind during the experiment. The trials of the experiment were carried out on different days with different atmospheric temperature, therefore there were some deviations of data between

each trial. However, the standard deviation is very minimal and this prove that the data collected are reliable.

Table 4.13: Standard Deviation for All Trials of Design 8.

<b>Mean Temperature Difference, <math>\Delta T</math> (°C)</b>	<b>Power, P from First Trial (W)</b>	<b>Power, P from Second Trial (W)</b>	<b>Power, P from Third Trial (W)</b>	<b>Standard Deviation, <math>\sigma</math> (W)</b>
0.3	0.000	0.000	0.000	0.000
4.3	0.000	0.000	0.000	0.000
7.1	0.093	0.092	0.124	0.018
10.8	0.249	0.271	0.271	0.013
14.3	0.263	0.425	0.426	0.093
17.5	0.601	0.597	0.598	0.002
20.4	0.792	0.794	0.796	0.002
22.8	0.950	0.935	0.939	0.008
25.1	1.155	1.100	1.118	0.028
27.5	1.378	1.313	1.380	0.038
30.8	1.652	1.474	1.505	0.095
32.5	1.678	1.680	1.706	0.016
33.5	1.692	1.695	1.807	0.066
34.6	1.540	1.795	1.806	0.151
34.9	1.953	1.818	1.829	0.075
35.6	1.991	1.781	1.785	0.120
36.8	2.019	1.841	1.842	0.102
<b>Average Standard Deviation, <math>\sigma</math> (W)</b>				<b>0.049</b>

#### 4.3.10 Summary of the Comparison on the Designs

Table 4.14 shows the summary of the comparison for design 1 to design 8 with the power generated and number of TEG modules used in each design.

Table 4.14: Comparison of the Designs.

<b>Design</b>	<b>Power Generated, P (W)</b>	<b>No. of TEGs</b>	<b>Explanation</b>
1	1.654	4	Four TEG modules connected in series were not able to provide sufficient power for the loads.
2	1.201	6	Six TEG modules were connected in series and parallel. Power output was significantly reduced due to parallel connection.
3	1.376	8	Clamps were added but failed to clamp evenly on all heat sinks due to the rods were bending.
4	0.915	9	Single piece of long copper heat sink was used to clamp on the TEG modules. However, the fins were too short and were not able to dissipate heat at a faster rate.
5	1.231	15	Four large heat sinks were used to cover 15 TEG modules. However, there were gaps between the heat sinks and TEG modules due to the slightly different thickness of TEG modules.
6	3.127	16	Heat sinks that have same surface area as the TEG module were used to eliminate the gaps. Case and Fins for fan were 3D printed to improve the air flow. Power output increased significantly. However, underperforming TEG modules at the four corners were limiting the overall power output. Too many TEG modules contribute to high concentration of heat at the centre.
7	3.237	9	TEG modules were reduced to nine pieces and separated with 50 mm gaps to prevent concentration of heat. However, 50 mm gaps were too far apart and the fan was unable to blow directly on the heat sinks at the two sides.
8	4.125	12	This design has even air flow on the heat sinks and similar temperature difference among all TEG modules. The prototype was able to self-sustain by powering up the fan to cool down the heat sink without external power source. Temperature difference was maintained at around 40 °C continuously.

#### 4.4 Efficiency of the Prototype

The energy output by the TEG prototype and energy input by the heater to heat up the aluminium plate were measured to evaluate the efficiency of the prototype. The measurements were recorded in Table 4.15 and the efficiency of the prototype was calculated using the equation 4.1. The obtained efficiency is 1.934 % as shown in equation 4.2.

Table 4.15: Measured Power of the Energy Input and Output.

<b>Input / Output</b>	<b>Measured Power, P (W)</b>
TEG (Output)	4.591
Heater (Input)	237.4

$$\% \text{ Efficiency, } \eta = \frac{\text{Energy Output}}{\text{Energy Input}} \times 100 \% \quad (4.1)$$

$$\% \text{ Efficiency, } \eta = \frac{4.591 \text{ W}}{237.4 \text{ W}} \times 100\% = 1.934 \% \quad (4.2)$$

The efficiency obtained for this study is not suitable to compare with previous research. This is because most of them were using different types of TEG module and cooling method. The cooling method commonly used were the fan powered by external source, wind from the moving of vehicles as well as water and ice. The efficiency of the TEG can be increased by using larger fan with higher rotational speed to increase the air flow to cool down the heat sink. However, for this experiment, the power produced by the TEG system is the limiting factor for the selection of fan to cool down the TEG system itself. Fan with lower power consumption was used and therefore, it has limited rotational speed and limited air flow to cool down the heat sink. If larger fan is used, it requires higher power input and is unable to be powered up by the TEG system. On the other hand, if smaller fan is used, the area of the air flow created is not sufficient to cover the all the heat sink of the TEG system.

#### 4.5 Develop Arduino Module – Wireless Device

The output of the TEG prototype from previous experiment was stepped-down to a constant voltage of 5 V using step-down power module. Figure 4.22 shows

the built prototype and the connections between each module. From the experiment, the Arduino module and fan were successfully powered up by design 8 of the TEG prototype and the sensor values were sent to the Ubidots cloud.

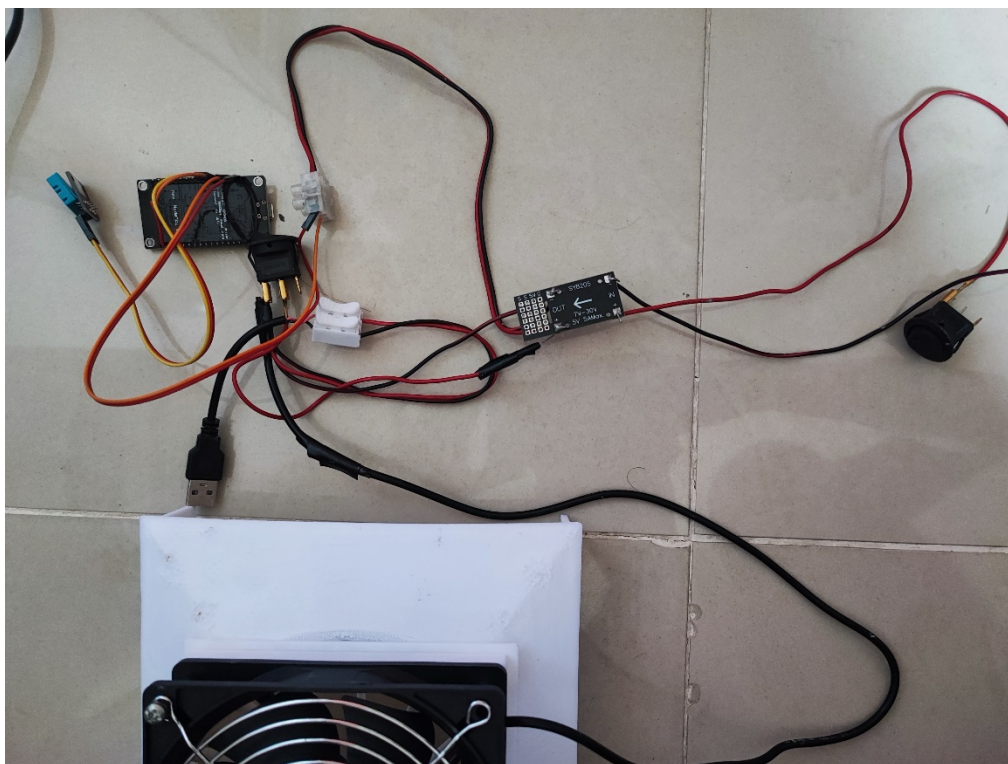


Figure 4.22: Set-up of Arduino Module.

Figure 4.23 shows the display of the dashboard with the value of the respective sensors.

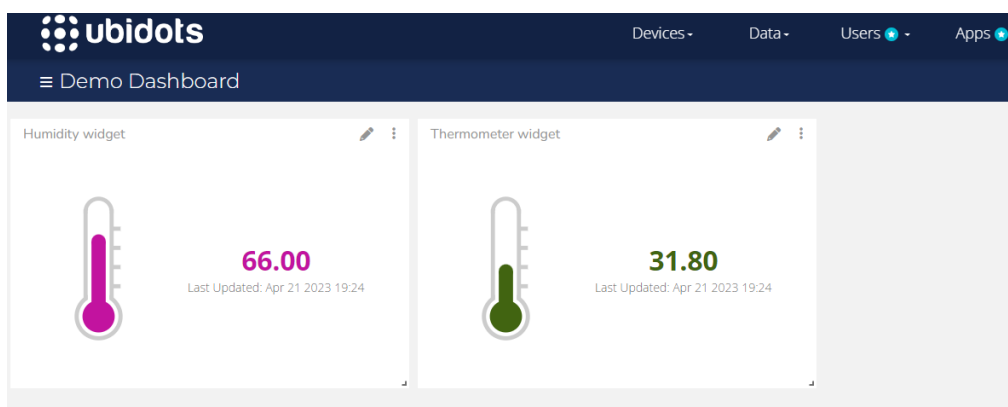


Figure 4.23: Dashboard of Ubidots showing Real-Time Data from ESP32 Arduino Board.

#### **4.6 Summary**

This chapter sums up the results obtained from the experiments, which were interpreted accordingly. The problems encountered at each stage were analysed and solved subsequently until the result was satisfying. Discussion and comparison were made to explain the reasons for the modifications.



## CHAPTER 5

### CONCLUSIONS AND RECOMMENDATIONS

#### 5.1 Conclusions

A TEG system was successfully built in this project. The prototype was able to self-sustain from surface temperature of 115 °C and atmospheric temperature of 30 °C. Fan was powered up by the TEG itself to cool down the heat sinks and maintain the temperature gradient. The remaining power generated was used to power up the Arduino module. It has a power output of 4.591 W with efficiency of 1.934 % as measured in experiment 2 from temperature difference of 39.8 °C. From experiment 1, comparison was done on different type of heat sink, thermal conductive paste and TEG module. The best heat sink is aluminium heat sink with fins height of 36 mm, whereas the best TEG module is TEG-127-3.5-2.8T250D. For thermal conductive paste, Frost X25 Thermal Paste with 10.5 W/m-K Thermal Conductivity has the best performance despite they did not have notable improvement on the performance. For experiment 2, comparison between the designs was done to select the best design. Design 8 is the best design after several modifications and improvements were done on each design. Air flow and arrangement of TEG modules are having significant impact on the power output of the prototype. In conclusion, the TEG system managed operate at surface temperature of 115 °C up to 200 °C where 200 °C is the maximum working temperature of the TEG module.

#### 5.2 Limitations

The limitations for this project are the fins height of the heat sink and the availability of TEG modules. Heat sink with fins height higher than 36 mm, which was used in this prototype, was not commonly available. Similarly, the types of TEG modules available in the market were limited and restricting the overall efficiency of the prototype.

### **5.3 Recommendations for Future Work**

The TEG prototype can be further improved to increase the efficiency as well as power generation. Thereby, the number of TEG modules used can be reduced which leads to lower product cost and smaller size of the product. One of the recommendations is using higher heat sinks to create larger surface area for the heat to dissipate at a faster rate. Therefore, the temperature gradient can be increased. Analysis on the optimum distance of the gaps between TEG modules and heat sinks can be carried out to maximise the cooling effect. Furthermore, using thicker TEG module could improve the power generation of the system. This is because thicker TEG module has larger gap between the two side and lowering the heat transfer rate across the TEG module. Therefore, higher temperature difference can be achieved.

Moreover, additional device such as supercapacitor can be added to act as a buffer for the TEG and stabilise the power output. Capacitor can accumulate the charge generated by the TEG system and power up higher power device for a short moment. Similarly, battery can be added into the system to store the charges and power up the device for a specific period depending on the requirements.

## REFERENCES

- Aranguren, P., Astrain, D. and Pérez, M.G., 2014. Computational and experimental study of a complete heat dissipation system using water as heat carrier placed on a thermoelectric generator. *Energy*, 74(C), pp.346–358.
- Bell, L.E., 2008. Cooling, Heating, Generating Power, and Recovering Waste Heat with Thermoelectric Systems. *Science*, 321(5895), pp.1457–1461. Available at: <https://www.science.org/doi/10.1126/science.1158899>.
- Belli, L. et al., 2019. Toward Industry 4.0 With IoT: Optimizing Business Processes in an Evolving Manufacturing Factory. *Frontiers in ICT*, 6.
- Bian, Q., 2020. Waste heat: the dominating root cause of current global warming. *Environmental Systems Research*, 9(1), p.8. Available at: <https://environmentalsystemsresearch.springeropen.com/articles/10.1186/s40068-020-00169-2>.
- Brückner, S. et al., 2015. Industrial waste heat recovery technologies: An economic analysis of heat transformation technologies. *Applied Energy*, 151, pp.157–167.
- Cao, Q., Luan, W. and Wang, T., 2018a. Performance enhancement of heat pipes assisted thermoelectric generator for automobile exhaust heat recovery. *Applied Thermal Engineering*, 130, pp.1472–1479.
- Cao, Q., Luan, W. and Wang, T., 2018b. Performance enhancement of heat pipes assisted thermoelectric generator for automobile exhaust heat recovery. *Applied Thermal Engineering*, 130, pp.1472–1479.
- Casano, G. and Piva, S., 2011. Experimental investigation of the performance of a thermoelectric generator based on Peltier cells. *Experimental Thermal and Fluid Science*, 35(4), pp.660–669.
- CMP (Firm), Institute of Electrical and Electronics Engineers. and Components, P.& M.T.Society., 2009. THERMINIC 2009: international workshop on THERMal INvestigation of ICs and Systems: 7-9 October 2009, Leuven, Belgium. 2009 EDA Pub, p. 234.
- Crane, D., Jackson, G. and Holloway, D., 2001. *Towards Optimization of Automotive Waste Heat Recovery Using Thermoelectrics*,
- Crane, D.T. and Jackson, G.S., 2004. Optimization of cross flow heat exchangers for thermoelectric waste heat recovery. *Energy Conversion and Management*, 45(9–10), pp.1565–1582.
- Crane, D.T. and Lagrandeur, J.W., 2010. Progress report on BSST-led US Department of Energy Automotive Waste Heat Recovery Program. *Journal of Electronic Materials*, 39(9), pp.2142–2148.

Drebushchak, V.A., 2008. The Peltier effect. *Journal of Thermal Analysis and Calorimetry*, 91(1), pp.311–315. Available at: <http://link.springer.com/10.1007/s10973-007-8336-9>.

Ekpu, M. et al., 2011. Investigation of effects of heat sinks on thermal performance of microelectronic package. *3rd IEEE International Conference on Adaptive Science and Technology, ICAST 2011, Proceedings*. 2011 pp. 127–132.

Espinosa, N., Lazard, M., Aixala, L. and Scherrer, H., 2010. Modeling a thermoelectric generator applied to diesel automotive heat recovery. *Journal of Electronic Materials*, 39(9), pp.1446–1455.

Eurostat, 2020, *Final energy consumption in industry - detailed statistics* [Online]. Available at: [https://ec.europa.eu/eurostat/statistics-explained/index.php?title=Final\\_energy\\_consumption\\_in\\_industry\\_-\\_detailed\\_statistics](https://ec.europa.eu/eurostat/statistics-explained/index.php?title=Final_energy_consumption_in_industry_-_detailed_statistics) [Accessed: 16 April 2023].

Faiz, M.S. and V.K. Maurya, 2017. Study of TEG When Connected in Series and Parallel Combinations Along With a DC-DC Converter. *Vivechan International Journal of Research*, 8(1), pp.76–86.

Fluch, J., Brunner, C. and Grubbauer, A., 2017. Potential for energy efficiency measures and integration of renewable energy in the European food and beverage industry based on the results of implemented projects. *Energy Procedia*, 123, pp.148–155. Available at: <https://linkinghub.elsevier.com/retrieve/pii/S187661021732814X>.

FoodDrinkEurope, 2019. Data & Trends. *EU Food & Drink Industry*.

Gabrian, *Copper vs. Aluminum Heatsinks: What You Need to Know* [Online]. Available at: <https://www.gabrian.com/copper-vs-aluminum-heatsinks/> [Accessed: 30 April 2023].

Ge, Y., Liu, Z., Sun, H. and Liu, W., 2018. Optimal design of a segmented thermoelectric generator based on three-dimensional numerical simulation and multi-objective genetic algorithm. *Energy*, 147, pp.1060–1069.

Goldsmid, H.J., 2014. Bismuth telluride and its alloys as materials for thermoelectric generation. *Materials*, 7(4), pp.2577–2592.

Haidar, J.G. and Ghojel, J.I., 2001. Waste heat recovery from the exhaust of low-power diesel engine using thermoelectric generators. *International Conference on Thermoelectrics, ICT, Proceedings*. 2001 pp. 413–418.

Han, M.K., Jin, Y., Lee, D.H. and Kim, S.J., 2017. Thermoelectric properties of Bi<sub>2</sub>Te<sub>3</sub>: CuI and the effect of its doping with Pb atoms. *Materials*, 10(11).

Hazen, B.T., Skipper, J.B., Ezell, J.D. and Boone, C.A., 2016. Big data and predictive analytics for supply chain sustainability: A theory-driven research agenda. *Computers and Industrial Engineering*, 101, pp.592–598.

Intel, *How to Apply Thermal Paste - Intel* [Online]. Available at: <https://www.intel.com/content/www/us/en/gaming/resources/how-to-apply-thermal-paste.html> [Accessed: 30 April 2023].

Jouhara, H. et al., 2021. Thermoelectric generator (TEG) technologies and applications. *International Journal of Thermofluids*, 9, p.100063. Available at: <https://linkinghub.elsevier.com/retrieve/pii/S266620272100001X>.

Jouhara, H. et al., 2018. Waste heat recovery technologies and applications. *Thermal Science and Engineering Progress*, 6, pp.268–289. Available at: <https://linkinghub.elsevier.com/retrieve/pii/S2451904918300015>.

Kanimba, E. et al., 2017. A modeling comparison between a two-stage and three-stage cascaded thermoelectric generator. *Journal of Power Sources*, 365, pp.266–272.

LaGrandeur, J. et al., 2006. *Automotive Waste Heat Conversion to Electric Power using Skutterudite, TAGS, PbTe and BiTe*,

Lan, Y., Minnich, A.J., Chen, G. and Ren, Z., 2010. Enhancement of Thermoelectric Figure-of-Merit by a Bulk Nanostructuring Approach. *Advanced Functional Materials*, 20(3), pp.357–376. Available at: <https://onlinelibrary.wiley.com/doi/10.1002/adfm.200901512>.

Leonov, V., 2013. Thermoelectric energy harvesting of human body heat for wearable sensors. *IEEE Sensors Journal*. 2013 pp. 2284–2291.

Li, M., Xu, S., Chen, Q. and Zheng, L.R., 2011. Thermoelectric-generator-based DC-DC conversion networks for automotive applications. *Journal of Electronic Materials*. May 2011 pp. 1136–1143.

Liu, C. et al., 2016. An experimental study of a novel prototype for two-stage thermoelectric generator from vehicle exhaust. *Journal of the Energy Institute*, 89(2), pp.271–281.

Manavalan, E. and Jayakrishna, K., 2019. A review of Internet of Things (IoT) embedded sustainable supply chain for industry 4.0 requirements. *Computers and Industrial Engineering*, 127, pp.925–953.

Meisner, G.P., 2010. Thermoelectric Generator Development for Automotive Waste Heat Recovery. *General Motors Global Research & Development*. 2010

Mostafavi, S.A. and Mahmoudi, M., 2018. Modeling and fabricating a prototype of a thermoelectric generator system of heat energy recovery from hot exhaust gases and evaluating the effects of important system parameters. *Applied Thermal Engineering*, 132, pp.624–636.

Niu, X., Yu, J. and Wang, S., 2009. Experimental study on low-temperature waste heat thermoelectric generator. *Journal of Power Sources*, 188(2), pp.621–626.

Pearson, M.R. et al., 2012. Energy harvesting for aerospace structural health monitoring systems. *Journal of Physics: Conference Series*. 2012 Institute of Physics Publishing.

PowerWatch, *FAQ – PowerWatch* [Online]. Available at: <https://www.powerwatch.com/pages/faqs> [Accessed: 21 August 2022].

Proto, A. et al., 2018. Human body energy harvesting solutions for wearable technologies. *2018 IEEE 20th International Conference on e-Health Networking, Applications and Services, Healthcom 2018*. 9 November 2018 Institute of Electrical and Electronics Engineers Inc.

Quan, R. et al., 2018. Performance investigation of an exhaust thermoelectric generator for military SUV application. *Coatings*, 8(1).

Reardon Hazel, 2022, *Thermoelectric materials* [Online]. Available at: <https://chem.au.dk/forskning/forskningscentre-og-projekter/og-projekter/og-projekter/center-for-materials-crystallography/research/energy-materials/thermoelectrics> [Accessed: 17 August 2022].

Riffat, S.B. and Ma, X., 2003. Thermoelectrics: A review of present and potential applications. *Applied Thermal Engineering*, 23(8), pp.913–935.

Romanjek, K. et al., 2015. High-Performance Silicon–Germanium-Based Thermoelectric Modules for Gas Exhaust Energy Scavenging. *Journal of Electronic Materials*, 44(6), pp.2192–2202.

Saeidi, A. and Taheri, P., 2020. *Numerical Design of a Guide Vane for an Axial Fan*,

Sandoz-Rosado, E. and Stevens, R.J., 2009. Experimental characterization of thermoelectric modules and comparison with theoretical models for power generation. *Journal of Electronic Materials*. July 2009 pp. 1239–1244.

Saqr, K.M., Mansour, M.K. and Musa, M.N., 2008. THERMAL DESIGN OF AUTOMOBILE EXHAUST BASED THERMOELECTRIC GENERATORS: OBJECTIVES AND CHALLENGES. *International Journal of Automotive Technology*, 9(2), p.155160.

Seebeck, T.J., Macmillan Encyclopedia of Energy. Available at: <https://www.encyclopedia.com/environment/encyclopedias-almanacs-transcripts-and-maps/seebeck-thomas-johann-1770-1831> [Accessed: 16 July 2022].

Shen, R., Gou, X., Xu, H. and Qiu, K., 2017. Dynamic performance analysis of a cascaded thermoelectric generator. *Applied Energy*, 203, pp.808–815.

Shu, G. et al., 2018. Configuration optimization of the segmented modules in an exhaust-based thermoelectric generator for engine waste heat recovery. *Energy*, 160, pp.612–624.

Snyder, G.J., 2004. Application of the compatibility factor to the design of segmented and cascaded thermoelectric generators. *Applied Physics Letters*, 84(13), pp.2436–2438.

Snyder, G.J. and Ursell, T.S., 2003. Thermoelectric efficiency and compatibility. *Physical Review Letters*, 91(14), pp.148301/1-148301/4.

Sofyan, S.E. et al., 2020. The performance of thermoelectric exhaust heat recovery system considering different heat source's fin arrangements. *IOP Conference Series: Earth and Environmental Science*. 6 April 2020 Institute of Physics Publishing.

Tech4All, *Matrix PowerWatch 2: Never Charge Your Watch Again – Tech4all - Let's Inspect Cool Tech* [Online]. Available at: <https://tech4all.net/matrix-powerwatch-2-never-charge-your-watch-again/> [Accessed: 21 August 2022].

Tian, H. et al., 2015. Comparison of Segmented and Traditional Thermoelectric Generator for Waste Heat Recovery of Diesel Engine. *Energy Procedia*. 2015 Elsevier Ltd, pp. 590–596.

Ubaidillah et al., 2014. Experimental study of thermoelectric generators. *Applied Mechanics and Materials*. 2014 Trans Tech Publications Ltd, pp. 299–303.

United Nations Environment Programme (UNEP), *GOAL 11: Sustainable cities and communities | UNEP - UN Environment Programme* [Online]. Available at: <https://www.unep.org/explore-topics/sustainable-development-goals/why-do-sustainable-development-goals-matter/goal-11> [Accessed: 15 July 2022].

Wahbah, M. et al., 2014. Characterization of human body-based thermal and vibration energy harvesting for wearable devices. *IEEE Journal on Emerging and Selected Topics in Circuits and Systems*, 4(3), pp.354–363.

Wilbrecht, S. and Beitelschmidt, M., 2018. The Potential of a Cascaded TEG System for Waste Heat Usage in Railway Vehicles. *Journal of Electronic Materials*, 47(6), pp.3358–3369.

World Weather & Climate Information, *Climate and average weather in Malaysia* [Online]. Available at: <https://weather-and-climate.com/average-monthly-Rainfall-Temperature-Sunshine-in-Malaysia> [Accessed: 18 July 2022].

Xiao, Y. et al., 2022. Research on Control Method of Waste Heat Utilization System Based on Multi-parameter Coupling. *Scientific Reports*, 12(1), p.11497. Available at: <https://www.nature.com/articles/s41598-022-15808-0>.

Xu, Z.Y., Wang, R.Z. and Yang, C., 2019. Perspectives for low-temperature waste heat recovery. *Energy*, 176, pp.1037–1043.

Yang, J., 2005. Potential applications of thermoelectric waste heat recovery in the automotive industry. *International Conference on Thermoelectrics, ICT, Proceedings*. 2005 Institute of Electrical and Electronics Engineers Inc., pp. 170–174.

Yu, J. and Zhao, H., 2007. A numerical model for thermoelectric generator with the parallel-plate heat exchanger. *Journal of Power Sources*, 172(1), pp.428–434.

Zhang, L., Tosho, T., Okinaka, N. and Akiyama, T., 2008. Design of cascaded oxide thermoelectric generator. *Materials Transactions*, 49(7), pp.1675–1680.

Zoui, M.A., Bentouba, S., Stocholm, J.G. and Bourouis, M., 2020. A review on thermoelectric generators: Progress and applications. *Energies*, 13(14).



## APPENDICES

### Appendix A: Gantt Chart

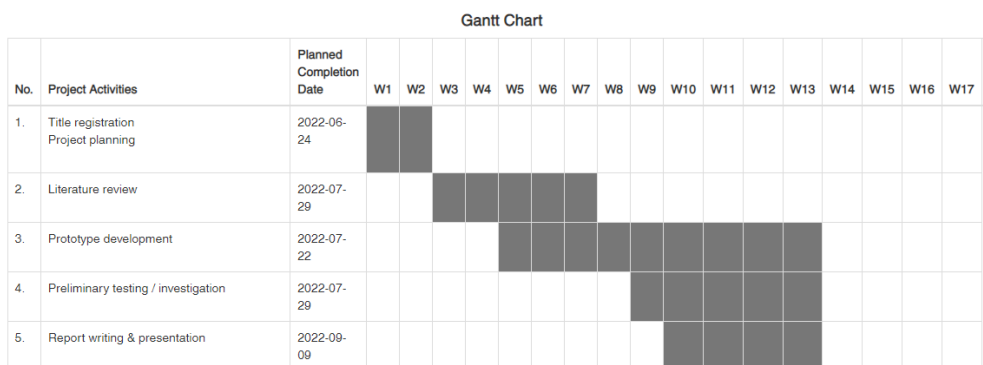


Figure A-1: Gantt Chart for FYP Part 1.

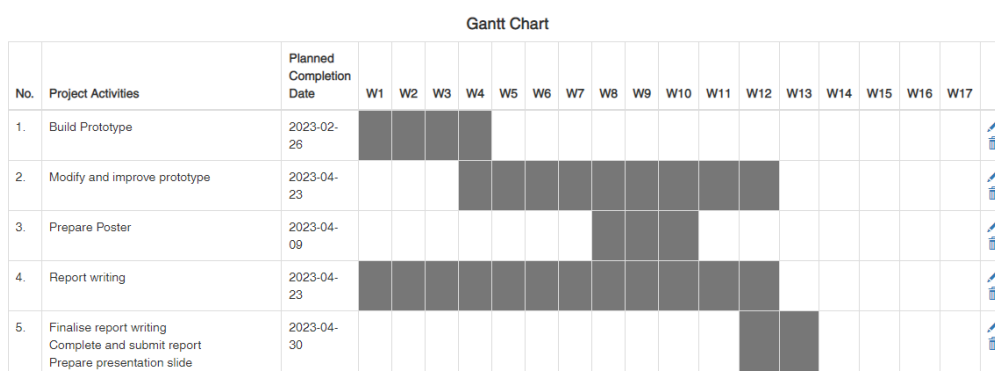


Figure A-2: Gantt Chart for FYP Part 2.

## Appendix B: Experimental Data for Design 8

Table B-1: Experimental Data for Design 8 for First Trial.

Hot Side (°C)	Cold Side (°C)	Temperature Difference, $\Delta T$ (°C)	Voltage under Load, $V_L$ (V)	Current under Load, $I$ (A)	Power under Load, $P$ (W)
34	33.6	0.4	0.95	0.000	0.000
38	33.8	4.2	2.37	0.000	0.000
41	33.8	7.2	2.99	0.031	0.093
45	34.0	11.0	3.36	0.074	0.249
49	34.6	14.4	3.56	0.074	0.263
53	35.4	17.6	3.71	0.162	0.601
57	36.4	20.6	4.00	0.198	0.792
61	38.0	23.0	4.34	0.219	0.950
65	39.4	25.6	5.09	0.227	1.155
69	40.7	28.3	5.49	0.251	1.378
74	42.2	31.8	6.77	0.244	1.652
78	44.1	33.9	9.48	0.177	1.678
81	45.1	35.9	10.99	0.154	1.692
85	47.9	37.1	13.05	0.118	1.540
88	50.1	37.9	12.85	0.152	1.953
92	53.3	38.7	13.92	0.143	1.991
96	55.3	40.7	14.42	0.140	2.019

Table B-2: Experimental Data for Design 8 for Second Trial.

Hot Side (°C)	Cold Side (°C)	Temperature Difference, $\Delta T$ (°C)	Voltage under Load, $V_L$ (V)	Current under Load, $I$ (A)	Power under Load, $P$ (W)
34	33.7	0.3	1.27	0.000	0.000
38	33.7	4.3	2.42	0.000	0.000
41	33.9	7.1	3.07	0.030	0.092
45	34.2	10.8	3.38	0.080	0.271
49	34.7	14.3	3.54	0.120	0.425
53	35.5	17.5	3.73	0.160	0.597
57	36.7	20.3	3.97	0.200	0.794
61	38.3	22.7	4.25	0.220	0.935
65	40.0	25.0	5.00	0.220	1.100
69	41.8	27.2	5.47	0.240	1.313
74	43.6	30.4	7.76	0.190	1.474

78	46.1	31.9	8.84	0.190	1.680
81	48.6	32.4	9.97	0.170	1.695
85	51.5	33.5	11.22	0.160	1.795
88	54.6	33.4	12.12	0.150	1.818
92	57.7	34.3	12.72	0.140	1.781
96	61.2	34.8	13.15	0.140	1.841

Table B-3: Experimental Data for Design 8 for Third Trial.

Hot Side (°C)	Cold Side (°C)	Temperature Difference, $\Delta T$ (°C)	Voltage under Load, $V_L$ (V)	Current under Load, I (A)	Power under Load, P (W)
34	33.7	0.3	1.13	0.000	0.000
38	33.7	4.3	2.50	0.000	0.000
41	33.9	7.1	3.10	0.040	0.124
45	34.3	10.7	3.39	0.080	0.271
49	34.8	14.2	3.55	0.120	0.426
53	35.7	17.3	3.74	0.160	0.598
57	36.8	20.2	3.98	0.200	0.796
61	38.3	22.7	4.27	0.220	0.939
65	40.2	24.8	5.08	0.220	1.118
69	41.9	27.1	5.52	0.250	1.380
74	43.9	30.1	7.92	0.190	1.505
78	46.3	31.7	8.98	0.190	1.706
81	48.8	32.2	10.04	0.180	1.807
85	51.8	33.2	11.29	0.160	1.806
88	54.7	33.3	12.19	0.150	1.829
92	58.1	33.9	12.75	0.140	1.785
96	61.2	34.8	13.16	0.140	1.842

Table B-4: Mean Data for Design 8 From All Trials.

Hot Side (°C)	Cold Side (°C)	Temperature Difference, $\Delta T$ (°C)	Voltage under Load, $V_L$ (V)	Current under Load, I (A)	Power under Load, P (W)
34.0	33.7	0.3	1.1	0.000	0.000
38.0	33.7	4.3	2.4	0.000	0.000
41.0	33.9	7.1	3.1	0.034	0.103
45.0	34.2	10.8	3.4	0.078	0.263
49.0	34.7	14.3	3.5	0.105	0.371
53.0	35.5	17.5	3.7	0.161	0.599

57.0	36.6	20.4	4.0	0.199	0.794
61.0	38.2	22.8	4.3	0.220	0.942
65.0	39.9	25.1	5.1	0.222	1.124
69.0	41.5	27.5	5.5	0.247	1.357
74.0	43.2	30.8	7.5	0.208	1.557
78.0	45.5	32.5	9.1	0.186	1.690
81.0	47.5	33.5	10.3	0.168	1.736
85.0	50.4	34.6	11.9	0.146	1.731
88.0	53.1	34.9	12.4	0.151	1.866
92.0	56.4	35.6	13.1	0.141	1.851
96.0	59.2	36.8	13.6	0.140	1.901

## Appendix C: Arduino Code for ESP32

```

#include "UbidotsEsp32Mqtt.h"
/*****

* Define Constants
*****/

const char* UBIDOTS_TOKEN = ""; // Ubidots TOKEN
const char* WIFI_SSID = "Test"; // Wi-Fi SSID
const char* WIFI_PASS = "abc12345"; // Wi-Fi password
const int PUBLISH_FREQUENCY = 1000; // Update rate in milliseconds
unsigned long timer;

Ubidots ubidots(UBIDOTS_TOKEN);

#include "DHT.h" // DHT11/DHT22 sensor
#define DHTPIN 13 // Defining the data output pin to Arduino
#define DHTTYPE DHT11 // Specify the sensor type (DHT11 or DHT22)

/*****

* Auxiliar Functions
*****/

void callback(char *topic, byte *payload, unsigned int length)
{
  Serial.print("Message arrived [");
  Serial.print(topic);
  Serial.print("] ");
  for (int i = 0; i < length; i++)
  {
    Serial.print((char)payload[i]);
  }
  Serial.println();
}

```

```
DHT dht(DHTPIN, DHTTYPE);

void setup()
{
  Serial.begin(115200);
  ubidots.connectToWifi(WIFI_SSID, WIFI_PASS);
  ubidots.setCallback(callback);
  ubidots.setup();
  ubidots.reconnect();

  timer = millis();
  dht.begin(); //To initialise DHT sensor
}

void loop()
{
  if (!ubidots.connected())
  {
    ubidots.reconnect();
  }

  if ((millis() - timer) > PUBLISH_FREQUENCY) // triggers the routine
  {
    float h= dht.readHumidity();
    float tC= dht.readTemperature();

    if (isnan(h) || isnan(tC))
    {
      Serial.println("Failed to read the DHT sensor. Check connections");
    }
    else
    {
      Serial.print("Humidity: ");
```

```
Serial.print(h);
Serial.print("%");
Serial.print(" || ");
Serial.print("Temperature: ");
Serial.print(tC);
Serial.print("C ");
}

ubidots.add ("Temperature",tC);
ubidots.add ("Humidity",h);
ubidots.publish ("esp8266");
timer = millis ();
}
ubidots.loop ();
}
```